UNIVERSIDADE ESTADUAL DE CAMPINAS
Faculdade de Engenharia Mecânica

Edilson Dantas Nóbrega

Modeling elastic metamaterials and phononic crystals by wave finite element method

Modelagem de metamateriais elásticos e cristais fonônicos pelo método de propagação de ondas por elementos finitos

CAMPINAS
2020

Edilson Dantas Nóbrega

Modeling elastic metamaterials and phononic crystals by wave finite element method
Modelagem de metamateriais elásticos e cristais fonônicos pelo método de propagação de ondas por elementos finitos

Doctoral Thesis presented to the School of Mechanical Engineering of the University of Campinas in partial fulfillment of the requirements for the degree of doctor in Mechanical Engineering, in the Area of Solid Mechanics and Machanical Design.

Tese de doutorado apresentada à Faculdade de Engenharia Mecânica da Universidade Estadual de Campinas como parte dos requisitos exigidos para obtenção do título de Doutor em Engenharia Mecânica, na Área de Mecânica dos Sólidos e Projeto Mecânico.

Orientador: Prof. Dr. José Maria Campos dos Santos

ESTE EXEMPLAR CORRESPONDE À VERSÃO DA TESE DEFENDIDA PELO ALUNO EDILSON DANTAS NÓBREGA, E ORIENTADO PELO PROF. DR. JOSÉ MARIA CAMPOS DOS SANTOS.

.....

ASSINATURA DO ORIENTADOR

CAMPINAS

2020

Ficha catalográfica
Universidade Estadual de Campinas
Biblioteca da Área de Engenharia e Arquitetura
Luciana Pietrosanto Milla - CRB 8/8129

Nóbrega, Edilson Dantas, 1985-
N669m Modeling elastic metamaterials and phononic crystals by wave finite element method / Edilson Dantas Nóbrega. – Campinas, SP : [s.n.], 2020.

Orientador: José Maria Campos dos Santos.
Tese (doutorado) – Universidade Estadual de Campinas, Faculdade de Engenharia Mecânica.

1. Guias de ondas. 2. Propagação de ondas. 3. Cristais fonônicos. 4. Metamateriais. 5. Métodos dos elementos finitos. I. Santos, José Maria Campos dos, 1953-. II. Universidade Estadual de Campinas. Faculdade de Engenharia Mecânica. III. Título.

Informações para Biblioteca Digital

Título em outro idioma: Modelagem de metamateriais elásticos e cristais fonônicos pelo método de propagação de ondas por elementos finitos
Palavras-chave em inglês:
waveguide
Wave propagations
Phononic crystals
Metamaterials
Finite element method
Área de concentração: Mecânica dos Sólidos e Projeto Mecânico
Titulação: Doutor em Engenharia Mecânica
Banca examinadora:
José Maria Campos dos Santos [Orientador]
José Roberto de França Arruda
Renato Pavanello
Domingos Alves Rade
Leopoldo Pisanelli Rodrigues de Oliveira
Data de defesa: 04-02-2020
Programa de Pós-Graduação: Engenharia Mecânica

Identificação e informações acadêmicas do(a) aluno(a)
- ORCID do autor: https://orcid.org/0000-0002-4388-311X
- Currículo Lattes do autor: http://lattes.cnpq.br/1599522390196102

UNIVERSIDADE ESTADUAL DE CAMPINAS

FACULDADE DE ENGENHARIA MECÂNICA

TESE DE DOUTORADO

Modeling elastic metamaterials and phononic crystals by wave finite element method

Modelagem de metamateriais elásticos e cristais fonônicos pelo método de propagação de ondas por elementos finitos

Autor: Edilson Dantas Nóbrega
Orientador: José Maria Campos dos Santos
A Banca Examinadora composta pelos membros abaixo aprovou esta Tese:

Prof. Dr. José Maria Campos dos Santos, Presidente
DMC - Faculdade de Engenharia Mecânica - UNICAMP

Prof. Dr. José Roberto de França Arruda
DMC - Faculdade de Engenharia Mecânica - UNICAMP

Prof. Dr. Renato Pavanello
DMC - Faculdade de Engenharia Mecânica - UNICAMP

Prof. Dr. Domingos Alves Rade
Instituto Tecnológico de Aeronáutica - ITA

Prof. Dr. Leopoldo Pisanelli Rodrigues de Oliveira
Escola de Engenharia de São Carlos - EESC/USP

A Ata da defesa com as respectivas assinaturas dos membros encontra-se no processo de vida acadêmica do aluno.

Campinas, 04 de Fevereiro de 2020.

Dedication

I dedicate this thesis to my dear parents and my wife.

Eu dedico esta tese aos meus queridos pais e a minha esposa.

Acknowledgments

Thank God for keeping me firm and focused on this project.

I would like to thank my wife and family for their patience, strength and support all these years.

Thanks also to my advisor Prof. Dr. Jose Maria Campos dos Santos for sharing his knowledge with me and for giving me the necessary support to complete this course.

I would like to thank the members of the newsstand for being willing to read this work and contributing to its completion. Thanks also to Prof. Dr. José Roberto de França Arruda and Prof. Dr. Renato Pavanello for the various suggestions offered during this research.

I am immensely grateful to UNICAMP's Faculty of Mechanical Engineering, which, together with the Department of Computational Mechanics, provided all the necessary infrastructure for the smooth running of this research. In particular, I thank the CPG-FEM team for all the professional support offered.

I would also like to thank my friends and lab colleagues, in particular Josh Labaki, Pricilla Brandao, Edson Jansen, Danilo Beli, Daniela Damasceno, Helio Vitor, Fernando Ortolano, Adriano Goto and Victor Gustavo. Together we shared many moments of lab research and fun outside.

I am grateful to FAPEMA, which through the universal processes 01415/17 and BD-08788/17 provided me with the necessary financial support for the development of this thesis.

I would also like to thank the Federal University of Maranhão, for providing financial support for the development of this thesis. I also take the opportunity to thank the group of researchers from the Mechanical Engineering course at UFMA, as their support was essential for the completion of this research.

Agradecimentos

Agradeço Deus por me manter firme e focado nesse projeto.

Eu gostaria de agradecer a minha esposa e a minha família pela paciência, força e apoio durante todos esses anos.

Agradeço também ao meu orientador Prof. Dr. José Maria Campos dos Santos por ter compartilhado comigo seus conhecimentos e por ter me dado o suporte necessário para a conclusão deste curso.

Eu gostaria de agradecer aos membros do banca por se disponibilizarem a ler este trabalho e contribuírem para a sua conclusão. Agradeço também ao Prof. Dr. José Roberto de França Arruda e ao Prof. Dr. Renato Pavanello pelas diversas sugestões oferecias durante essa pesquisa.

Sou imensamente grato à Faculdade de Engenharia Mecânica da UNICAMP que, juntamente com Departamento de Mecânica Computacional, ofereceram toda a infraestrutura necessária para bom andamento desta pesquisa. Em especial, agradeço à equipe da CPG-FEM por todo o suporte profissional oferecido.

Eu gostaria de agradecer também aos meus amigos e colegas de laboratório, em especial, Josh Labaki, Pricilla Brandão, Edson Jansen, Danilo Beli, Daniela Damasceno, Helio Vitor, Fernando Ortolano, Adriano Goto e Victor Gustavo. Juntos compartilhamos muitos momentos de pesquisa no laboratório e de diversão fora dele.

Agradeço FAPEMA, que através dos processos universal-01415/17 e BD-08788/17 me proporcionou o apoio financeiro necessário ao desenvolvimento desta tese.

Eu também gostaria de agradecer a Universidade Federal do Maranhão, por proporcionar um suporte financeiro para o desenvolvimento desta tese. Aproveito a oportunidade para agradecer também ao grupo de pesquisadores do curso de Engenharia Mecânica da UFMA, pois o apoio deles foi essencial para a conclusão desta pesquisa.

Good fortune is what happens when the opportunity meets with planning.

Thomas Alva Edison

Boa sorte é o que acontece quando a oportunidade encontra o planejamento.

Thomas Alva Edison

Resumo

Nesta tese, estruturas elásticas periódicas unidimensionais e bidimensionais são modeladas usando o método de elementos finitos das ondas (WFE), a fim de calcular bandas de frequências proibidas e respostas forçadas harmônicas para avaliar a atenuação de vibração estrutural. Bandas proibidas ou "band gaps", são faixas de frequência onde as ondas não podem se propagar. Band gaps ocorrem devido a estruturas que exibem alterações periódicas em sua geometria ou propriedade conhecidas como Cristais Fonônicos (PCs) ou a adição de ressonadores locais chamadas de Metamateriais Elásticos (EMs). Tais sistemas mecânicos foram estudados por vários pesquisadores nestas duas ultimas décadas e suas aplicações estruturais variam de barras a placas ou até estruturas tridimensionais. Uma contribuição deste trabalho consiste na modelagem de PCs e EMs para estruturas do tipo barra usando o WFE, bem como evidenciar a possibilidade da sua aplicação usando pacotes comerciais de elementos finitos. Nestes casos, os PCs são estruturas mecânicas periódicas cujo período é composto por elementos finitos de barra com propriedades do material ou geometrias contendo diferenças significativas. Os EMs são também estruturas periódicas onde o período é composto por elementos finitos de barra contendo um ou mais ressonadores locais mecânicos fixados periodicamente. Exemplos simulados por WFE são verificados com aqueles obtidos pelos métodos de elementos finitos (FE) convencional e do elemento espectral (SE), bem como são validados com os dados experimentais obtidos em uma barra de PC real. Outra contribuição é a modelagem por WFE de PCs usando estruturas do tipo pórtico e placa plana com período na forma triangular. Exemplos simulados de ambos modelos são verificados pelo método do FE. Também, EMs de estruturas tipo placa plana são modelados com ressonadores locais contínuos (CLR) usando o WFE. Um CLR é um modelo tridimensional de ressonador local. Resultados numéricos de um modelo de placa plana com CLRs periódicos sujeita à flexão são verificados pelo método do FE. Os dados experimentais obtidos em um ME de placa plana real, construído por manufatura aditiva, validam os resultados numéricos obtidos por WFE. A modelagem de PCs usando elementos finitos de barra de alta ordem formulados por WFE é apresentada. Resultados simulados por WFE com modelos de barra de alta ordem são verificados com os do SE e validados com os dados experimentais de uma barra de PC real.

Palavras-chave: guias de ondas, propagação de ondas, cristais fonônicos, metamateriais, método dos elementos finitos.

Abstract

In this thesis, one-dimensional and two-dimensional periodic elastic structures are modeled using the finite element wave method (WFE), in order to calculate prohibited frequency bands and forced harmonic responses to assess the attenuation of structural vibration. Prohibited bands or band gaps are frequency bands where the waves cannot propagate. Band gaps occur due to structures that exhibit periodic changes in their geometry or properties known as Phonic Crystals (PCs) or the addition of local resonators called Elastic Metamaterials (EMs). Such mechanical systems have been studied by several researchers in the past two decades and their structural applications vary from rods to plates or even three-dimensional structures. A contribution of this work consists of the modeling of PCs and EMs for rod-type structures using WFE, as well as highlighting the possibility of its application using commercial finite element packages. In these cases, the PCs are periodic mechanical structures whose period is composed of finite rod elements with material properties or geometries containing significant differences. EMs are also periodic structures where the period is composed of finite rod elements containing one or more local mechanical resonators fixed periodically. Examples simulated by WFE are verified with those obtained by the conventional finite element (FE) and spectral element (SE) methods, as well as being validated with the experimental data obtained in a real PC rod. Another contribution is the WFE modeling of PCs using frame and plain plate structures with a triangular shape. Simulated examples of both models are verified by FE method. In addition, EMs of flat plate structures are modeled with continuous local resonators (CLR) using WFE. A CLR is a three-dimensional model of a local resonator. Numerical results of a flat plate model with periodic CLRs subject to bending are verified by FE method. The experimental data obtained in a real flat plate EM, built by additive manufacturing, validate the numerical results obtained by WFE. It also presents the modeling of PCs using high-order finite rod elements formulated by WFE. Results simulated by WFE with high order rod models are verified with those of the SE and validated with the experimental data of a real PC rod.

Keywords: waveguide, wave propagations, phononic crystals, metamaterials, finite element method.

List of Illustrations

List of Tables

List of Abbreviations and Acronyms

Matrices and Vectors

$\mathbf{A}$ - matrix of WFE eigenvalue problem
$\mathbf{B}$ - matrix of WFE eigenvalue problem
$\mathbb{C}$ - Matrix of reflection/transmission in terms of the basis wave modes
$\mathbf{D}$ - Dynamic stiffness matrix
$\mathbf{F}$ - Force vector
$\mathbb{F}$ - Normalized force vector
$\mathbf{I}$ - Identity matrix
$\mathbf{J}$ - Unit symplectic matrix
$\mathbf{L}$ - Zhong matrix
$\mathbf{K}$ - Stiffness matrix
$\mathbf{k}$ - Wavenumber matrix
$\mathbf{k_{i,j}}$ - Stiffness matrix of resonators
$\mathbf{M}$ - Mass matrix
$\mathbf{m_{i,j}}$ - Mass matrix of resonators
$\mathbf{N}$ - Zhong matrix
$\mathbf{\Phi}$ - Wave modes matrix
$\boldsymbol{\mu}$ - Eigenvalues matrix j
$\mathbf{T}$ - Transfer matrix
$\mathbf{q}$ - State vector
$\mathbf{u}$ - Displacement vector
$\mathbf{w}$ - Displacement vector
$\mathbf{\Psi}$ - Coupling waveguide matrix
$\mathcal{Q}$ - Wave amplitude vector for coupling waveguide
$\mathcal{F}$ - Normalized force vector for coupling waveguide

Superscripts

* - related to left-going waves

H - vector conjugate transpose

T - vector/matrix transpose

^{N_p} - Number of periodic coupling waveguide

^{m} - Actual slice

Subscripts

l - relative to left degrees fo freedom

r - relative to right degrees fo freedom

i - relative to internal degrees fo freedom

i - index

$_0$ - relative to initial boundary conditions

$_{ex}$ - relative to external forces

$_q$ - Waveguide index

$_p$ - Waveguide index

Latin Letters

S - cross-section area

E - Young's modulus

f - frequency

f_i - natural frequency of the i resonator

i - imaginary unit $\sqrt{-1}$

L - Cell/slice length

N_c - Number of periodic slices

n - number of degrees of freedom which discretizes the left (or the right) cross-section of a substructure/slice

x,y,z - cartesian axes

y - direction of wave propagation in one-dimensional periodic systems

Greek Letters

$\boldsymbol{\alpha}$ - attenuation constant
ρ - mass density
μ - eigenvalue
ν - Poisson's ratio
η - structural damping
Δ - frequency step
ω - angular frequency
θ - angle between the strip and the horizontal direction

Acronyms

ACS - Attenuation Constant Surface
DOFs - Degrees of Freedom
EM - Wave Finite Element
FEM - Finite Element Method
FE - Finite Element
FRF - Frequency Response Function
LR - Local Resonance
MAC - Modal Assurance Criterion
PC - Phononic Crystal
PWE - Plane Wave Expansion
SEM - Spectral Element Method
WFE - Wave Finite Element
WFEM - Wave Finite Element Method
WSEM - Wave Spectral Element Method

Other Notations

$1D$	-	one-dimensional
$2D$	-	two-dimensional
$3D$	-	three-dimensional
$\Re()$	-	real part of a number
$\Im()$	-	imaginary part of a number
$\|\ \|$	-	absolute value of a number
$\{\}^T$	-	Transposto de um vetor
$\|\|\ \|\|$	-	Norm of a vector
normal font-weight	-	scalars
bold font-weight	-	vectors and matrices

Table of Contents

1 INTRODUCTION

1.1 Motivation

Vibrations in structures can be described in terms of wave propagation in engineering problems. Normally, this approach is used at mid and high frequencies, when the wavelength is small compared to the size of the structure. The following can be cited among its many applications: free and forced vibrations, non-destructive testing, vibration transmission through of the structures and acoustic problems. For simple cases the problem is easy to solve once the characteristics of wave propagation are known. With the objective of better utilization and the application of many techniques in science and industry, it is of great importance to understand the wave propagation theory. This study of rods, beams, frames, plates and shells allows non-destructive testing in many cases. Furthermore, acoustic problems, such as noise and resonance, can be detected and processed as a technique for monitoring structural integrity.

The propagation of waves in mechanical systems was initiated in the seventeenth century from Newton's work (Newton (1687) apud Brillouin (1946)), in which he assumed that the speed of sound in the air would be similar to the elastic waves in a lattice of point masses connected to springs (Fig. 1.1) for one-dimensional propagation. The reason to use this type of model was because at that time, continuous structures had been considered insoluble problems. From this point onwards, a series of researches started working with this theory. However, only with the contribution of Floquet (1883), which proposed analytical solutions to differential equations with periodic coefficients, the study around of one-dimensional periodic structures was extended to continuum models. In 1928, this study of wave propagation was extended to the 3D spatial periodicity case by Bloch (1928). Studies of the wave behavior in periodic structures were conducted by Brillouin (1946), in which the zone theory for 3D wavenumber presently known as Brillouin zones were proposed.

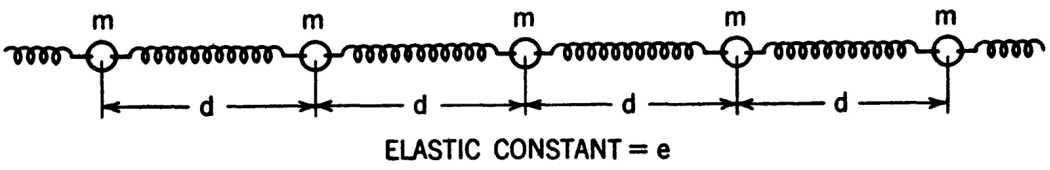

Figure. 1.1: Newton's one-dimensional lattice.
Source: Brillouin (1946)

The engineering studies of periodic structures using wave propagation began to spread in the mid-70s with Mead's works (Mead, 1970, 1973, 1974, 1975). The effect of wave propagations in engineering periodic structures known as "propagation constant" are currently studied by many researchers who use this concept together with the Bloch-Bloch's theorem. This increases the number of possibilities of finding new methods and types of structures. In recent decades, new methods have been developed that use the same basic concepts of periodicity together with approximated solution as a way of reducing computational cost and to solving complex engineering models that can neither be solved analytically nor numerically using traditional methods (Mace *et al.*, 2005; Mencik and Ichchou, 2005; Duhamel *et al.*, 2006; Mace and Maconi, 2008; Waki *et al.*, 2009a). One of them is the Wave Finite Element (WFE) method, which consists of modeling a small slice of elastic waveguide by the Finite Element (FE) Method, where applying the periodicity condition with Floquet-Bloch's theorem, it is possible to obtain the transfer matrix eigenproblem. The solution provides the attenuation constant and wave-modes, from which wavenumbers, wave motion amplitudes and Frequency Response Functions (FRFs) are obtained. The method has been applied in various types of finite element models, such as beams, thin plates, cylindrical shells, including wiht different material properties, couplings and mediums. Some of these periodic elastic structures are known as phononic materials like the Phononic Cristals (PCs) and Metamaterials.

In the last decade, applied research on PCs and metamaterials has been abundant. However, some fundamental assessments from the engineering point of view, such as model simulation (analytical, numerical and hybrid) and experimental approaches developed for conventional materials and structures, need to be employed to understand and explore metamaterial systems (HUSSEIN *et al.*, 2014). One of the most attractive characteristic of acoustic and elastic metamaterials is their wave filtering behavior. This provides some frequency ranges known as band gaps or forbidden bands where the waves cannot propagate. Band gaps are generated on spatial periodicity of the impedance mismatch domains which produce the Bragg scattering effect. Also, Locally Resonant (LR) mechanism (LIU *et al.*, 2000) provide band gaps at sub-wavelength, which are well below the Bragg scattering band gaps.

In this thesis, we are searching development and application of a numerical approach to the wave propagation in periodic structures. In particular, we are interested in elastic structures with changes in material and geometry or with attached resonators that occur periodically along their length and width, known as Phononic Crystals and Metamaterials.

1.2 Literature review

The study around periodic structures has increased over the last two decades, as shown by Silva (2015). This section presents some research of periodic structures and their applications to metamaterials and Phononic Crystals.

1.2.1 Periodic structure

Recently, some researchers have improved the study of one-dimensional wave propagation in structures. Mencik and Ichchou (2005) introduced the Finite Element (FE) method in the study of wave propagation in which a propagative approach was formulated based on a finite element model. This improved the wave property study, expanding to complex guided structures. However, this was possible only due to the work of Zhong and Williams (1995) which proposed a new formulation to solve the eigenvalue problem. It is an eigenproblem wherein the main parameters are the displacement instead of displacement/force and then, reduction of the problem of the inversion of ill-conditioned matrices. Duhamel *et al.* (2006) as one of the precursor to the Wave Finite Element (WFE) method demonstrated its efficacy from of forced response for a finite beam and plate-strip by using the Dynamic Stiffness Matrix (DSM) method with propagation matrices. The method has been applied in various types of finite element models. The solution provides the wavenumber and corresponding wave-modes of a structure slice, from which a dispersion diagram and frequency response functions (FRFs) of a whole structure are obtained. An issue of wave propagation in guided elastodynamic structures filled with acoustic fluid is proposed in which many simplified analytical models are incorporated (MENCIK AND ICHCHOU, 2006). This demonstrated that WFE is not low frequency limited (SILVA, 2015). The WFE was extended to wave propagation in two-dimensional structures by Mace and Maconi (2008), who analyzed numerical examples of thin isotropic and orthotropic plates.

In 2007, some applications of the WFE method to the free and forced vibrations of one-dimensional waveguides were studied in complicated structures (WAKI, 2007). These applications included free wave propagation in a plate strip with free edges, a ring and a cylindrical strip, where complicated phenomena such as curve veering, non-zero cut-on phenomena and bifurcations were observed as results of wave coupling in the wave domain. Complex structures of unknown wave characteristics were studied by WFE (ICHCHOU *et al.*, 2009). As a result, reflections and transmission waves inside of these structures could be investigated. But, the WFE method by DSM approach

has numerical difficulties, despite being easy to apply. If all the wave modes are included instead, the calculated result breaks down. This is because of the poor numerical conditioning associated with highest order wave modes, which are the very rapidly decaying waves. These complications were discussed by Waki *et al.* (2009b) and same methods to avoid or remove them were described.

Nascimento (2009) implemented a new formulation which used the DSM that combine the WFE method proposed by Mace *et al.* (2005) with the analytical natural forces obtain from movement equations (DOYLE, 1997), that were called the Wave Spectral Element Method (WSEM). These applications were made for Timoshenko and curved beams, Levy plates and high order rod models (Mindlin-Herrmann rod model) and were validated with the SEM and WFE methods. Later, other research was conducted that included the study of the high order rod model of Mindlin-McNiven (NOBREGA, 2015), which was validated using a new finite element for the high order rod model.

In 2010, the WFE method with DSM approach was used to obtain the response for the waveguide to a convected harmonic pressure (CHP) via inverse Fourier transform (RENNO AND MACE, 2010). On the other hand, the forced response of an elastic structure was computed by the WFE method using Neumann-to-Dirichlet problems involving single as well as coupled structures (MENCIK, 2010). This approach improved the convergence of the WFE method when multi-layered systems were specifically dealt with, creating a different form of the wave-based boundary conditions that is quite stable and easy to solve. Mencik (2011) introduced a study which included coupled elastic systems at junctions with uncertain eigenfrequencies in the WFE method by using model reduction. He improved the selection method of the wave modes of the junction. In this case, the mode selection can be performed in a single pre-processing step, in which it is not necessary to select the modes empirically. In this case, the wave propagation is still one-dimensional of each elastic system. Only in 2011, a response to a CHP for the two-dimensional (2D) waveguide was computed, where the forced response of an infinite 2D homogeneous medium was obtained (RENNO AND MACE, 2011).

Ichchou *et al.* (2011) introduced, for the first time, the stochastic finite element method (SFEM) to compute the wave propagation in random periodic media, in which he combines the uncertainty treatments with the WFE technique. This approach is called stochastic wave finite element (SWFE). Further research in structures with a random parameter was made after this, which included variability of coupling loss factors (BEN SOUF *et al.*, 2013b) and energy propagation in random viscoelastic media (BEN SOUF *et al.*, 2013a). Later, this method was computed for a second order perturbation (BOUCHOUCHA *et al.*, 2017) and extended to 1D and 2D forms (SINGH *et*

al., 2020).

A study of a hybrid finite element/wave method was made with the aim to compute the reflection and transmission coefficients of joins in the coupling of waveguides (Renno and Mace, 2013, 2014). Other research was performed in this same direction. In this case, a wave finite element-based formulation for flat shells was presented by Mencik (2013), wherein the coupling of these structures was computed using an assembly of the wave amplitudes. Besides, the forced response was computed from a model reduction strategy, in which a norm-wise error analysis was proposed for any waveguide to reduce the wave basis (MENCIK, 2012).

Lee (2009) proposed several of research that use the periodicity effect to obtain analytical solution of elastic standard structures (rod, beam, truss, etc.). This approach is known as the Spectral Element Method (SEM). This technique was combined with FEM, which resulted in a semi-analytical method called WSEM (NASCIMENTO, 2009). But this method was still restricted to simple structures, such that for modeling complex structures it required cumbersome analytical formulations. However, this problem was circumvented by Silva *et al.* (2013), who build spectral finite elements from a finite element model of a slice of a structural waveguide with an arbitrary cross section and, potentially, of arbitrary order. This approach was called the Wave Spectral Finite Element Method (WSFEM).

A new advanced technique to compute forced response using the WFE was created, which circumvented numerical issues like ill-conditioning and instability (MENCIK, 2014). However, although the WFE was computed for a finite element model to complex geometries, it was still restricted to symmetric models. This was broken down when a generalized eigenproblem based on the $S + S^{-1}$ transformation was proposed, in which periodic structures with arbitrary-shaped slices could be computed by WFE (MENCIK AND DUHAMEL, 2015).

Many applications of one-dimensional propagation with the WFE approach were studied in recent years. For instance, the following can be cited: acoustic radiation of axisymmetric fluid-filled pipes (BHUDDI *et al.*, 2015); a 2D frame structure under plane stresses and a 3D aircraft fuselage involving stiffened cylindrical shells, in which some another approaches were developed, ie. the Receptance Matrix (RM) (SILVA *et al.*, 2015); periodic structures with local perturbations (MENCIK AND DUHAMEL, 2016); a strategy to compute the dynamic flexibility modes of structures with cyclic symmetry (MENCIK, 2017); rotating periodic structures, which include asymmetric wave propagation due to the gyroscopic effect (BELI *et al.*, 2018).

But there are also advances in the research of models with two-dimensional periodicity, such as: the wave finite element application to prediction of noise transmission and radiation in infinite panels, where fluid-structure interaction was modeled in two-dimensional media (YANG *et al.*, 2017); and a hybrid FE/WFE approach to compute the wave transmission through two-dimensional structures, in which a coupling was made between two plates using a join modeled by WFE and FE methods, respectively (MITROU *et al.*, 2017).

1.2.2 Metamaterial

A theoretical and experimental study of longitudinal wave propagation in a rod structure including periodic local resonators was presented by Wang *et al.* (2006). They showed that both results produce an asymmetric band gap attenuation which is influenced by local resonator stiffness and mass ratios. Nevertheless, this work was centered on the band gaps conception and its property to attenuate vibration, without exploring the band gap formation mechanisms fully. Later, analytical models of resonant structures were provided to understand these band gap mechanisms formation (XIAO *et al.*, 2011), wherein the formulations were derived based on the transfer matrix method. It was demonstrated, for instance, that there are asymmetric/symmetric attenuation behaviors within a resonance gap.In addition, it has been proven that, with the inclusion of the resonator system, they cause not only the resonance gap, but also the Bragg effect.

More recently, a theoretical and numerical study of a locally resonant elastic metamaterial rod system with periodic multi-degree-of-freedom (M-DOF) resonators was presented by Xiao *et al.* (2012a). The band gap behavior and vibration attenuation performance was analyzed in a more systematic way. A new metamaterial rod model, based on a combination of the spectral element method and Floquet-Bloch's theorem was proposed, which will be called here the Wave Spectral Element Method (WSEM) (XIAO *et al.*, 2012a). They provided explicit expressions to predict band edge frequencies, demonstrated that both Bragg- and resonance-type band gaps co-exist in metamaterial rods and that multiple resonance band gaps can be achieved using M-DOF Local Resonators. These authors had also applied WSEM for band gap investigation in flexural metamaterial beams with local resonators (XIAO *et al.*, 2013). An analytical model of plate metamaterals was also presented that increased the sound absorption, in this case the study was about coupled vibroacoustic modeling of acoustic metamaterials (CHEN *et al.*, 2014). Still studying the mechanisms for the formation of the band gap, Colombi *et al.* (2014) showed that it is possible to concentrate energy on a specific point of the structure by creating a defect in the periodic distribution of the resonators system. Its was still concluded, that independent of a random or regular arrangement of the resonators,

the metamaterial shows large bandgaps.

Khajehtourian and Hussein (2014) presented a study of wave dispersion in a nonlinear elastic metamaterial rod system with periodically attached local resonators. The type of nonlinearity considered is large elastic deformation. The metamaterial rod model is based on a combination of the standard transfer matrix method and Floquet-Bloch's theorem. The results demonstrate that nonlinearities on metamaterial rods can affect band gap position, width, and its type (Bragg scattering or local resonance). They showed that large deformation alone may induce a pair of Bragg- and resonance-type band gaps to merge in to one hybrid and form a combined wide band gap. They also showed that as the wave amplitude increases, the effect of the nonlinearity on the metamaterial rod system is no longer negligible and the error incurred by assuming linear elastic wave propagation theory increases quickly.

Casadei and Bertoldi (2014) presented a study of a beam metamaterial wherein the resonators are represented by airfoil-shaped attached at a beam by means of a linear and torsional spring. An analytical and numerical study was conducted on the influence of fluid speed on the band gaps. Dispersion characteristics of the fluid-coupled waveguide were computed by the transfer matrix method where the aerodynamic coupling in system was considered.

Another kind of metamaterial, called metaconcrete was proposed by Mitchell *et al.* (2014), in which sand and gravel aggregates of standard concrete would be replaced with spherical inclusions consisting of a heavy metal core coated with a soft outer layer. These type of structures are able to scatter the energy from localized oscillatory motions, which causes a reduction of the stress in the mortar phase, enhancing its ability to sustain the applied dynamic actions without damage. Research that was also based in inclusions to generate band gaps due to local resonance was introduced by Torrent *et al.* (2014). In this case, the resonance was caused by arrangements of scatterers attached to a thin elastic plate. This metamaterial was modeled based on the multiple scattering theory.

In 2015, an elastic metamaterial plate was composed in which the resonators were represented bu two-degree of freedom mass-string systems modeled as Multi-stopband with the aim to represent vibration absorbers (PENG *et al.*, 2015). Besides the study of resonance with M-DOFs, the effect that the resonators geometric form implies in the band gab behavior and how this influences its tuning characteristics was investigated (WANG *et al.*, 2015). The acoustic behaviors of these models was studied by considering defect inclusions.

An acoustic duct metamaterial was developed analytically and validated with the finite element method (FAROOQUI *et al.*, 2016b). The sound attenuation was produced by use of locally resonant periodic aluminum patches. In this case the aluminum patches represented the Helmholtz resonator that create frequency stop bands at the low frequency zone. An experimental validating was made from the transmission spectra of resonant aluminum patches flush-mounted to acoustic duct walls (FAROOQUI *et al.*, 2016a).

There is research that developed elastic metamaterial plates with the aim to create the cloak effect (LEE AND KIM, 2016). Metamaterial cloaking has the capability to control incident waves that are guided around them without being affected by the object itself, which torn this structure invisible or insensible. An other interesting application for metamaterials was made by (QI *et al.*, 2016), by creating a planar acoustic metamaterial with the objective of studying the acoustic energy harvesting. This was made by introduction of a piezoelectric material in a structure position where the acoustic energy is concentrated, for instance, in a metamaterial defect position.

The WFE method was used to compute wave propagation in elastic metamaterials for the first time by Silva *et al.* (2016). The aim of this study was to use the WFE for passive vibration control. Two numerical examples were presented: an one-dimensional structure with resonators spaced periodically along its length; and a 3D fuselage-like structure with an array of local resonators attached periodically. After, other research was presented using the same approach for a different application (NÓBREGA AND DOS SANTOS, 2019). In this case the resonator was modeled using many DOFs, which was called Continuous Local Resonator (CLR). A 3D wave propagation modeled by WFE using the metamaterial concept was developed by Poggetto *et al.* (2019).The local resonance effect was explored in several applications in plate during this period (Wang *et al.*, 2016a; Titovich *et al.*, 2016; Wang *et al.*, 2016b; Liu *et al.*, 2018; Miranda *et al.*, 2019), which include analytical, numerical and experimental analyses.

The uncertain material construction it has also been used to compute wave propagation in elastic metamaterial structure. Duranteau *et al.* (2016) used a subwavelength dipolar resonance to obtain random acoustic waves. After, a beam was computed by wave finite element method to obtain uncertain behavior from random parameter (MACHADO *et al.*, 2016). Beli *et al.* (2019) analyzed the variability in 3D printed metamaterial beams, ie., he evaluated the variation in attenuation in metamaterial beams due to 3D printing, which was motivated by the differences between numerical and experimental measurements.

1.2.3 Phononic cristals

Recently, some researchers studied the effect in structures when periodic inclusions are added (XIAO *et al.*, 2012b), these is a change in geometry (NOBREGA *et al.*, 2016) or material (XIANG AND SHI, 2009), or even by material inclusions (SUN AND WU, 2007). Also known as Phononic Crystals or metamaterials, this kind of structure has a "wave filtering" property, thus waves cannot propagate freely through the periodic structures within some frequency ranges, which are also called band gaps (XIAO *et al.*, 2012a). In (SILVA *et al.*, 2011a), an analytical spectral element for periodic rods was modeled with the aim to see this band gap effect on the audio frequency range. The existence of the band gaps in the dynamic responses were demonstrated with experimental and numerical tests. This trait of Phononic Crystals is sometimes created by inclusions or material characteristics that have a smaller wavelength when compared to its base material or geometry. Xiang *et al.* (2012) demonstrated that it is possible to apply the Phononic Crystal characteristics to create a vibration isolator using periodic foundations. By using a one-dimensional periodic material, a foundation composed of rubber and reinforced concrete was capable of creating band gaps in the same critical band frequencies of the civil structure. In the work of Zhang *et al.* (2013) the Transfer Matrix (TM) method and Bloch theorem are used to investigate PC Euler beams on a two-parameter foundation. They show that a PC Euler beam on this kind of foundation has better vibration isolation characteristics, when compared with the homogeneous Euler beam.

The band gap phenomenon was shown in many models of structures, like rods, beams, plates, etc., ie., a study of a silicon PC plate, where the inclusion was composed of air (MOHAMMADI *et al.*, 2008). PCs are structures that can be modeled by using alternated material or transversal sections along its length (MIRANDA *et al.*, 2019). Hussein *et al.* (2014) presented a historical approach to the evolution of research on these new types of materials. This review showed elastic configurations ranging from trusses and ribbed shells to phononic crystals and metamaterials. PC rods and Beams are also modeled to control wave propagation in elastic structures piezoelectric material (Ponge *et al.*, 2016; Croënne *et al.*, 2016). The advance in use of these electric devices is because the material itself can be changed depending on necessity without any structural adjustment. Taking into account these characteristics, a structural system can be easily adjusted to filter critical frequencies band.

The local resonance is also used to enlarge the band frequency affected by the band gap of a PC plate as observed in Assouar and Oudich (2012). In this case, the inclusions are composed of two different material. PC structures can be constructed for material inclusions, but they can be

made also, from material extraction (LUCKLUM *et al.*, 2012), where the scatter is represented by geometric variation. The scattering effect can be also represented by a junction of some of these structural characteristics, for instance, Assouar *et al.* (2014) made a hybrid elastic PC plate that has both inclusions and holes arranged along its length. He built a plate with pillars and holes with scattering function to create stop bands with a significant widening and lowering of the acoustic band gap.

A lot of other researches was made over these years, which include from everything simple design with analytical (HVATOV AND SOROKIN, 2015) and numerical applications (SHU *et al.*, 2016), to complex projects such as topological guiding analysis of wave propagations (GUO *et al.*, 2017). A review of Phononic Crystals and Metamaterials was made which include a historical evolution of the behavior presented of this kind of structures up until the present day (WANG *et al.*, 2020). A prospection of future promising study from of this emerging field was presented.

1.3 Objectives

The main objective of this thesis is to explore new formulations to model structural phononic crystal and elastic metamaterials based on the Wave Finite Element method. The specific objectives of this thesis are listed as follows:

- To numerically and experimentally evaluate the elementary rod model of conventional finite element to modeling PCs and MEs using WFE;
- To demonstrate the applicability of commercial FE software to calculate structural PCs and EMs using WFE;
- To investigate the bandgap in couping flat PC plates with a triangular shape in order to evaluate two levels of Bragg scattering band gaps;
- To compute the WFE method using continuous local resonators (CLRs) designed as a mass-spring system in elastic structures;
- To analyze flexural band gaps in EM plates with CLR in comparison with experimental tests;
- To analyze the effect of band gaps on PC rods with higher order models.

1.4 Outline of the thesis

In Chapter 2, the wave finite element (WFE) is presented for 1D, 2D and 3D structures with wave propagation in one direction. The eigenproblem is provided for symmetric and asymmetric structures. The formulation of waveguides coupling to two consecutive plates is extended to several consecutively coupled plates by using the scattering matrix. Finally, a new formulation is obtained for the case that we have periodic couplings, which may make it possible to reduce the computational cost and to obtain the dispersion diagram.

In this thesis, both Bragg and local resonance band gaps to achieve multiband and broadband vibration in rods are explored. Parametric influence on the bandgap behavior, as well as the bandgap formation mechanisms, are examined. Two examples illustrating its efficiency and accuracy to model an elastic metamaterial rod unit-cell using a 1D simple rod and a 3D solid finite element are demonstrated and the results present good approximation to the experimental data (Nobrega *et al.*, 2016; Nobrega and Dos Santos, 2015). These research are addressed in Chapters 3 and 4.

A investigate of wave propagation along periodic structures made of several PC beams arranged in a triangular shaped pattern. Each of these beams was itself made of a periodic distribution of different material strips. This creates two levels of periodic variations. Two-scale band gaps are created, one due to the variation of the angle and the other due to the material change. This research is addressed in Chapter 5, where the same study is made with flat plates. Results observed in the FRFs show that band gap occur due to change of material, but the biggest effect appears with the change of direction of the waveguide that is made by rotating the wave modes (NOBREGA *et al.*, 2018).

Is still shown, an elastic metamaterial reinforced-plate modeling by WFE and conventional FE methods. Continuous local resonators (CLR) are designed as a mass-spring system constructed using a solid cubical block (mass) connected by four very small beams (springs) to the plate stiffener-beams. In order to attenuate the plate excitation responses, the CLRs are designed to be tuned at the second plate natural frequency. Then, the CLR's first natural frequency is tuned approximately equal to that. The reinforced-plate metamaterial behavior is analyzed using the dispersion diagram and forced responses (FRFs). The forced response calculated by WFE is verified using the conventional FE method. Results show that band gaps occur in more than one mode and the corresponding responses at these modes are attenuated (NOBREGA AND DOS SANTOS, 2019).

This research is addressed in Chapter 6.

Another example plate with CLR was printed on 3D printer with UV curing technology. Numerical results are obtained by a model of the FE methods and PWE method of this plate. The results are validated with the experimental data (MIRANDA *et al.*, 2019). After this, an analysis of FRF and dispersion diagram is computed by the WFE method and results are discussed and compared with the FE method and experimental data, Chapter 7.

In Chapter 8, a study of a higher order rod is made, where the dispersion diagram and FRFs are computed by WFE method and the results are compared with the STM method. Analysis of three high order mode is made: Love's rod, with only one mode; Mindlin-Herrmann's rod, with two modes; and Mindlin-McNiven's rod, with three modes.

In Chapter 9, general conclusions regarding this thesis are drawn. Then, original contributions of this study are highlighted in a list of the publications that resulted during progress of the thesis.

2 WAVE FINITE ELEMENT METHOD

The method is presented here for the analysis of wave propagation in elastic structures. In this method the mass and stiffness matrices of a small slice of the structure modeled by the conventional finite element method is used for the application of periodicity conditions in the propagation of a harmonic perturbation across the structure. The periodicity conditions result in an eigenvalue / vector problem whose formulation produces the equations of force-displacement relations of the structure. The method has been used for free and forced vibration analysis (DUHAMEL *et al.*, 2006) with applications to uni and bidimensional models (Mace and Maconi, 2008; Mencik, 2008).

2.1 Finite element and transfer matrix

The WFE method consists to model a slice (Fig. 2.1(b)) of the periodic structure (Fig. 2.1(a)) by FE method and find the dynamic stiffness matrix, using the equilibrium equation given as,

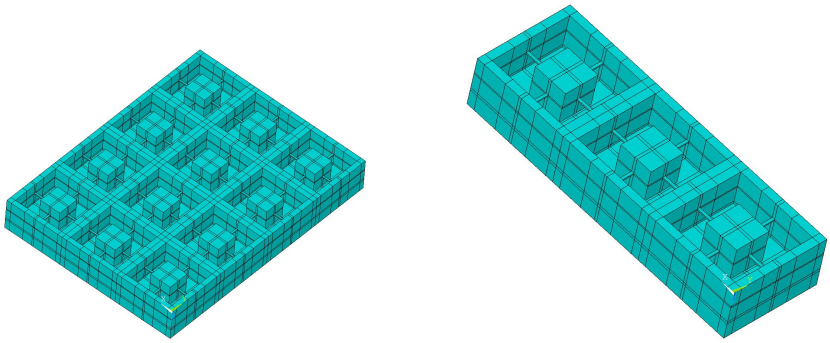

Figure. 2.1: Model of a periodic structure: (a) plate; (b) slice

$$(\mathbf{K} - \omega^2 \mathbf{M})\mathbf{u} = \mathbf{F} \quad \text{or} \quad \mathbf{D}\mathbf{u} = \mathbf{F}, \tag{2.1}$$

where, $\mathbf{K}$ and $\mathbf{M}$ are the stiffness and mass matrix, $\mathbf{u}$ is the displacement vector, $\mathbf{F}$ is the external force vector, and ω is the circular frequency. The dynamic stiffness matrix ($\mathbf{D}$) can be partitioned as:

$$\begin{bmatrix} \mathbf{D}_{ii} & \mathbf{D}_{il} & \mathbf{D}_{ir} \\ \mathbf{D}_{li} & \mathbf{D}_{ll} & \mathbf{D}_{lr} \\ \mathbf{D}_{ri} & \mathbf{D}_{rl} & \mathbf{D}_{rr} \end{bmatrix} \begin{Bmatrix} \mathbf{u}_i \\ \mathbf{u}_l \\ \mathbf{u}_r \end{Bmatrix} = \begin{Bmatrix} \mathbf{F}_i \\ \mathbf{F}_l \\ \mathbf{F}_r \end{Bmatrix}, \tag{2.2}$$

where l, i and r represents the left, internal and right degrees-of-freedom (DOF), respectively. To computing the WFE method is necessary to obtain a relationship between the left and right sides of the slice. This relation is performed by the transfer matrix. Because of this, it is necessary to condense the internal DOFs of the dynamic stiffness matrix. Considering $\mathbf{F}_i = 0$ in the Eq.(2.2), the internal displacement can be obtained by:

$$\mathbf{u}_i = \mathbf{D}_{ii}^{-1}(\mathbf{D}_{il}\mathbf{u}_l + \mathbf{D}_{ir}\mathbf{u}_r). \tag{2.3}$$

Substituting Eq. (2.3) into Eq. (2.2) the condensed dynamic stiffness matrix is obtained as,

$$\begin{bmatrix} \mathbf{D}_{ll} & \mathbf{D}_{lr} \\ \mathbf{D}_{rl} & \mathbf{D}_{rr} \end{bmatrix} \begin{Bmatrix} \mathbf{u}_l \\ \mathbf{u}_r \end{Bmatrix} = \begin{Bmatrix} \mathbf{F}_l \\ \mathbf{F}_r \end{Bmatrix}, \tag{2.4}$$

where, $\mathbf{D}_{ll} = \mathbf{D}_{ll} - \mathbf{D}_{li}\mathbf{D}_{ii}^{-1}\mathbf{D}_{il}$, $\mathbf{D}_{rl} = \mathbf{D}_{rl} - \mathbf{D}_{ri}\mathbf{D}_{ii}^{-1}\mathbf{D}_{il}$, $\mathbf{D}_{lr} = \mathbf{D}_{lr} - \mathbf{D}_{li}\mathbf{D}_{ii}^{-1}\mathbf{D}_{ir}$, $\mathbf{D}_{rr} = \mathbf{D}_{rr} - \mathbf{D}_{ri}\mathbf{D}_{ii}^{-1}\mathbf{D}_{ir}$.

Equation (2.4) can be transformed in a transfer matrix formulation by creating a state vector $\mathbf{q} = \{\mathbf{u} \quad \mathbf{F}\}^T$, and applying this in the Eq. (2.4) to obtain,

$$\underbrace{\begin{Bmatrix} \mathbf{u}_r \\ -\mathbf{F}_r \end{Bmatrix}}_{\mathbf{q}_r} = \underbrace{\begin{bmatrix} -\mathbf{D}_{lr}^{-1}\mathbf{D}_{ll} & -\mathbf{D}_{lr}^{-1} \\ \mathbf{D}_{rl} - \mathbf{D}_{rr}\mathbf{D}_{lr}^{-1}\mathbf{D}_{ll} & -\mathbf{D}_{rr}\mathbf{D}_{lr}^{-1} \end{bmatrix}}_{\mathbf{T}} \underbrace{\begin{Bmatrix} \mathbf{u}_l \\ \mathbf{F}_l \end{Bmatrix}}_{\mathbf{q}_l}. \tag{2.5}$$

2.2 Floquet-Bloch's theorem and eigenvalue problem

Applying the Floquet-Bloch's theorem for a m slice and considering consecutive slices, displacement continuity condition, and the force balance (Mead, 1973):

$$\begin{Bmatrix} \mathbf{u}_r^{(m)} \\ -\mathbf{F}_r^{(m)} \end{Bmatrix} = \begin{bmatrix} \boldsymbol{\mu}_q & \mathbf{0} \\ \mathbf{0} & \boldsymbol{\mu}_F \end{bmatrix} \begin{Bmatrix} \mathbf{u}_l^{(m)} \\ \mathbf{F}_l^{(m)} \end{Bmatrix} \quad \text{or} \quad \mathbf{q}_r = \boldsymbol{\mu}\mathbf{q}_l, \tag{2.6}$$

the Eq. (2.5) becomes an eigenproblem given by,

$$\mathbf{T} \begin{Bmatrix} \mathbf{u}_l^{(m)} \\ \mathbf{F}_l^{(m)} \end{Bmatrix} = \boldsymbol{\mu} \begin{Bmatrix} \mathbf{u}_l^{(m)} \\ \mathbf{F}_l^{(m)} \end{Bmatrix} \quad \text{or} \quad \mathbf{T}\mathbf{q}_l = \boldsymbol{\mu}\mathbf{q}_l, \tag{2.7}$$

where $\boldsymbol{\mu} = e^{-i\mathbf{k}L}$ are the eigenvalues, $\boldsymbol{\alpha} = -i\mathbf{k}L$ is the attenuation constant given as function of the wavenumber $\mathbf{k}$, L the slice length and i the imaginary unit. To avoid ill-conditioning likely to occur in matrix $\mathbf{D}_{lr}^{-1}$ for symmetric structures, the Eq. (2.7) can be rewritten in a representation by displacement vector alone (ZHONG AND WILLIAMS, 1995), where $\mathbf{F}_l = \{-\mathbf{D}_{ll}\mathbf{u}_l - \mathbf{D}_{lr}\mathbf{u}_r\}$ and $\mathbf{F}_r = \{-\mathbf{D}_{rl}\mathbf{u}_l - \mathbf{D}_{rr}\mathbf{u}_r\}$, then the Eq. (2.6) be came:

$$\mu \underbrace{\begin{bmatrix} \mathbf{I}_n & \mathbf{0} \\ -\mathbf{D}_{ll} & -\mathbf{D}_{lr} \end{bmatrix}}_{\mathbf{L}} \underbrace{\begin{Bmatrix} \mathbf{u}_l \\ \mathbf{u}_r \end{Bmatrix}}_{\mathbf{w}} = \underbrace{\begin{bmatrix} \mathbf{0} & \mathbf{I}_n \\ \mathbf{D}_{rl} & \mathbf{D}_{rr} \end{bmatrix}}_{\mathbf{N}} \underbrace{\begin{Bmatrix} \mathbf{u}_l \\ \mathbf{u}_r \end{Bmatrix}}_{\mathbf{w}} \tag{2.8}$$

where $\mathbf{I}_n$ is the identity matrix of rank n and $\mathbf{w}$ is the displacement vector associated to the slice. It can also be shown that μ and $\mathbf{Lw} = \Phi$ are eigenvalues and eigenvectors of Eq. (2.7), respectively. The wave that traveling to the right and left directions are represented by $|\mu_j| \leq 1$ and $|\mu_j| \geq 1$ eigenvalues respectively with the corespondent Φ_j, where $j = 1,2,\ldots,n$. In matrix form, the wave shapes are:

$$\boldsymbol{\Phi} = \begin{bmatrix} \boldsymbol{\Phi}_u & \boldsymbol{\Phi}_u^\star \\ \boldsymbol{\Phi}_F & \boldsymbol{\Phi}_F^\star \end{bmatrix}, \quad \mu = \begin{bmatrix} \mu & \mathbf{0} \\ \mathbf{0} & \mu^\star \end{bmatrix} \tag{2.9}$$

where $\boldsymbol{\Phi}_u$ and $\boldsymbol{\Phi}_F$ are related to the displacement/rotation and force components respectively with n order. And the symbol * represent the wave modes that traveling in the left direction related to modes.

If the structure is not symmetric, then it may be used the so-called $\mathbf{S} + \mathbf{S}^{-1}$ transformation (MENCIK AND DUHAMEL, 2016), (PATEL, 1993), which keep the symplectic structure of the problem by a generalized eigenproblem where the wave that out going from right to left are $\mu_j^\star$. This new problem is given by:

$$\left((\mathbf{N}'\mathbf{J}\mathbf{L}'^T + \mathbf{L}'\mathbf{J}\mathbf{N}'^T) - \lambda_j \mathbf{L}'\mathbf{J}\mathbf{L}'^T\right)\mathbf{z_j} = 0 \tag{2.10}$$

where

$$\mathbf{L}' = \begin{bmatrix} \mathbf{0} & \mathbf{I}_n \\ -\mathbf{D}_{lr} & \mathbf{0} \end{bmatrix}, \quad \mathbf{N}' = \begin{bmatrix} \mathbf{D_{rl}} & \mathbf{0} \\ -(\mathbf{D}_{ll} + \mathbf{D}_{rr}) & -\mathbf{I}_n \end{bmatrix}$$

,

$$(\mathbf{N}'\mathbf{J}\mathbf{L}'^T + \mathbf{L}'\mathbf{J}\mathbf{N}'^T) = \begin{bmatrix} \mathbf{D}_{rl} - \mathbf{D}_{lr} & \mathbf{D}_{ll} + \mathbf{D}_{rr} \\ -(\mathbf{D}_{ll} + \mathbf{D}_{rr}) & \mathbf{D}_{rl} - \mathbf{D}_{lr} \end{bmatrix}$$

and

$$\mathbf{L'JL'}^T = \mathbf{N'JN'}^T = \begin{bmatrix} \mathbf{0} & -\mathbf{D}_{rl} \\ \mathbf{D}_{lr} & \mathbf{0} \end{bmatrix} \quad \text{with} \quad \mathbf{J} = \begin{bmatrix} \mathbf{0} & \mathbf{I}_n \\ -\mathbf{I}_n & \mathbf{0} \end{bmatrix}$$

Knowing that $\lambda_j = \mu_j + 1/\mu_j$ is possible find the wave parameters μ_j and $1/\mu_j$ by solving the quadratic equation $x^2 - \lambda_j x + 1$. Its respective wave shapes can be found from the eigenvalue $\mathbf{z}_j$ of the Eq. 2.10 as follows:

$$\mathbf{\Phi}_j = \begin{bmatrix} \mathbf{I}_n & \mathbf{0} \\ \mathbf{D}_{rr} & \mathbf{I}_n \end{bmatrix} \mathbf{w'}_j \quad \text{with} \quad \mathbf{w'}_j = \mathbf{J}(\mathbf{L'}^T - \mu_j^\star \mathbf{N'}^T)\mathbf{z}_j$$

and

$$\mathbf{\Phi}_j^\star = \begin{bmatrix} \mathbf{I}_n & \mathbf{0} \\ \mathbf{D}_{rr} & \mathbf{I}_n \end{bmatrix} \mathbf{w'}^\star_j \quad \text{with} \quad \mathbf{w'}^\star_j = \mathbf{J}(\mathbf{L'}^T - \mu_j \mathbf{N'}^T)\mathbf{z}_j$$

The wave mode are computed for a great number of frequencies ω_m. The problem is to identify between all the defined modes in a frequency ω_{m+1} which correspond the mode i defined in the previous frequency ω_m (Fig. 2.2(a)). Then, sufficiently small $\Delta\omega$ wave mode j defined at angular frequency $\omega + \Delta\omega$ is such that:

$$\left| \frac{\Phi_i(\omega)^H \Phi_i(\omega + \Delta\omega)}{\|\Phi_i(\omega)\| \|\Phi_i(\omega + \Delta\omega)\|} \right| = max \left\{ \left| \frac{\Phi_i(\omega)^H \Phi_j(\omega + \Delta\omega)}{\|\Phi_i(\omega)\| \|\Phi_j(\omega + \Delta\omega)\|} \right| \right\}. \tag{2.11}$$

This is the Modal Assurance Criterion - MAC (ALLEMANG, 2003). It is used to estimate a correlation between the wave shapes, where j is the mode of frequency $\omega + \Delta\omega$ with higher correlation with the mode i of the frequency ω. In the figure 2.2 is shown the dispersion curves organized (Fig.2.2(b)) and unorganized (Fig. 2.2(a)) modes of a slice with ten Kirchhoff-Love plate element according to the figure 2.3.

2.3 Wave expansion

The state vectors $\mathbf{q}^{(m)}$ for a finite structure can be expressed as (SILVA *et al.*, 2014):

$$\mathbf{q}^{(m)} = \sum_{j=1}^{n} (\Phi_j Q_j^{(m+1)} + \Phi_j^\star Q_j^{\star(m+1)}) = \sum_{j}^{n} (\Phi_j \mu_j Q_j^m + \Phi_j^\star \mu_j^\star Q_j^{\star m}), \tag{2.12}$$

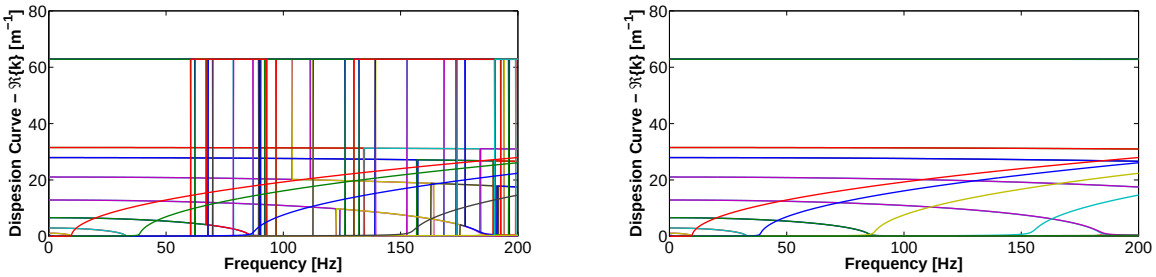

(a) Unorganized mode (b) Organized mode

Figure. 2.2: Dispersion curve of a slice with 10 Kirchhoff-Love plate element.

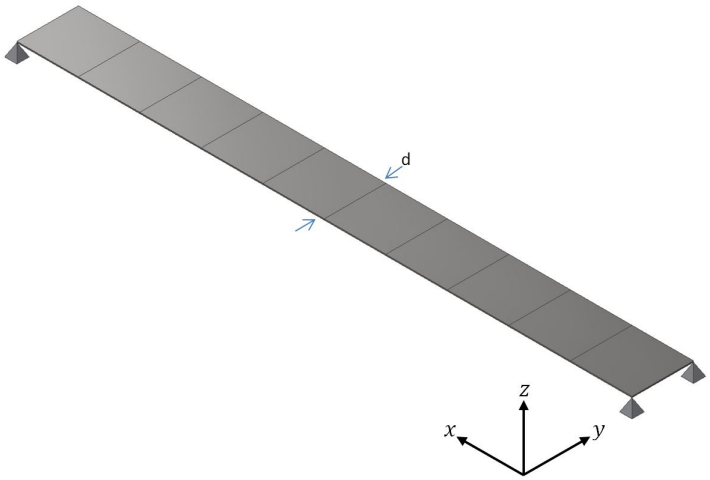

Figure. 2.3: Slice with 10 Kirchhoff-Love plate element.

with $m = 1,2,3,...,N,N+1$, where N is the slice number, k_j is the wavenumber. $\mathbf{Q}_j^{(m+1)}$ and $\mathbf{Q}_j^{(m)}$ are the wave vector amplitudes at the interface $m+1$ and m, respectively (Fig. 2.4). Defining the amplitude vectors $\mathbf{Q} = \mathbf{Q}^{(1)}$ and $\mathbf{Q}^{\star} = \mathbf{Q}^{\star\,(N+1)}$ at the extremities of a structure, as illustrated in Figure 2.5, the Eq. (2.12) may be rewritten as follows:

$$\mathbf{q}_l^{(m)} = \mathbf{\Phi}\,\boldsymbol{\mu}^{m-1}\,\mathbf{Q} + \mathbf{\Phi}^{\star}\,\boldsymbol{\mu}^{N+1-m}\,\mathbf{Q}^{\star}, \quad m = 1\ldots N+1. \tag{2.13}$$

One way to solve the Eq. (2.13) is by finding the wave amplitudes $(\mathbf{Q}, \mathbf{Q}^{\star})$ in the boundary through the Neumann and Dirichlet conditions at the left and right side of the structure. Consider that have a force on the left $(\mathbf{F}_0)$ and a displacement/rotation $(\mathbf{u}_0)$ on the right sides of the structure, the Eq.

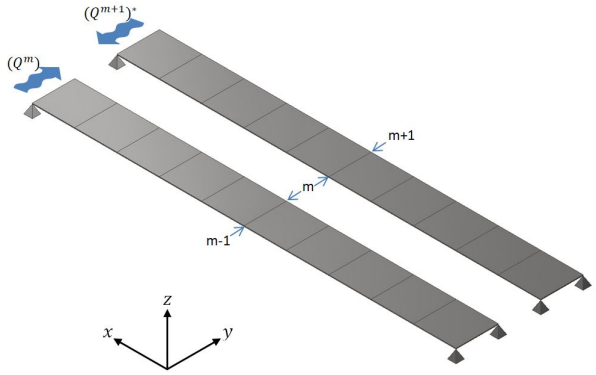

Figure. 2.4: Example of a two consecutive slices.

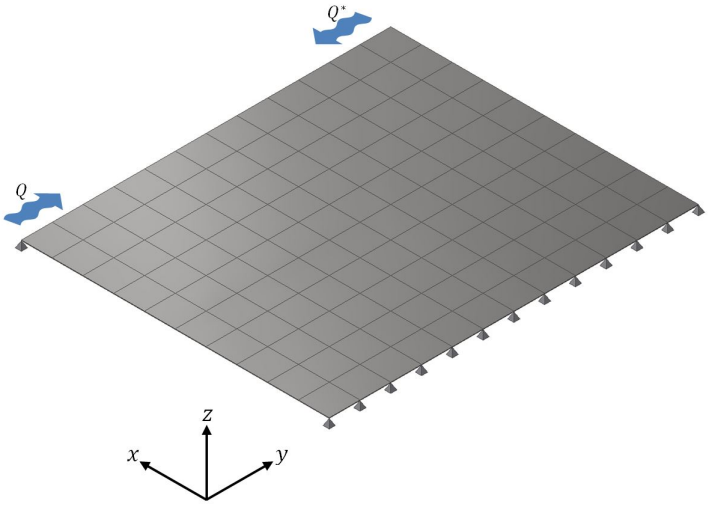

Figure. 2.5: Example of a plate containing 12 slices where $\mathbf{Q} = \mathbf{Q}^{(1)}$ and $\mathbf{Q}^\star = \mathbf{Q}^{\star\,(N+1)}$.

(2.13) be comes:

$$\boldsymbol{\Phi}_{\mathrm{F}}\,\mathbf{Q} + \boldsymbol{\Phi}_{\mathrm{F}}^{\star}\,\boldsymbol{\mu}^{N}\,\mathbf{Q}^{\star} = -\mathbf{F}_{0}, \tag{2.14}$$

$$\boldsymbol{\Phi}_{\mathrm{q}}\,\boldsymbol{\mu}^{N}\,\mathbf{Q} + \boldsymbol{\Phi}_{\mathrm{q}}^{\star}\,\mathbf{Q}^{\star} = \mathbf{u}_{0}. \tag{2.15}$$

The computation of $\mathbf{Q}$ and $\mathbf{Q}^{\star}$ follows from the inversion of the resulting matrix system

$$\begin{bmatrix} \boldsymbol{\Phi}_{\mathrm{F}} & \boldsymbol{\Phi}_{\mathrm{F}}^{\star}\boldsymbol{\mu}^{N} \\ \boldsymbol{\Phi}_{\mathrm{u}}\,\boldsymbol{\mu}^{N} & \boldsymbol{\Phi}_{\mathrm{u}}^{\star} \end{bmatrix} \begin{bmatrix} \mathbf{Q} \\ \mathbf{Q}^{\star} \end{bmatrix} = \begin{bmatrix} -\mathbf{F}_{0} \\ \mathbf{u}_{0} \end{bmatrix}, \tag{2.16}$$

However, the inversion of the matrix in the Eq. (2.16) may suffer with singularity problem. This can be observed both in the ratios between the diagonal components $\boldsymbol{\mu}^{N}$ and in the divisions between the components of modes $\boldsymbol{\Phi}_{\mathrm{u}}$ and $\boldsymbol{\Phi}_{\mathrm{F}}$, that can have value extremely big. This problem is solved by rewriting the Eq. (2.16) as follows:

$$\begin{bmatrix} \mathbf{I}_{n} & \boldsymbol{\Phi}_{\mathrm{F}}^{-1}\,\boldsymbol{\Phi}_{\mathrm{F}}^{\star}\boldsymbol{\mu}^{N} \\ \boldsymbol{\Phi}_{\mathrm{u}}^{\star\,-1}\,\boldsymbol{\Phi}_{\mathrm{u}}\,\boldsymbol{\mu}^{N} & \mathbf{I}_{n} \end{bmatrix} \begin{bmatrix} \mathbf{Q} \\ \mathbf{Q}^{\star} \end{bmatrix} = \begin{bmatrix} -\boldsymbol{\Phi}_{\mathrm{F}}^{-1}\,\mathbf{F}_{0} \\ \boldsymbol{\Phi}_{\mathrm{u}}^{\star\,-1}\,\mathbf{u}_{0} \end{bmatrix}, \tag{2.17}$$

Then, by the solution of Eq. 2.17, the amplitude ratios of the waves are obtained which can be replaced in Eq. 2.13 to find the displacement and forces.

3 METAMATERIAL ROD WITH ATTACHED RESONATORS USING MULTI-DEGREES-OF-FREEDOM

This Chapter is based in the reference Nobrega *et al.* (2016) and Nobrega and Dos Santos (2015). The bandgap determination of periodic system is formulated using analytical (Wave Spectral Element - WSE) and numerical (Wave Finite Element - WFE) methods. They are computationally implemented, evaluated and compared with results from the literature and between methods. It is also explored both Bragg and local resonance band gaps to achieve multiband and broadband vibration in rods. Parametric influence on the bandgap behavior, as well as the bandgap formation mechanisms are examined. In addition, a bandgap sensitivity analysis is computed.

3.1 Metamaterial cell model

Find the dynamic stiffness matrix (DSM) of a EM rod is an intrinsic condition for WFE method (Cap. 2). It is possible by considering a locally resonant elastic metamaterial rod system with infinite cells with periodic externally attached identical M-DOFs resonators (Fig. 3.1) with L length. Where a mass-spring system in series represent the M-DOFs resonators with N degrees-freedom. This can be represented by the equilibrium equation of the resonator given by :

$$\left(\underbrace{\begin{bmatrix} k_1 & \mathbf{k}_{lr} \\ \mathbf{k}_{rl} & \mathbf{k}_{rr} \end{bmatrix}}_{\mathbf{K}} - \omega^2 \underbrace{\begin{bmatrix} m_0 & \mathbf{0} \\ \mathbf{0} & \mathbf{m}_{rr} \end{bmatrix}}_{\mathbf{M}} \right) \underbrace{\begin{Bmatrix} u_0 \\ \mathbf{u}_r \end{Bmatrix}}_{\mathbf{u}} = \underbrace{\begin{Bmatrix} F_0 \\ \mathbf{F}_r \end{Bmatrix}}_{\mathbf{F}} \quad \text{or} \quad \mathbf{Du} = \mathbf{F} \tag{3.1}$$

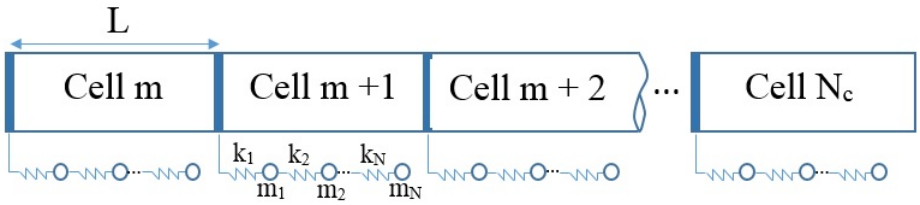

Figure. 3.1: EM rod with N_C consecutive cells. Each cell have a resonator with N degrees-freedom.

where $\mathbf{D} = \mathbf{K} - \omega^2\mathbf{M}$, the index l and r represent left and right sides of resonators, m_0, q_0 and F_0 are the mass, displacement and force, respectively of the attachment point between the resonator and the rod cell. This approach was initially proposed Xiao *et al.* (2012b) from the Wave

Spectral Element Method (WSEM). The submatrices and subvectors of the Eq. (3.1) are given by:

$$\mathbf{k}_{rl} = \mathbf{k}_{lr}^{T} = \begin{bmatrix} -\mathbf{k}_1 \\ 0 \\ 0 \\ \vdots \\ 0 \end{bmatrix}, \quad \mathbf{k}_{rr} = \begin{bmatrix} k_1 + k + 2 & -k_2 & 0 & \dots & 0 \\ -k_2 & k_2 + k_3 & -k_3 & \dots & \vdots \\ 0 & -k_3 & \ddots & \dots & 0 \\ \vdots & \vdots & \dots & k_{N-1} + k_N & -k_N \\ 0 & 0 & \dots & -k_N & k_N \end{bmatrix},$$

$$\mathbf{m}_{rr} = \begin{bmatrix} m_1 & 0 & 0 & \dots & 0 \\ 0 & m_2 & 0 & \dots & 0 \\ 0 & 0 & \ddots & \dots & \vdots \\ \vdots & \vdots & \dots & m_{N-1} & 0 \\ 0 & 0 & \dots & 0 & m_N \end{bmatrix}, \quad \mathbf{u}_r = \begin{bmatrix} u_1 \\ u_2 \\ \vdots \\ u_{N-1} \\ u_N \end{bmatrix} \quad \text{and} \quad \mathbf{F}_r = \begin{bmatrix} F_1 \\ F_2 \\ \vdots \\ F_{N-1} \\ F_N \end{bmatrix},$$

Once that, no exist external force in resonator ($\mathbf{F}_r = 0$), the Eq. (3.1) can be rewritten as $F_0 = D_0 u_0$, where $D_0 = k_1 - \mathbf{k}_{lr}(\mathbf{k}_{rr} - \omega^2 \mathbf{m}rr)^{-1}\mathbf{k}rl$ is the resonator dynamics stiffness at the attachment point. This approach can be use for both method, WSEM and for the proposed method, the WFEM.

The equilibrium equation for a finite rod slice is similar to Eq. (3.1). But, its Dynamic Stiffness Matrix (DSM) is given by $\mathbf{D}_{rod} = \mathbf{K}_{rod} - \omega^2 \mathbf{M}_{rod}$, where $\mathbf{K}_{rod}$ and $\mathbf{M}_{rod}$ are obtained from a analytical or numeric rod model. For the analytic case presented by Xiao *et al.* (2013), the DSM developed from of the Spectral Element Method (SEM) is given by the equation 3.2 (LEE, 2009), which is proposed as reference method.

$$\mathbf{D}^{e}_{Slicesem} = EA\beta \begin{bmatrix} \cot(\beta L) & -\csc(\beta L) \\ -\csc(\beta L) & \cot(\beta L) \end{bmatrix}, \tag{3.2}$$

The numerical case is formulated here as a new way to compute metatmaterial rods, in which the DSM is developed from of the Finite Element Method (FEM). In this case, the DSM is given by dynamic stiffness element matrices represented by $\mathbf{D}^{e}_{Slicefem} = \mathbf{K}^{e}_{Slicefem} - \omega^2 \mathbf{M}^{e}_{Slicefem}$, where

$$\mathbf{K}^{e}_{Slicefem} = \frac{ES}{L} \begin{bmatrix} 1 & -1 \\ -1 & 1 \end{bmatrix}, \quad \mathbf{M}^{e}_{Slicefem} = \frac{\rho SL}{6} \begin{bmatrix} 2 & 1 \\ 1 & 2 \end{bmatrix} \tag{3.3}$$

are FEM stiffness and mass element matrix, respectively. The dynamic stiffness global matrix is given by, $\mathbf{D}_{Slicefem} = \mathbf{K}_{Slicefem} - \omega^2\mathbf{M}_{Slicefem}$, where $\mathbf{K}_{Slicefem}$ and $\mathbf{M}_{Slicefem}$ are the stiffness and mass global matrix, respectively, which are an assembly of as many stiffness and mass element matrices as required to obtain convergence.

This $D_{Slicefem}$ matrix can be partitioned as in Eq. 2.2 and by coupling the local resonator with the finite rod, results:

$$\underbrace{\begin{bmatrix} D_{ll} + D_0 & \mathbf{D}_{lr} \\ \mathbf{D}_{rl} & \mathbf{D}_{rr} \end{bmatrix}}_{D_S} \begin{Bmatrix} u_l \\ \mathbf{u} \end{Bmatrix} = \begin{Bmatrix} F_l \\ \mathbf{F} \end{Bmatrix} \tag{3.4}$$

where D_S is the dynamic stiffness matrix of the elastic metamaterial Slice. As result, the WFE method is used to obtain the wavenumber and wave modes from of this matrix.

3.2 Numerical Verification

Examples with single (S-DOF) and multi (M-DOF) degree-of-freedom attached local resonators are modeled in an elastic system of rod. They are organized in three examples as shown in Tab. 3.2 and Its geometry and property are in Tab. 3.1. In the results, the WFE and WSE methods are compared. More details are in the Nobrega *et al.* (2016) and Nobrega and Dos Santos (2015).

Table. 3.1: Elastic metamaterial rod geometric parameters and material properties.

Geometry/Property	Value
Unit-cell length (L)	0.05 m
Cross section area (S)	50×10^{-6} m^2
Number of unit-cells (N_c)	8
Young's modulus (E)	1.5×10^{10} Pa
Mass density (ρ)	1200 kg/m^3
Structural damping (η)	0.02

In the simulated examples, an equivalent mass $m_0 = 0.016$ is included at the attachment point of the local resonator, which represent the mass of stiffness local. Besides, it is included a structural hysteretic damping (η) as a complex Young's modulus, $E_c = E[1 + i\eta]$.

Fig. 3.2 shows vibration transmittance for the EM rod model of S-DOF local resonator tuned

Table. 3.2: Three examples of attached local resonator with different parameters.

Resonator		Stiffness [N/m]		Mass [kg]		N. Freq. [Hz]	
Example	DOF's	k_1	k_2	m_1	m_2	f_1	f_2
1	Single	5.120×10^6	-	0.0476	-	1650	-
2	Single	2.302×10^7	-	0.0476	-	3500	-
3	Two	1.079×10^7	2.555×10^6	0.0298	0.0178	1650	3500

in 1650 Hz. Where it is possible to see a good agreement between WFE (red line) and WSE (blue line) methods when comparing Its vibration transmittance results (Example 1). It is possible due to use of 50 internal DOFs per FE cell in order to obtain the nearest result to the WSEM. As expected, the bandgap appear around of the natural frequency tuned at the local resonator. Of course, the biggest attenuation occur exactly in resonance frequency of the resonator. In addition, the bandgap width increase when the resonance frequency is tuned in higher frequencies, as can be see in the figure 3.3 (Example 2). Where the width frequency for local resonator at 3500 Hz goes from just over 1 kHz to over 3 kHz using the same mass resonator.

Using M-DOFs local resonators it is possible to obtain multiples band gaps. The Fig. 3.4 shows a vibration transmittance which has two band gaps, one around of $1650\ Hz$ and other one in 3500 Hz. This occur due to the local resonator with 2-DOFs, where the natural frequencies (f_1 and f_2) are the same as the examples 1 and 2. It is possible see that the band gaps occur in close to the examples 1 and 2. However, the band gaps width are less than the S-DOfs ones. This occur because M-DOF local resonator have the same mass, i.e. the sum of each mass ofthe example 3 is equal to the mass of S-DOF in examples 1 and 2, e.g. $m_1 + m_2 = 0.0476$ kg. For all simulated examples the comparative results prove that the WFE method can be used as a good approximated solution for the metamaterial models.

Figures 3.5, 3.6 and 3.7 shows the point receptance FRF's band gaps for the S-DOF example with the resonator tuned in $f_1 = 1650Hz$, S-DOF example with the resonator tuned in $f_2 = 3500Hz$ and for the 2-DOFs example with the resonator tuned in $f_1 = 1650Hz$ and $f_2 = 3500Hz$. Figure 3.8 shows that effect of WFEM approximation as the frequency range increases and the requirements of at least 10 cell/wavelength is violated. In these cases the inclusion of internal points in the cell and /or the use of a FEM element with high order interpolation function will minimize this divergences.

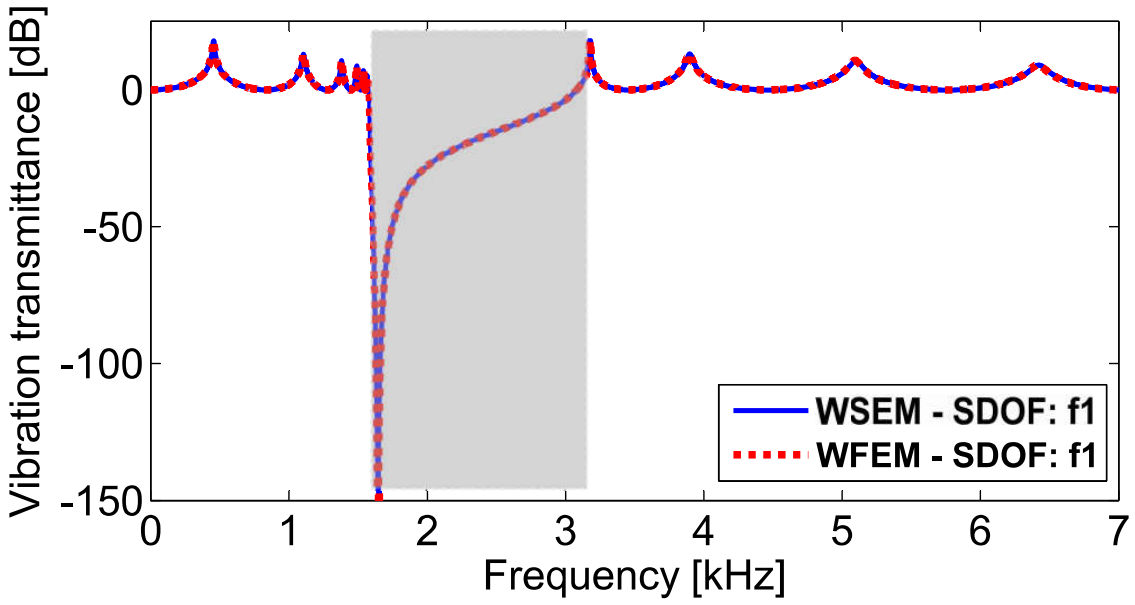

Figure. 3.2: Vibration transmittance showing a bandgap at $f_1 = 1650$ Hz of metameterial rod calculated by WSE and WFE methods.

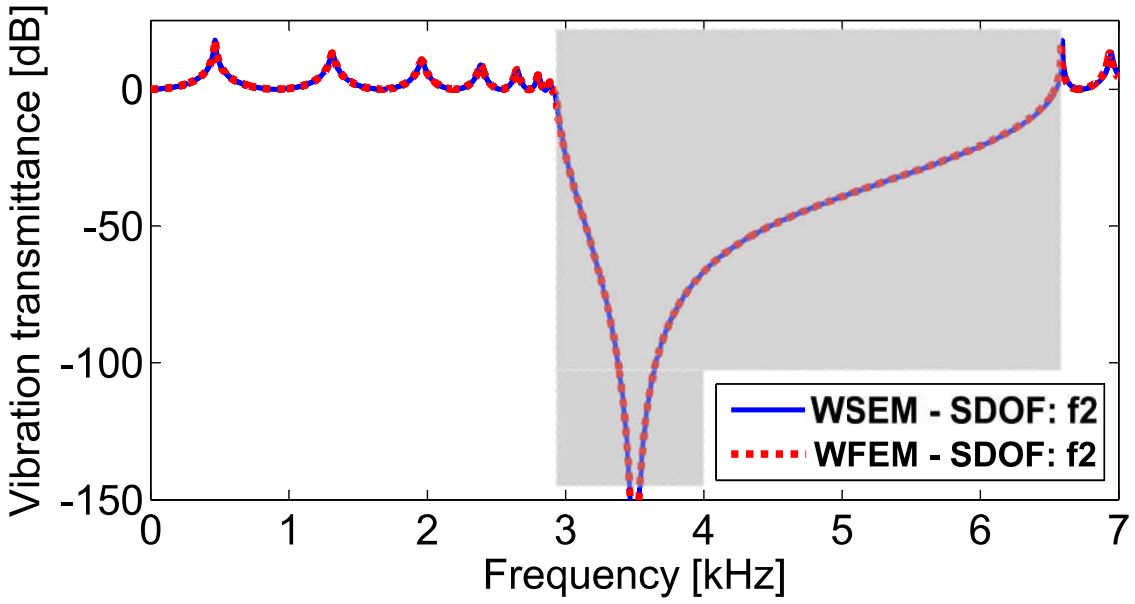

Figure. 3.3: Vibration transmittance showing a bandgap at $f_2 = 3500$ Hz of metameterial rod calculated by WSE and WFE methods.

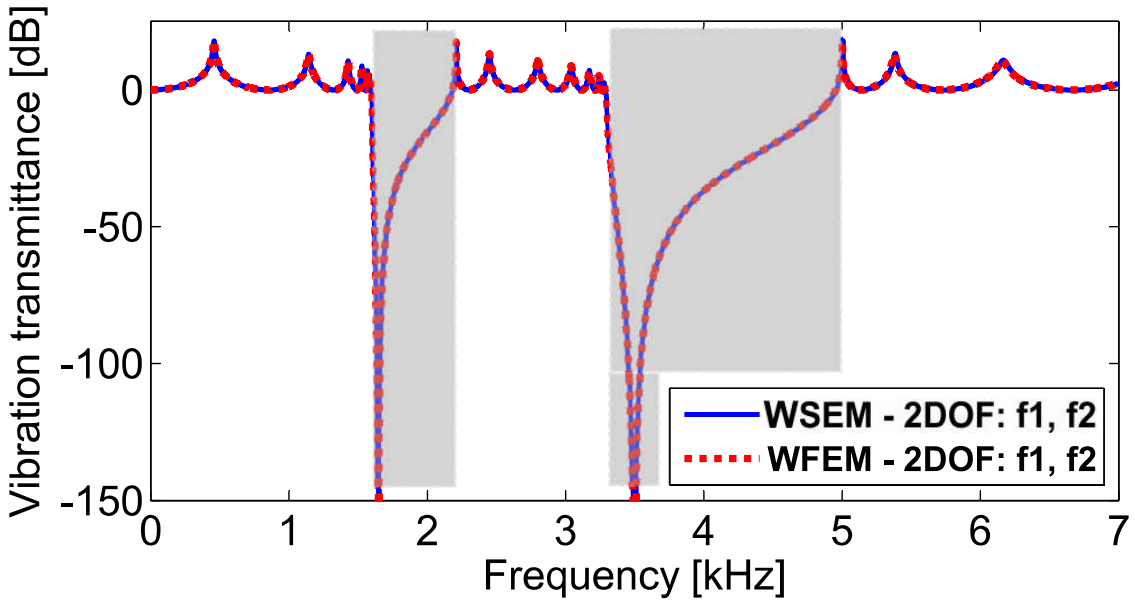

Figure. 3.4: Vibration transmittance showing band gaps at $f_1 = 1650$ Hz and $f_2 = 3500$ Hz of metameterial rod calculated by WSE and WFE methods.

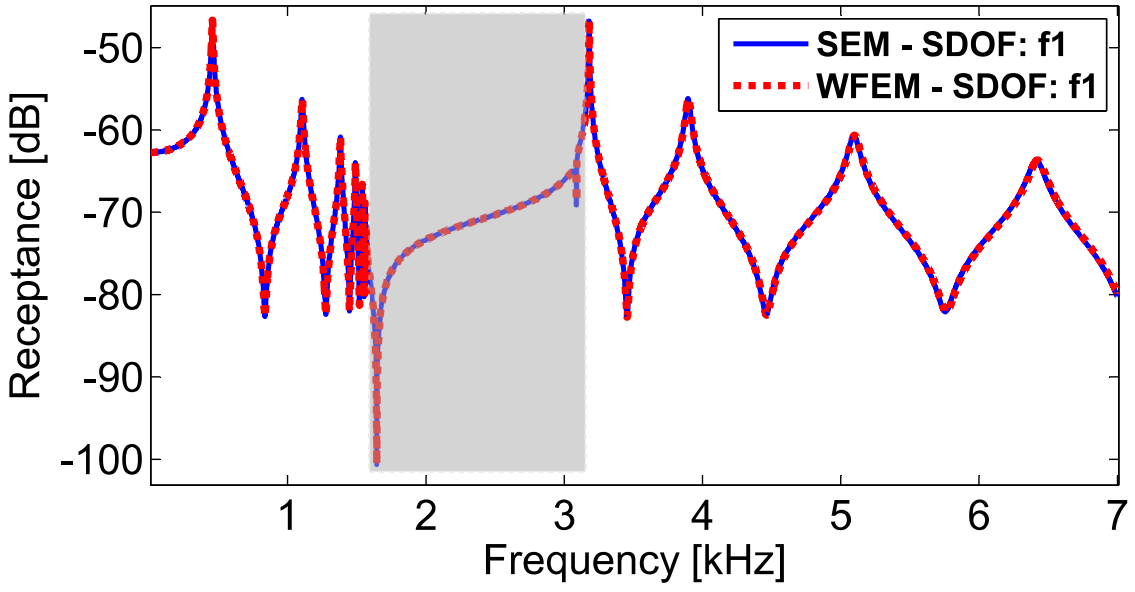

Figure. 3.5: Point receptance FRF band gaps with S-DOF example with $f_1 = 1650$ Hz.

3.3 Bandgap sensitivity analysis

Know the behavior of band gaps due to parameters variations can be interesting for practical applications. Its sensitivity can be seen by means position, width and attenuation performance in

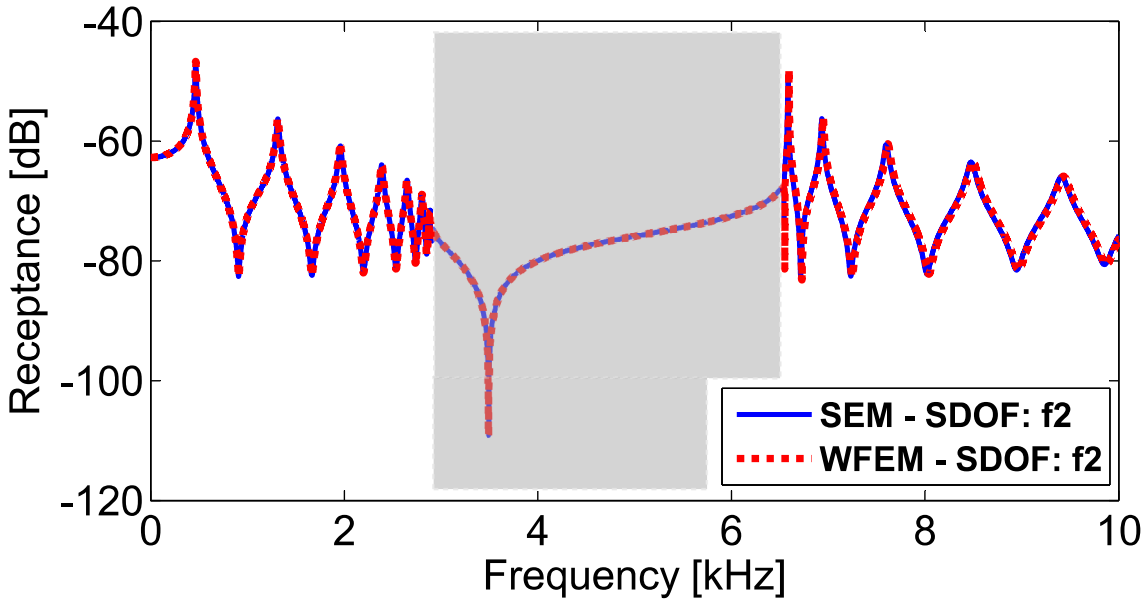

Figure. 3.6: Point receptance FRF bandgap with S-DOF example with $f_1 = 3500$ Hz.

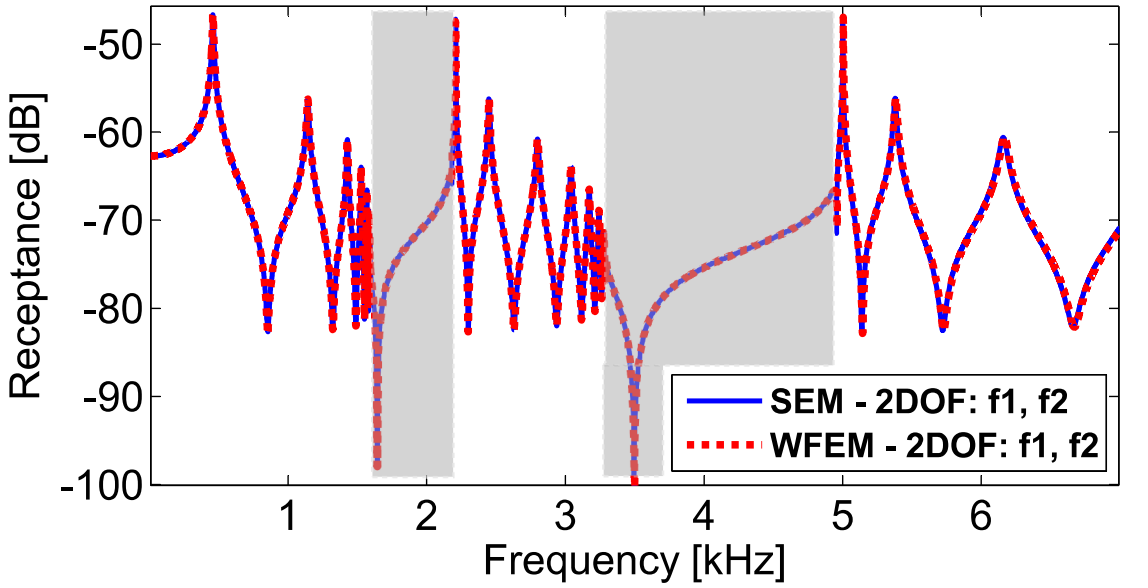

Figure. 3.7: Point receptance FRF band gaps with 2-DOF's with $f_1 = 1650$ Hz and $f_2 = 3500$ Hz.

the band gaps. In general, the attenuation constant is used to represent this behavior, which may be described by $\Re(\mu) = f(E,A,\rho,L,\omega,m_0,k_1,m_1,k_2,m_2,\ldots)$. As focus of this work is how the WFE method can describe band gaps, It will be followed Xiao *et al.* (2013), which the sensitivity analysis of the attenuation constant is related with local resonator stiffness and the frequency, $\Re(\mu) = f(\omega,k_1)$. This representation is called *Attenuation Constant Surface*-ACS (XIAO *et al.*, 2011).

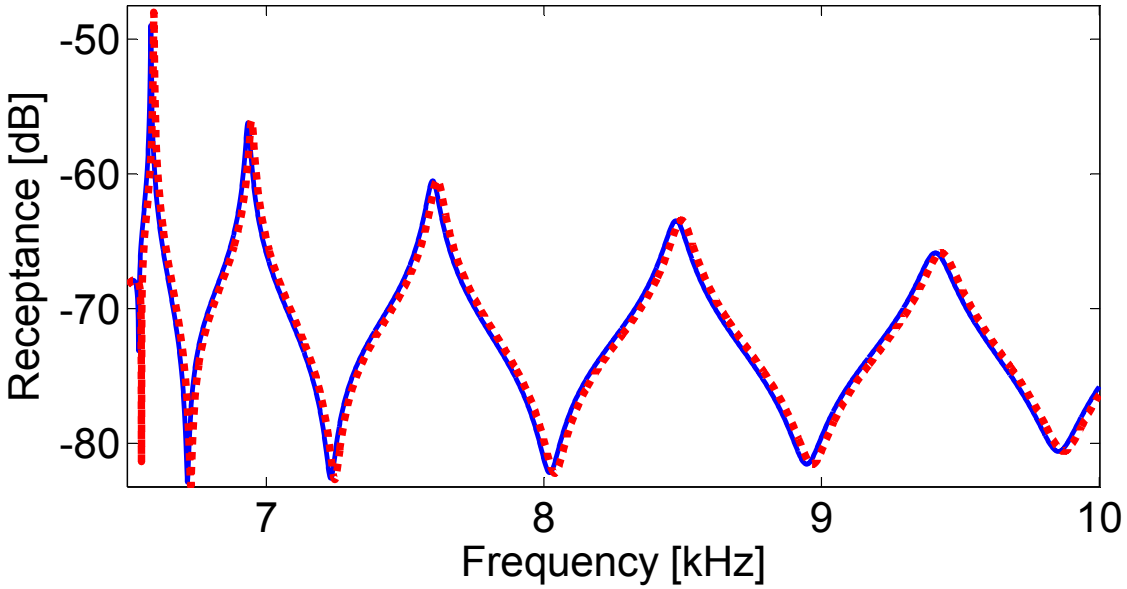

Figure. 3.8: Point receptance FRF bandgap with S-DOF with $f_2 = 3500$ Hz zoomed between 6.5-10 kHz.

Figure 3.9 displays a comparison between four ACS's to the elastic metamaterial rod with S-DOF resonator calculated by: a) SEM; b) WFEM with 1 internal dof; c) WFEM with 5 internal dof's; and d) WFEM with 50 internal dof's. At each plan-form ACS the hot color region (red) represents the bandgap range with nonzero attenuation constants. To the SEM results (Figure 3.9(a)) there are three band gaps in the frequency range considered. As reported by (XIAO *et al.*, 2013) the bandgap with the maximum attenuation constant is the locally resonance bandgap, while the others are Bragg-scattering band gaps. When the locally resonance bandgap and the nearest Bragg bandgap merge, the attenuation constant becoming zero (bandgap coupling phenomenon) (XIAO *et al.*, 2011). Figure 3.9(b) shows that WFEM results with a single internal dof fails to converge to the SEM results. By increasing internal DOF's to five the WFEM results (Figure 3.9(c)) seems to be improved. However, a more careful verification shows that the bandgap coupling points do not coinciding with the corresponding ones of the SEM results. By including a relatively high number (fifth) of internal DOF's (Figure 3.9(d)) the difference between WFEM and SEM results are minimized and a better convergence is reached.

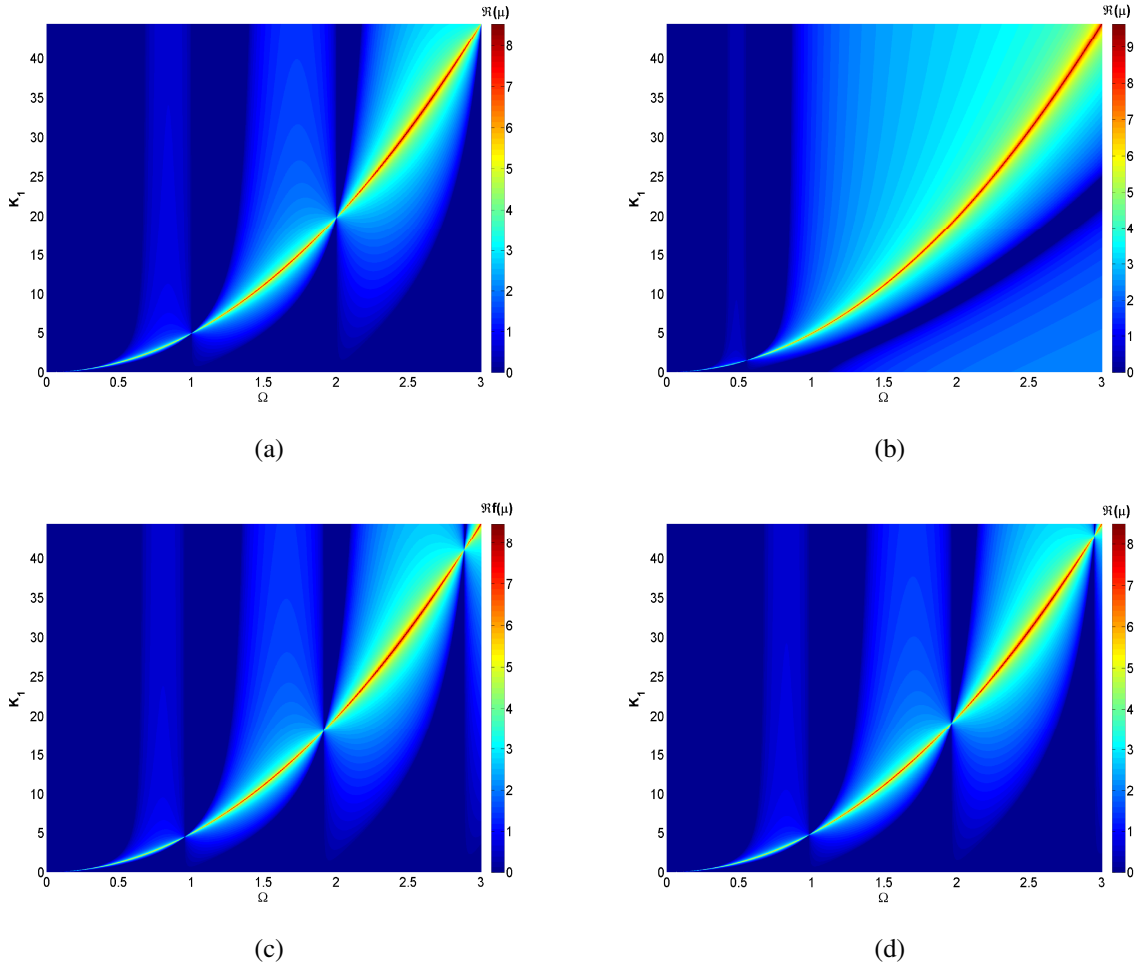

Figure. 3.9: *Attenuation Constant Surface*-ACS of elastic metamaterial rod cell with S-DOF resonator calculated by: a) SEM and b) WFEM with 1 internal dof's; c) WFEM with 5 internal dof's; d) WFEM with 50 internal dof's. $K_1 = k_1/(EA/L)$ and $\Omega = (L\omega/\pi)/\sqrt{\rho/E}$.

3.4 Conclusion

Elastic metamaterials rod with M-DOF locally resonators was presented, which the wave propagation was studied in terms of attenuation constants, vibration transmittance and FRF. This rod was modeled as a periodic structure from of a hybrid method, witch is combination of FEM and wave propagation known as the Wave Finite Element Method. The validation of this methodology was confirmed by a comparison with the analytical method, the Spectral Element Method. Three simulated examples with WFEM elastic metamaterial rod system consisting of a uniform rod with periodically attached S-DOF and 2-DOF's resonators were evaluated. For all results, the WFEM presented good agreement in comparison with the SEM. It was performed as sensitivity analysis,

the *Attenuation Constant Surface*-ACS (XIAO *et al.*, 2011), where a constant attenuation varies depending on the resonator stiffness and the frequency. The ACS WFEM results calculated increased the converge to the SEM results when high number of internal DOFs were added. Finally, it can be conclude that the WFEM method presents a good performance to calculate elastic metamaterials rod provided that the used finite element be a satisfactory interpolation functions and the number of DOFs respect the wave propagation limit of 10 cells/wavelength.

4 EXPERIMENTAL VALIDATION OF PC ROD MODEL

A real elastic PC waveguide was used to perform an experimental test (NOBREGA *et al.*, 2016). The PC waveguide was designed to be an assembly of parts including two resonator and a waveguide portion (Fig. 4.1(a)). It was originally developed to be used in another research project (LI AND BRIK, (in French) as a metamaterial beam-like (flexural waves) and shaft-like (torsional waves) structures with spatial periodic distribution and local resonators (Fig. 4.1(b)).

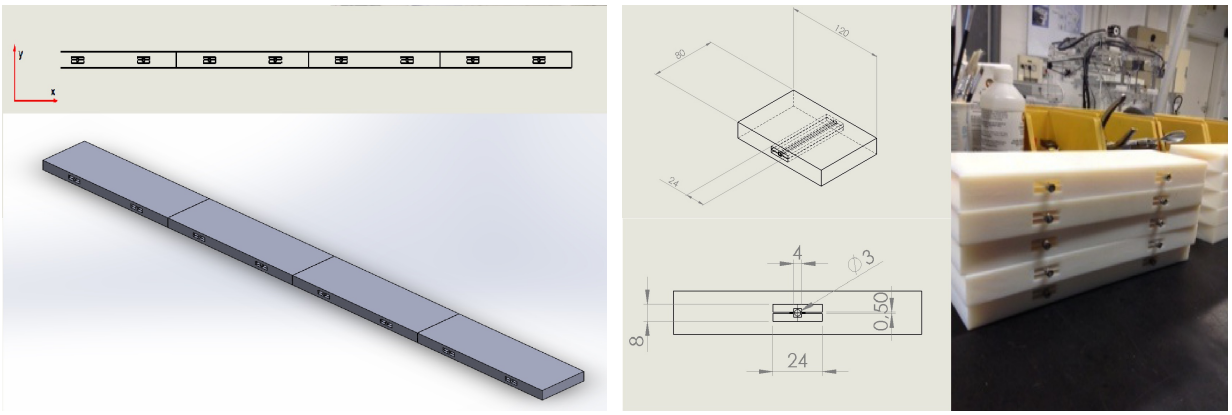

(a) (b)

Figure. 4.1: Design of PC waveguide: (*a*) waveguide assembly; (*b*) local resonator dimensions and physical aspect.

For this work it was configured as a rod-like (longitudinal waves) structure, which maintains the spatial periodic distribution, but the local resonators becomes inactive since they are not sensitive to longitudinal movements. Then, the experimental evaluation presented here is relate only to Bragg-type band gap formation in a PC rod. Therefore, the spatial periodic distribution was assumed as an empty cavity in the rod and this region was modeled as cross section area change. Fig. 4.2 shows the views for the original metamaterial unit-cell with local resonators for beam/shaft and with the simplification to be used with the rod spatial periodic distribution (PC rod).

4.1 Numerical results

The PC rod was built by bonding 10 equal parts of prismatic rod (0.24 x 0.08 x 0.02 m) with male and female conic ends. Each part includes two local resonator separated by 0.0979 m and they were fabricated in a 3D printer. The final assembly of PC rod includes also two extra rod parts at the ends without cross section variation. The actual PC rod geometric parameters and material

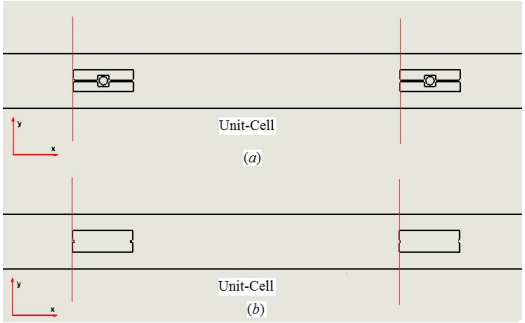

Figure. 4.2: Unit-cell model for the metamaterial: (a) with local resonator for beam/shaft structure; (b) with rod spatial periodic distribution.

properties are summarized in Table 4.1.

Table. 4.1: Actual metamaterial rod geometric parameters and material properties.

Geometry/Property	Value
Unit-cell length (L)	0.12 m
Periodic part length (L_p)	2.41 m
Total length (L_t)	2.88 m
Cross section area ($S = b \times h$)	0.080 x 0.020 m^2
Cross section area at cavity ($S_r = b \times h_c$)	0.080 x 0.012 m^2
Number of unit-cells (N_c)	20
Young's modulus* (E)	2.495 x 10^9 Pa
Mass density* (ρ)	1.3 x 10^3 kg/m^3
Structural damping (η)	0.02

*manufacturing nominal value.

Fig. 4.3 shows the experimental setup with the details of impact hammer and accelerometers positions. This figure also shows a typical measured inertance FRF including the ordinary coherence function. It must be emphasized an interesting behavior of the measured inertance FRF, which presents an oscillatory behavior before the band gap indicating low damping, while after the band gap the curve becomes smooth indicating a high damping behavior. Fig. 4.4 shows the dispersion curves calculated with the numerical methods (WSEM, WFEM, WFEM-ANSYS, WFEM-ANSYS-3D) where it can be identified the Bragg limit ($\beta = \pi/L = 26.18$), and the band gap position and width for this PC rod.

In order to increase the flexibility of WFEM to solve complex engineering models, a hybrid approach using WFEM and a FEM commercial software is proposed. It consists of coupling WFEM with the commercial finite element analysis software ANSYS (Mechanical APDL Release 14.5) to calculate elastic PC rods. The PC rod unit-cell is modeled with ANSYS using an appropriated

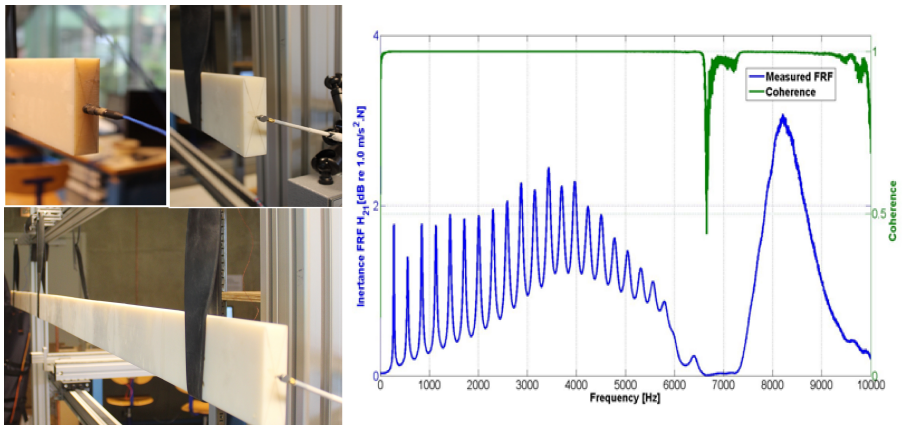

Figure. 4.3: Rod measurement setup and a typical measured inertance FRF (blue line) and corresponding ordinary coherence function (green line).

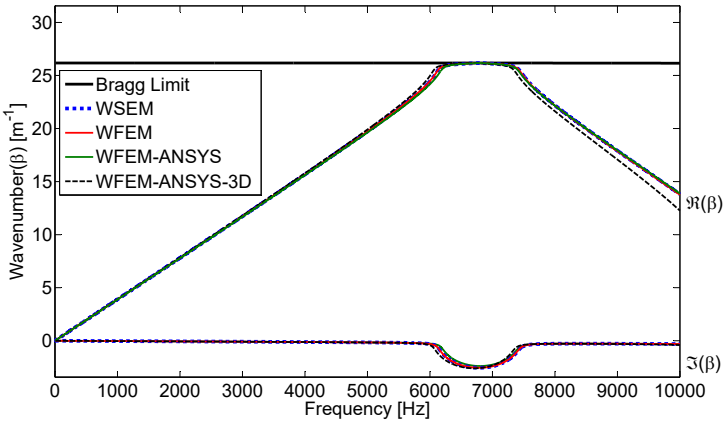

Figure. 4.4: Dispersion curves calculated by WSEM, WFEM, WFEM-ANSYS and WFEM-ANSYS-3D.

element type from its element library. Then, using a MATLAB code, the dynamic stiffness matrix is calculated and periodicity conditions are applied to obtain the receptance FRFs. Two examples of PC rod unit-cell modeling are performed: one called WFEM-ANSYS using a simple 1D element rod (LINK180), and other called WFEM-ANSYS-3D using a more complex 3D solid element (SOLID185). Fig. 4.5(a) shows the PC rod unit-cell modeled with ANSYS 1D element rod with 2 nodes and 1 DOF/node. The rod unit-cell was discretized with 40 internal elements, which means 41 nodes and DOFs. Fig. 4.5(b) shows the PC rod unit-cell modeled with ANSYS 3D solid element with 8 nodes and 3 DOFs/node. The rod unit-cell was discretized with 25 internal elements, which means 200 nodes and 600 DOFs.

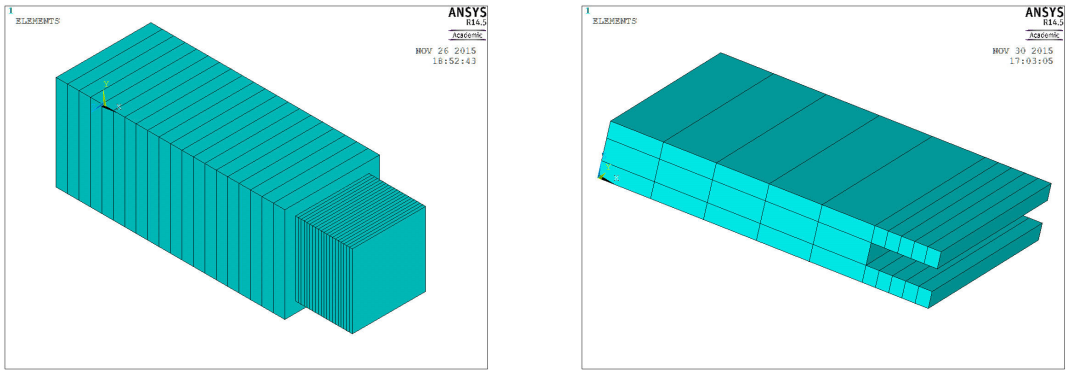

(a) (b)

Figure. 4.5: PC rod unit-cell modeled with ANSYS: (*a*) 1D rod element in which the geometry change is represented by only a variation area; and (*b*) 3D solid element is used to model a real slice where the geometry change is a hollow hole in slice.

For the first evaluation the simulated receptance FRFs calculated by WSEM, WFEM, WFEM-ANSYS and WFEM-ANSYS-3D using material properties of Table 4.1 are compared with the experimental FRFs. Fig. 4.6 illustrates that the FRF calculated by numerical methods (WSEM, WFEM and WFEM-ANSYS, WFEM-ANSYS-3D) present good agreement among them, but there are some mismatch and different behaviors related with its corresponding experimental FRFs. Before band gap positions, all numerical FRFs present the same oscillatory behaviors as its corresponding experimental FRF. At the band gap position, all simulated FRFs present similar width as the experimental, but they are shifted to the left of experimental band gap position. After band gap positions, all simulated FRFs return to the oscillatory behaviors, in total disagree with the smooth behavior of corresponding experimental FRFs.

This oscillatory response (low damping) before band gap position followed by a smooth response (high damping) after band gap position is a characteristic behavior of the elastic metamaterial rod, which is not very well captured by the numerical models presented here. For the WFEM-ANSYS-3D model the receptance FRF shows another band gap around 9.0 kHz, not included in the others numerical models. It comes from the greater number of wave-modes include in the 3D model as compared with the others 1D models, associated with the uncertainty of the values of material properties (Young modulus and mass density) specified by the plastic manufacturer, which is not guaranteed in the addictive manufacturing process used to make the actual metamaterial rod.

In order to reduce the mismatch between experimental and simulated FRFs a try-and-error model updating procedure was performed. By varying material property parameters E and ρ the

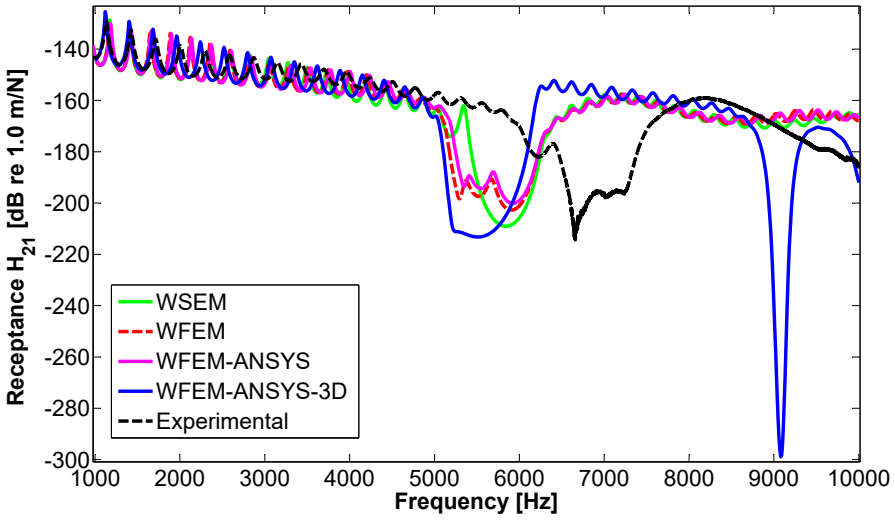

Figure. 4.6: Simulated FRFs calculated by WSEM, WFEM, WFEM-ANSYS, WFEM-ANSYS-3D with material properties of Table 4.1 and experimental FRFs of transfer receptance.

shift between simulated and experimental band gap position was reduced until the band gaps are almost coincident. These results were founded using the combination of Young's modulus E = 3.2 x 10^9 Pa and mass density ρ = 1,180 kg/m^3. Fig. 4.7 shows the simulated FRFs (WSEM, WFEM, WFEM-ANSYS, WFEM-ANSYS-3D) obtained with updated parameters and the experimental FRF.

Although the model updating process brings the simulated and experimental FRFs more close for the band gaps, still have different behaviors between experimental and simulated FRFs after the band gaps. A model updating varying the parameter structural damping η was performed without success. Considering that the behavior before and after band gap are strongly different, actually contradictory, an updating process for the whole frequency band of analysis will be not possible. Then, a selective model updating varying η was applied for two frequency band: DC-5.7 kHz and 5.7-10 kHz. Using a try-and-error updating process the best curve fitting for the FRFs was obtained with the structural damping $\eta = 0.015$ to DC-5.7 kHz and $\eta = 0.05$ to 5.7-10 kHz. Fig. 4.8 shows the comparison between simulated (WSEM, WFEM, WFEM-ANSYS, WFEM-ANSYS-3D) using updating structural damping and experimental results for the measured FRF. It can be seen that all numerical FRFs after the band gap change their behavior from oscillatory to smooth as the experimental ones, however still remains significant differences in amplitudes.

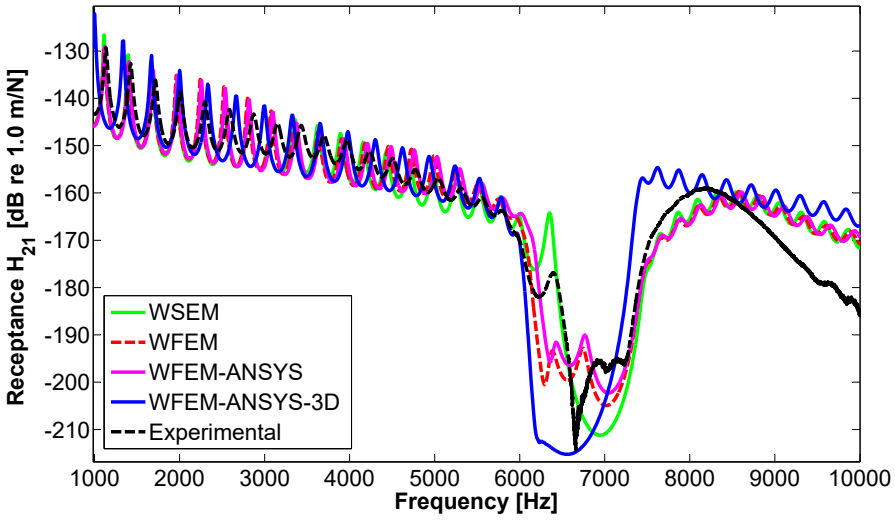

Figure. 4.7: Simulated FRFs (SEM, WSEM, WFEM, WFEM-ANSYS, WFEM-ANSYS-3D) using updating material property parameters and experimental FRFs of transfer receptance.

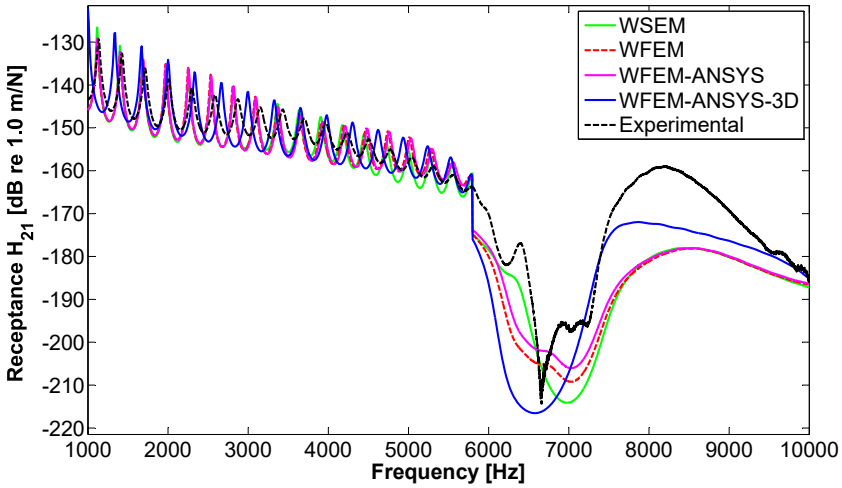

Figure. 4.8: Simulated FRFs calculated by WSEM, WFEM, WFEM-ANSYS, WFEM-ANSYS-3D with updating material property parameters and experimental FRFs of transfer receptance.

4.2 Conclusion

Band gap in PC rod was presented from of numerical methodology called wave finite element method (WFEM). Based on a combination of FEM and Floquet-Bloch's theorem, the WFEM was

proposed as an engineering tool to calculate these type of structures.The use of WFE for the calculation of periodic structures was demonstrated through the inclusion of models by commercial FEM packages, which through the use of commercial finite element software (ANSYS Mechanical APDL Release 14.5) allowed the inclusion of models with complex geometry or PC unit cell non -uniform. This approach extends the WFEM application to model complex PC systems. However, WFE inherits the same approximation problems from the finite element model, where the greater the frequency range, the greater the numerical error. An interesting behavior of PC rod was observed in the experimental test results in relation to the damping variation, where it is low for vibration response before band gap and high for this response after band gap. Finally, it was presents a comparison between WSEM, WFEM and WFEM/ANSYS methods from of dispersion curves of a PC cell and its FRFs was compared with the experimental FRFs obtained from a real PC rod. It was shown that it is possible to obtain a good agreement between the numerical and experimental results, both for the presented method (WSEM) and for those proposed (WFEM, WFEM / ANSYS), where it was possible to locate the position and width of the band gap close to the experimental.

5 THE INFLUENCE ON THE WAVE PROPAGATION PROPERTIES BY COUPLING OF WAVEGUIDES IN PC STRUCTURES

In this Chapter, a brief approach to waveguide coupling using wave modes Φ and autovalue μ obtained by WFE is made. The objective here is to calculate the WFE for a substructure and make several consecutive couplings of it to obtain a formulation for periodic couplings. Finally, to apply this approach in PC structures.

5.1 Waveguides coupling

Within the PC structure, several structures of different materials are connected in a periodic way, and coupling conditions apply at the interfaces between two consecutive structures. According to Eq. (2.13), for any structure (i) composed of N_i substructures having n_i DOFs on each left/right boundary, the state vector at the m^{th} substructure is now given by the following expression:

$$\mathbf{u}_{l,i}^{(m)} = \mathbf{\Phi}_i \, \boldsymbol{\mu}_i^{m-1} \, \mathbf{Q}_i + \mathbf{\Phi}_i^{\star} \, \boldsymbol{\mu}_i^{N_i+1-m} \, \mathbf{Q}_i^{\star}, \tag{5.1}$$

with again $\mathbf{Q}_i = \mathbf{Q}_i^{(1)}$ and $\mathbf{Q}_i^{\star} = \mathbf{Q}_i^{\star\,(N_i+1)}$ (as illustrated in Figure 5.1).

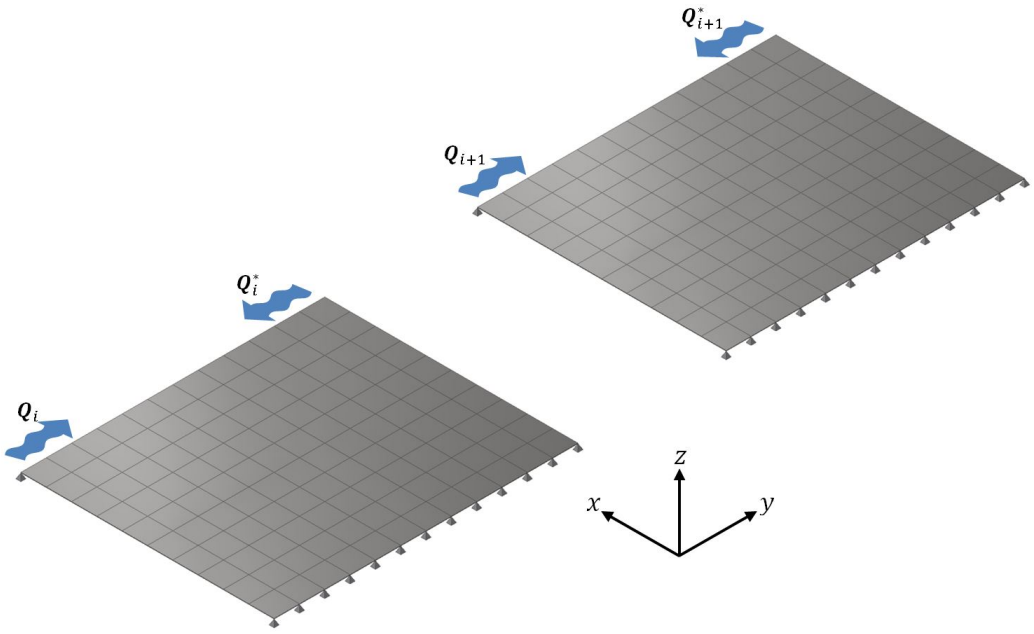

Figure. 5.1: Coupling of two consecutive strips.

At the interface between two consecutive structures (i) and $(i+1)$ where an external excitation $\mathbf{F}_{ex}$ may apply, the coupling conditions are written:

$$\mathbf{q}_i^{(N_i+1)} = \mathbf{q}_{i+1}^{(1)} \tag{5.2}$$

$$\mathbf{F}_{L,i}^{(N_i+1)} + \mathbf{F}_{ex} = \mathbf{F}_{L,i+1}^{(1)}, \tag{5.3}$$

that is, in matrix form,

$$\boldsymbol{\Phi}_{\mathrm{q},i}\,\boldsymbol{\mu}^{N_i}\,\mathbf{Q}_i + \boldsymbol{\Phi}^{\star}_{\mathrm{q},i}\,\mathbf{Q}^{\star}_i = \boldsymbol{\Phi}_{\mathrm{q},i+1}\,\mathbf{Q}_{i+1} + \boldsymbol{\Phi}^{\star}_{\mathrm{q},i+1}\,\boldsymbol{\mu}_{i+1}^{N_{i+1}}\,\mathbf{Q}^{\star}_{i+1} \tag{5.4}$$

$$-\boldsymbol{\Phi}_{\mathrm{F},i}\,\boldsymbol{\mu}^{N_i}\,\mathbf{Q}_i - \boldsymbol{\Phi}^{\star}_{\mathrm{F},i}\,\mathbf{Q}^{\star}_i + \mathbf{F}_{ex} = -\boldsymbol{\Phi}_{\mathrm{F},i+1}\,\mathbf{Q}_{i+1} - \boldsymbol{\Phi}^{\star}_{\mathrm{F},i+1}\,\boldsymbol{\mu}_{i+1}^{N_{i+1}}\,\mathbf{Q}^{\star}_{i+1}. \tag{5.5}$$

Taking into account that in our case $n_i = n_{i+1} = n$ (the case $n_i \neq n_{i+1}$ may be considered by using Lagrange multipliers, as developed for instance in Mencik (2013)), the above equations may be simplified into the following matrix system:

$$\mathbf{A}\begin{bmatrix} \mathbf{Q}^{\star}_i \\ \mathbf{Q}_{i+1} \end{bmatrix} = \mathbf{B}\begin{bmatrix} \boldsymbol{\mu}_i^{N_i}\mathbf{Q}_i \\ \boldsymbol{\mu}_{i+1}^{N_{i+1}}\mathbf{Q}^{\star}_{i+1} \end{bmatrix} + \begin{bmatrix} \mathbf{0} \\ -(\boldsymbol{\Phi}_{\mathrm{F}\,i+1})^{-1}\mathbf{F}_{ex} \end{bmatrix} \quad \text{where} \tag{5.6}$$

$$\mathbf{A} = \begin{bmatrix} \mathbf{I}_n & -(\boldsymbol{\Phi}^{\star}_{\mathrm{q},i})^{-1}\,\boldsymbol{\Phi}_{\mathrm{q},i+1} \\ -(\boldsymbol{\Phi}_{\mathrm{F},i+1})^{-1}\boldsymbol{\Phi}^{\star}_{\mathrm{F},i} & \mathbf{I}_n \end{bmatrix} \quad \mathbf{B} = \begin{bmatrix} -(\boldsymbol{\Phi}^{\star}_{\mathrm{q},i})^{-1}\boldsymbol{\Phi}_{\mathrm{q},i} & (\boldsymbol{\Phi}^{\star}_{\mathrm{q},i})^{-1}\boldsymbol{\Phi}^{\star}_{\mathrm{q},i+1} \\ (\boldsymbol{\Phi}_{\mathrm{F},i+1})^{-1}\boldsymbol{\Phi}_{\mathrm{F},i} & -(\boldsymbol{\Phi}_{\mathrm{F},i+1})^{-1}\boldsymbol{\Phi}^{\star}_{\mathrm{F},i+1} \end{bmatrix}.$$

As in (MENCIK, 2013) the latter matrix system may be finally put in the following form:

$$\begin{bmatrix} \mathbf{Q}^{\star}_i \\ \mathbf{Q}_{i+1} \end{bmatrix} = \mathbb{C}\begin{bmatrix} \boldsymbol{\mu}_i^{N_i}\,\mathbf{Q}_i \\ \boldsymbol{\mu}_{i+1}^{N_{i+1}}\,\mathbf{Q}^{\star}_{i+1} \end{bmatrix} + \mathbb{F} \quad \text{with} \tag{5.7}$$

$$\mathbb{C} = \begin{bmatrix} \mathbb{C}^{\star}_{i,i} & \mathbb{C}^{\star}_{i,i+1} \\ \mathbb{C}_{i+1,i} & \mathbb{C}_{i+1,i+1} \end{bmatrix} = \mathbf{A}^{-1}\,\mathbf{B} \quad \text{and} \quad \mathbb{F} = \begin{bmatrix} \mathbb{F}^{\star}_i \\ \mathbb{F}_{i+1} \end{bmatrix} = \mathbf{A}^{-1}\begin{bmatrix} \mathbf{0} \\ -(\boldsymbol{\Phi}_{\mathrm{F},i+1})^{-1}\mathbf{F}_{ex} \end{bmatrix},$$

where $\mathbb{C}$ is the scattering matrix. In the equation 5.7, $\mathbb{C}_{i,i}$ and $\mathbb{C}_{i+1,i+1}$ are square matrices of size $n \times n$ that express the reflection coefficients of the wave modes of the structures respectively (i) and $(i+1)$ at the interface. The $n \times n$ matrices $\mathbb{C}^{\star}_{i,i+1}$ and $\mathbb{C}_{i+1,i}$ contain the transmission coefficients between the wave modes of the two structures at the interface. Finally, the vector $\mathbb{F}$ takes into account possible excitation sources at the interface.

For p structures connected to each other, a complete matrix system may be built by applying Eq. (5.7) at all the interfaces between structures (i) and $(i+1)$ for $i = 1 \ldots p-1$, and boundary conditions at the left end of structure (1) and the right end of structure (p). As an example, if the same Newmann / Dirichlet boundary conditions as in the previous section apply, Eqs. (2.14) and

(2.15) become

$$\mathbf{Q}_1 + (\mathbf{\Phi}_{\mathrm{F},1})^{-1}\mathbf{\Phi}^{\star}_{\mathrm{F},1}\,\boldsymbol{\mu}_1^{N_1}\,\mathbf{Q}^{\star}_1 = -(\mathbf{\Phi}_{\mathrm{F},1})^{-1}\mathbf{F}_0, \tag{5.8}$$

$$(\mathbf{\Phi}^{\star}_{\mathrm{q},p})^{-1}\,\mathbf{\Phi}_{\mathrm{q},p}\,\boldsymbol{\mu}_p^{N_p}\,\mathbf{Q}_p + \mathbf{Q}^{\star}_p = (\mathbf{\Phi}^{\star}_{\mathrm{q},p})^{-1}\,\mathbf{q}_0. \tag{5.9}$$

In the latter case, the computation of the unknown wave amplitudes for the set of p structures follows from the inversion of the final system

$$\mathbf{\Psi}\,\mathcal{Q} = \mathcal{F} \quad \text{where} \quad \mathcal{Q} = \begin{bmatrix} \mathbf{Q}_1 \\ \mathbf{Q}^{\star}_1 \\ \mathbf{Q}_2 \\ \mathbf{Q}^{\star}_2 \\ \vdots \\ \mathbf{Q}_p \\ \mathbf{Q}^{\star}_p \end{bmatrix}, \quad \mathcal{F} = \begin{bmatrix} -(\mathbf{\Phi}_{\mathrm{F},1})^{-1}\mathbf{F}_0 \\ \mathbb{F}^{\star}_1 \\ \mathbb{F}_2 \\ \mathbb{F}^{\star}_2 \\ \vdots \\ \mathbb{F}_p \\ (\mathbf{\Phi}^{\star}_{\mathrm{q},p})^{-1}\,\mathbf{q}_0 \end{bmatrix}, \quad \text{and} \tag{5.10}$$

$$\mathbf{\Psi} = \begin{bmatrix} \mathbf{I_n} & (\mathbf{\Phi}_{\mathrm{F},1})^{-1}\mathbf{\Phi}^{\star}_{\mathrm{F},1}\boldsymbol{\mu}_1^{N_1} & \mathbf{0} & \mathbf{0} & \dots & \mathbf{0} & \mathbf{0} \\ -\mathbb{C}^{\star}_{1,1}\boldsymbol{\mu}_1^{N_1} & \mathbf{I_n} & \mathbf{0} & -\mathbb{C}^{\star}_{1,2}\boldsymbol{\mu}_2^{N_2} & \dots & \mathbf{0} & \mathbf{0} \\ -\mathbb{C}_{2,1}\,\boldsymbol{\mu}_1^{N_1} & \mathbf{0} & \mathbf{I_n} & -\mathbb{C}_{2,2}\boldsymbol{\mu}_2^{N_2} & \dots & \mathbf{0} & \mathbf{0} \\ \mathbf{0} & \mathbf{0} & -\mathbb{C}^{\star}_{2,2}\,\boldsymbol{\mu}_2^{N_2} & \mathbf{I_n} & \dots & \mathbf{0} & \mathbf{0} \\ \vdots & \vdots & \vdots & \vdots & \ddots & \vdots & \vdots \\ \mathbf{0} & \mathbf{0} & \mathbf{0} & \mathbf{0} & \dots & \mathbf{I_n} & -\mathbb{C}_{p,p}\boldsymbol{\mu}_p^{N_p} \\ \mathbf{0} & \mathbf{0} & \mathbf{0} & \mathbf{0} & \dots & (\mathbf{\Phi}^{\star}_{\mathrm{q},p})^{-1}\mathbf{\Phi}_{\mathrm{q},p}\boldsymbol{\mu}_p^{N_p} & \mathbf{I_n} \end{bmatrix}.$$

The displacements/rotations and forces at any location of any structure are then computed from Eq. (5.1).

The same kind of formulation applies when modifying the orientation of a structure by introducing a θ angle between the structure and horizontal direction (Fig. 5.2), but in this case, the wave modes matrices are multiplied by rotation matrices $\mathcal{L}_i$ depending on θ as $\mathcal{L}_i\mathbf{\Phi}_i$ and $\mathcal{L}_i\mathbf{\Phi}^{\star}_i$.

5.2 Investigating simple designs of periodic structures frame and their influence on the wave propagation properties

This section focuses on that topic by exploring the wave propagation along simple periodic structures made of straight beam elements - which incorporate bending and longitudinal motions -

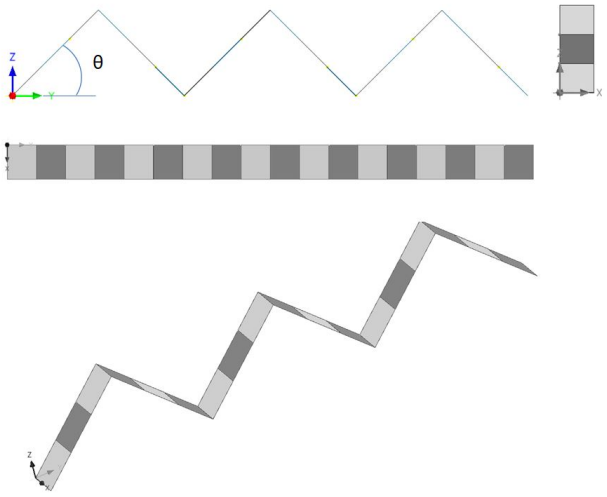

Figure. 5.2: Coupling of p consecutive strips with change direction θ of the wave propagation.

which are connected together at a certain angle ("triangle" shaped patterns). A parametric analysis is proposed to analyze the influence of the coupling angle. Emphasis is placed on the physical understanding of the wave mode conversion phenomenon which results in the occurrence of band gaps for several types of wave modes. The computation of the wave modes and forced response is achieved with the wave finite element (WFE) method. It provides an efficient numerical means to compute the response of periodic structures. It can be of finite length and subject to arbitrary kinds of boundary conditions in low- and mid-frequency range. A parametric analysis is proposed to highlight the influence of the topology patterns, and boundary conditions on the attenuation of the vibration levels of PC structures (band gap effects). The accuracy and efficiency of the proposed approach are discussed through numerical comparisons with the finite element (FE) method. In this section it is proposed to analyze wave propagation in a structure generated by coupling waveguides (frames) which alternate material propriety (steel and aluminum) and space direction to form a PC frame. Figure 5.3 shows a PC frame scheme including perspective and projection views (front, top and right).

5.2.1 Numerical results

Fourth cases are studied with a frame element. Case 1 consists of a straight line frame with only one material. Case 2 the waveguides frame are coupled in triangle form with $\theta = 45$ degrees. Case 3, straight line frame are coupled with two alternate materials. Case 4, the frame are coupled in triangle form ($\theta = 45$) with two alternate materials. For all cases the forced response is calculate

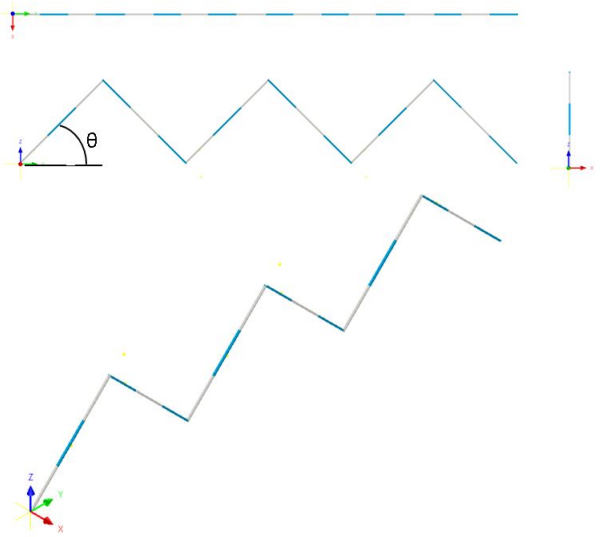

Figure. 5.3: PC frame with 18 waveguide including direction angle (θ) and alternating materials: steel (gray) and aluminum (blue).

using WFE and FE and the results are compared. The material properties are: $E_{steel} = 210e9$ Pa, $\rho_{steel} = 7800$ kg/m^3, $E_{al} = 700e9$, $\rho_{steel} = 2700$ kg/m^3, $\nu = 0.3$, $\eta = 0.005$. Slice dimensions are: length ($L = 0.001$ m), height ($h = 0.001$ m), and width ($b = 0.001$ m). Each sub-frame are made with 24 slices for WFE method and 24 elements for FE method. The results are calculated with 6 and 18 sub-frames coupled each other for both methods with clamped-free boundary conditions. The structure is excited in the free end with a unit force in "y" direction.

Figure 5.4 shows displacement response for Case 1 and 2 calculated by WFE and FE methods. The results are convergent and it can seen that for the Case 1 (Fig. 5.4(a)) the structure behaved as a rod due to direction of the excitation force along the frame length. For the Case 2 a different behavior is obtained due to the angle periodic discontinuity.

It can be observed in figure 5.4(b) where is shown that to a angle $\theta = 45$ it have a behavior of beam but with some special differences that can see better on the transmittance response, fig. 5.4(c). This behavior occur due to change of wave propagation direction on the structure. This effect cause something like bandpap phenomenon. When we coupling behavior of phononic crystals (fig. 5.5(a) and 5.5(b)) to the periodic wave propagation direction we have a reduction of the band width of the bandgap. But appear other band gaps as can be seen in the figures 5.6(a) and 5.6(b). If to increase the size of the structure keeping the same configuration is possible to see the increase of the band gaps, figures 5.7(a) and 5.7(b).

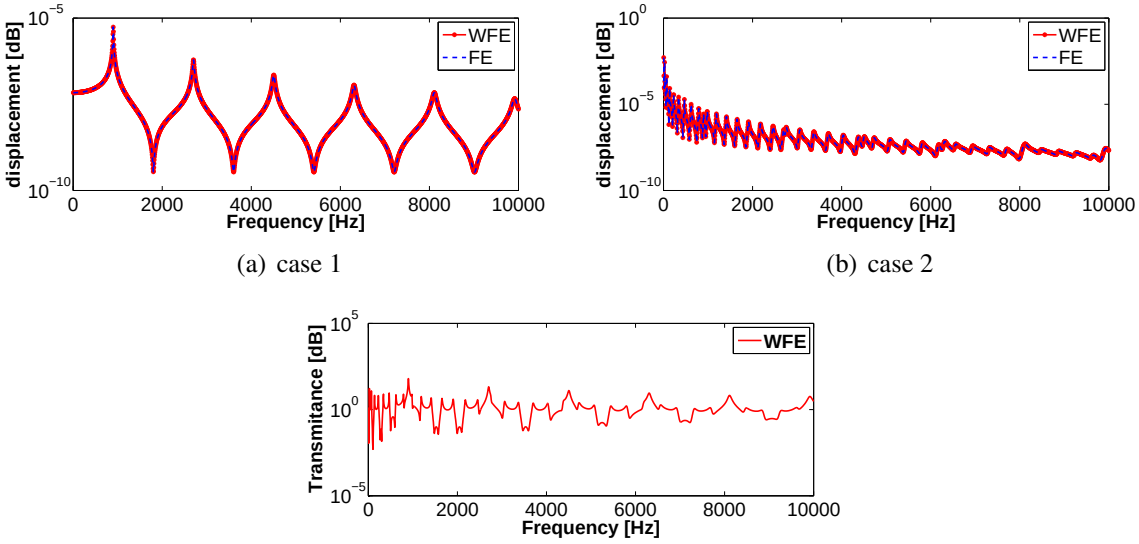

(a) case 1

(b) case 2

(c) case 2

Figure. 5.4: Case 1 and 2 displacement response by: WFE (red) and FE (blue).

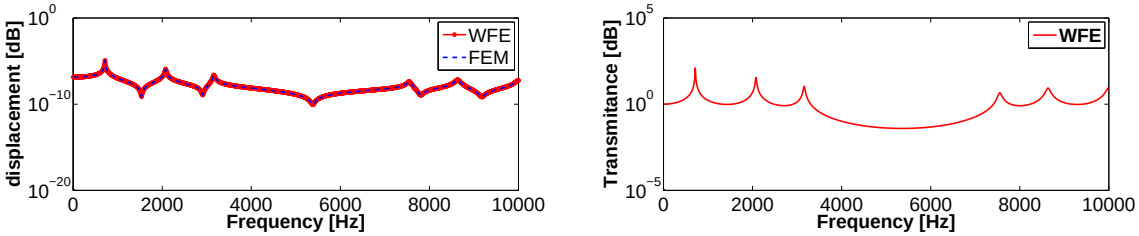

(a)

(b)

Figure. 5.5: Case 3 displacement response by: WFE (red) and FE (blue).

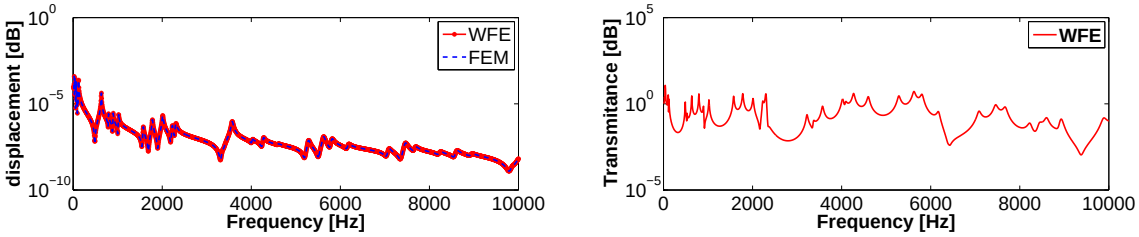

(a)

(b)

Figure. 5.6: Case 4 displacement response by: WFE (red) and FE (blue)

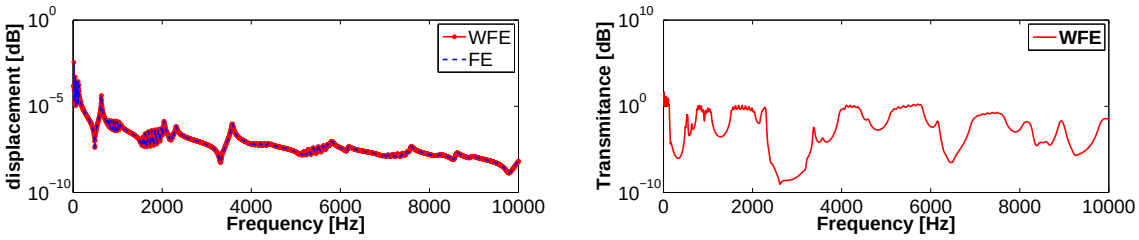

(a) (b)

Figure. 5.7: Case 4 displacement response with 18 waveguides by: WFE (red) and FE (blue).

5.3 investigating simple designs of phononic crystal plates and their influence on the wave propagation properties

This section is referenced in Nobrega *et al.* (2018). The intend is to investigate the wave propagation along periodic structures consisting of several PC flat plates arranged through a triangular shaped pattern, each rectangular plate being itself made of a periodic distribution of different material strips. In such structures involving two levels of periodic variations (related respectively to the variation of material properties in each plate, and to the angle variation between the plates), two-scale band gaps are expected to occur on different frequency bands. At a first level, band gaps are produced by the Bragg scattering effect when wavelengths of traveling waves become of the same order of magnitude than the width of a material strip. At a second level, wider attenuation zones might be achieved for appropriate angles between two PC flat plates, exploiting in particular the conversion mode phenomenon linked to the change of orientation between the plates. The aim of this is to study the influence of the coupling angle between the PC flat plates and of the periodicity pattern in each plate on the dispersion curves of the propagating modes and the frequency response functions (FRFs) of structures composed of a finite number of PC flat plates. The WFE method constitutes an efficient tool to perform this analysis.

5.3.1 Results for Flat plates

Numerical experiments are performed for various PC structures made up of an assembly of 6 plates arranged along a triangular pattern. Each plate is composed of an alternation of 3 strips (either two steel strips and one aluminum strip, or two aluminum strip and one steel strip), as depicted in Figure 5.8. The dimensions (specified in Table 5.1) and meshing properties of the different strips are chosen similar, each strip being composed of 12 identical substructures of width $d = 0.05$ in the

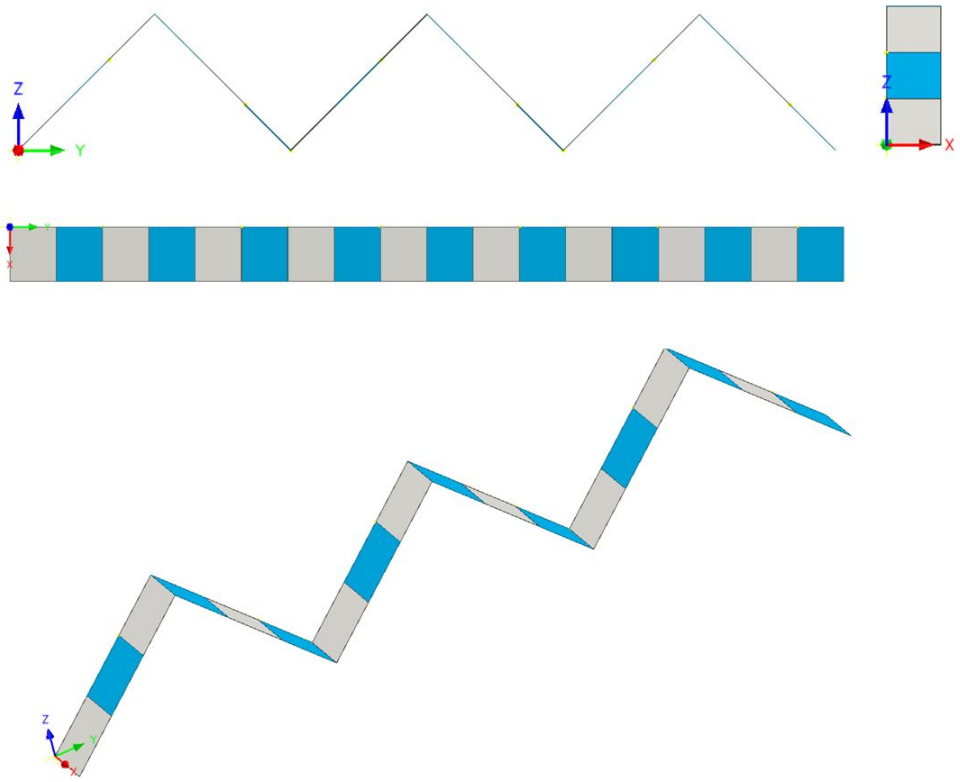

Figure. 5.8: PC structure composed of 18 alternate strips made of steel (grey color) and aluminum (blue color).

direction of propagation (y for $\theta = 0°$). The mesh of each substructure contains 1 shell element in the direction of propagation and 10 elements in the $x-$direction. The differences between the strips are linked to the properties of the chosen materials, which are also detailed in Table 5.1; for both materials, a damping is considered through a loss factor $\eta = 0.005$. The influence of the coupling angle between the plates on the responses of the PC structures is investigated by making the angle θ (between the first plate direction and the horizontal axis) varying from $0°$ to $60°$ with a step of $15°$.

Material and geometrical properties of the strips	Steel	Aluminum
$E\,[Pa]$	210^9	70^9
$\rho\,[kg/m^3]$	7800	2700
η	0.005	0.005
ν	0.3	0.3
$h\,[m]$	0.001	0.001
$L_x\,[m]$	0.5	0.5
$L_y\,[m]$	0.6	0.6

Table. 5.1: Strip configurations.

The 18 strips involved in the PC structure are supposed simply supported along their longitudinal edges. The whole PC structure is free on its left end ($y = 0$) and clamped on its right extremity ($y = y_{end}$ which depends on the θ value). A punctual harmonic excitation is applied at the node of coordinates $(0.05,0,0)$ located on the free end, with a magnitude of $1N$ in the z direction. The frequency range considered in this study is $[0; 100]$ Hz with a frequency step of 0.2 Hz.

For comparison purposes, the case of a structure composed of a single material (chosen as steel) is also presented, for the same angle configurations ($\theta = 0°$ to $\theta = 45°$ by $15°$).

The frequency responses of the structures are computed using the WFE formulations described in the Chapter 2, and compared to the reference solution obtained with the classic FE method. In the following, two quantities are considered to analyze the results obtained in the different configurations: the displacement in the $z-$direction at the forcing position (node of coordinates $(0.05,0,0)$ on the left end), and the transmittance, defined as the ratio of the reaction force in the $z-$direction at the node of coordinates $(0.05,y_{end},0)$ located on the right end to the excitation force.

The results obtained for the steel structure with $\theta = 0°$ are first presented in Figure 5.9 (displacement). A good agreement can be found in Figure 5.9 between the WFE results (solid line in blue color) and the FEM results (dotted line in red color), throughout the frequency range, with error levels far below 1%. In terms of computational times, the elapsed time obtained in Matlab for the WFE method is 607s, while the FE computation requires $2e4$s. The gain of computational time in this case reaches here about 97%, hence highlighting the efficiency of the proposed approach.

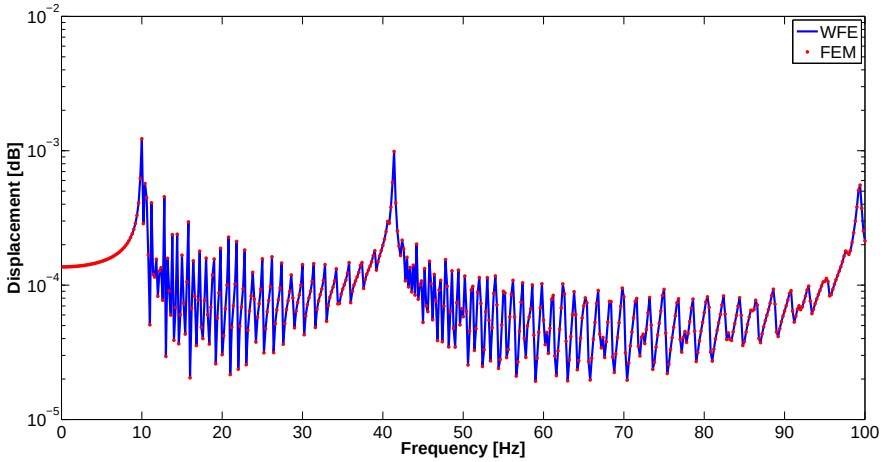

Figure. 5.9: Displacement of the steel structure with $\theta = 0°$ obtained from the WFE method (solid blue line) and the FE method (dotted red line)

The transmittance levels are affected in accordance with the prior observations on the vibration levels. A bandgap effect is created as soon as a nonzero θ angle is introduced (Fig. 5.10); the efficiency of the band gaps may be improved by increasing the value of the θ angle, the lowest levels of transmittance being in both cases obtained for $\theta = 60°$. The presence of alternate steel and aluminum strips affects locally the transmittance levels as compared to purely steel PC structure by lowering the transmittance levels at some frequencies (Fig. 5.11), for instance between 30 and 40Hz, or around 68Hz. Choosing materials with even larger discrepancies in their properties could therefore enable to increase the bandgap effects within multi-material PC structures.

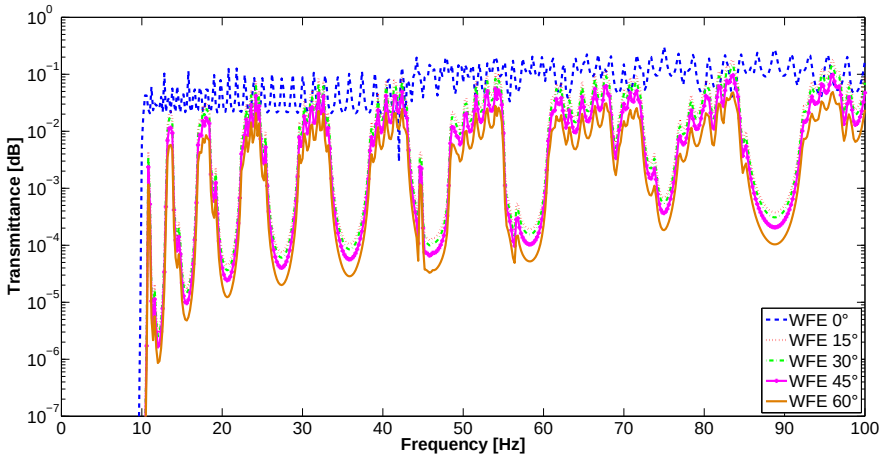

Figure. 5.10: Transmittances of the steel structure with angles θ of $0°$, $15°$, $30°$, $45°$ and $60°$ obtained from the WFE method

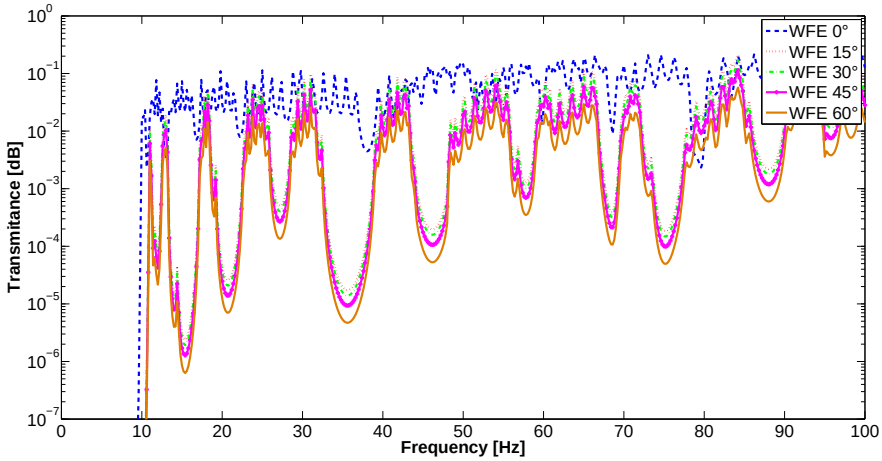

Figure. 5.11: Transmittances of the structure with alternate steel and aluminum strips and angles θ of $0°$, $15°$, $30°$, $45°$ and $60°$ obtained from the WFE method

5.4 Conclusion

In this chapter, two level PC structures composed of multi-material plates arranged along a triangular pattern have been investigated using the WFE method. The developed approach has proved efficient, in terms of accuracy and computational time, to compute the frequency responses of such structures as compared to the classic FE method. The numerical experiments carried out have shown that the triangular shape of the PC structure favors the expected band gap effect, which is all the more efficient when the structure is sharp, i.e. for small angle values between the plates or even in frames. The use of alternate steel / aluminum strips on each substructure (plate and frame) is seen to modify locally the vibration and transmittance levels in limited frequency ranges. Choosing materials with more discrepant properties could therefore enable to improve the efficiency of the band gaps in desired frequency regions.

6 METAMATERIAL PLATE USING CONTINUOUS LOCAL RESONATOR

In this section is referenced in Nobrega and Dos Santos (2019). It is shown an elastic metamaterial reinforced-plate modeling by WFE and conventional FE methods. Continuous local resonators (CLR) are designed as a mass-spring system constructed using a solid cubical block (mass) connected by four very small beams (springs) to the plate stiffener-beams (Figure 6.1). In order to attenuate the plate excitation responses, the CLRs are designed to be tuning at the second plate natural frequency. Then, the CLR's first natural frequency is tuned approximately equal to that. The reinforced-plate metamaterial behavior are analyzed using the dispersion diagram and forced responses (FRFs). The forced response calculated by WFE is verified using conventional FE method. The results shows that band gaps occur in more than one mode and the corresponding responses at these modes are attenuated. It is presented a some results of this publication.

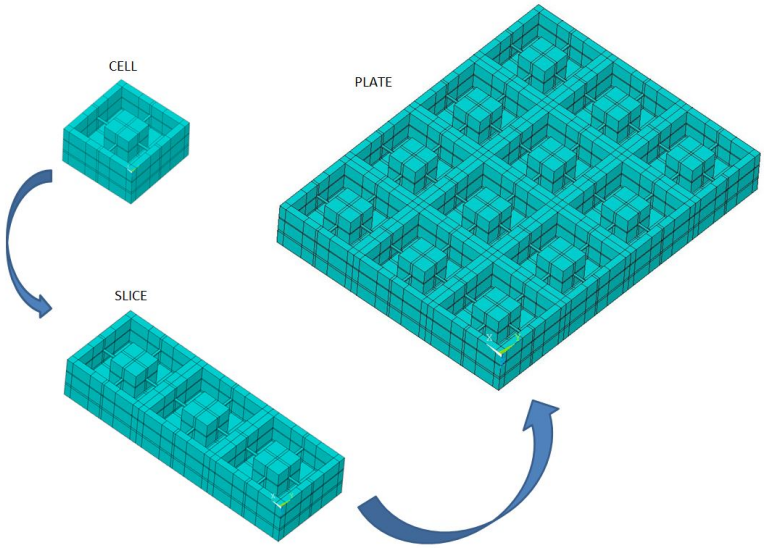

Figure. 6.1: Plate model.

6.1 Metamaterial and Continuous Local Resonator

Basically in this case, the metamaterial consists of a structure composed by divided in identical 18 identical and symmetric unit-cells arranged as an array of 3 x 6 cells (Fig. 6.1). Each unit-cell consists of a plate surrounded by stiffener-beams with a Continuous local resonator (CLR) inside. The CLR is a local resonator made with a solid cubical block (mass) connected by four small beams (springs) to the stiffener-beams. The cell was modeled with the first natural frequency tuned to the

second natural frequency of the reinforced-plate, in order to create a bandgap on this frequency. A numerical modal analyses of the CLR was performed with commercial software ANSYS considering the solid cubical block with the four small beams free and the stiffeners-beams and plate fixed. The results shows that the six first natural frequencies in a frequency band DC up to 2000 Hz are 778, 1209, 1209, 1454, 1454, 1846 with the corresponding mode shapes flexural-z, torsional-x, torsional-y, longitudinal-x, longitudinal-y, torsional-z (Fig. 6.2).

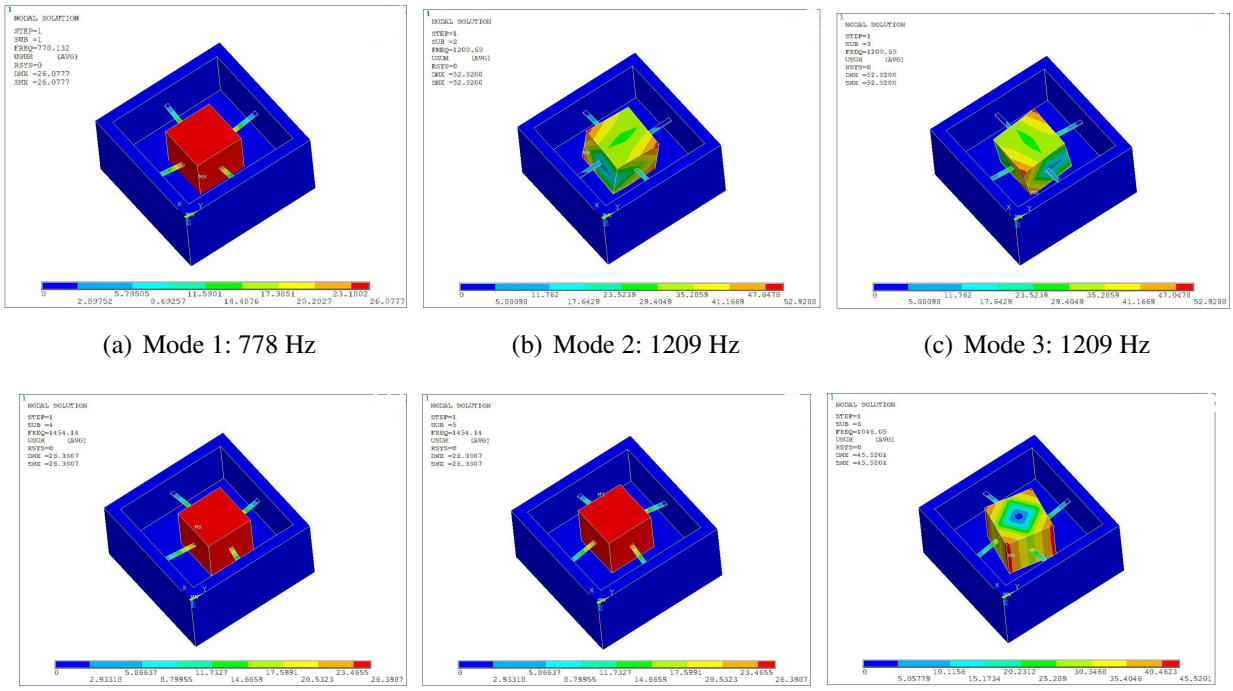

(a) Mode 1: 778 Hz (b) Mode 2: 1209 Hz (c) Mode 3: 1209 Hz

(d) Mode 4: 1454 Hz (e) Mode 5: 1454 Hz (f) Mode 6: 1846 Hz

Figure. 6.2: Cell modal analysis: the fist six modes.

6.2 Numerical Results

In this section the force response by WFE method is verified by conventional FE method and dispersion curves of a metamaterial reinforced-plate slice are calculated. The slice (Fig. 6.3(b)) was modeled by commercial software ANSYS using 2610 element type solid (SOLID185). Geometric parameters and material property are shown in Table 6.1. The plate was exited free-free in the direction z in position $y = 0$ with a load $F = 1\ N$ per node.

Figure 6.4 shows a comparison between two plates with six slices of three cells, but one with

Table. 6.1: Simulated metamaterial plate geometric parameters and material properties.

Geometry/Property	Value
Cell length[m]	37×10^{-3}
Plate thickness [m]	1×10^{-3}
Stiffener beam cross section base [m]	3×10^{-3}
Stiffener beam cross section height [m]	13.5×10^{-3}
Resonator beam cross section base [m]	1×10^{-3}
Resonator beam cross section height [m]	0.5×10^{-3}
Resonator beam length [m]	9×10^{-3}
Resonator mass side (cube) [m]	7×10^{-3}
Young's modulus (E) [Pa]	0.72×10^{9}
Mass density (ρ) [kg/m^3]	700
Structural damping (η)	0.02

resonators (Fig. 6.3(a)) and the other without resonators (Fig. 6.3(b)). As expected, the result for the plate with resonators split the second natural frequency (close to 700 Hz) in the plate without resonators in two others, and creates a bandgap with a significant amplitude attenuation at the band frequency between of approximately 600Hz and 900 Hz. However, this caused a bandgap in the interest band making a shift in the natural frequency of the structure. Moreover, the transmittance of plate with resonators caused a bandgap in the same frequencies of the natural frequencies of the cell as can seen more precisely in the comparison of figure (6.2(a)) to figure (6.4) where the difference is 2 Hz. Due to the fact that resonators were made of many DOFs, others band gaps was created around of 1,200 Hz and 1,450 Hz, which mate with the others frequencies in the modal analysis of the cell (Fig. 6.2(b), 6.2(c), 6.2(d) and 6.2(e)).

The dispersion curves were computed to a slice without and with resonators, Fig. (6.5) and (6.6), respectively. This results show the six first plate modes. It is possible to see that the slice with resonator caused a band gaps around of each natural frequencies of cell (computed by modal analysis (Fig. 6.2)). It can seen that occur in several wave modes. Probability, this was caused because of the influence of resonators that created a coupling band gaps, where many modes have gap in the similar band of frequency.

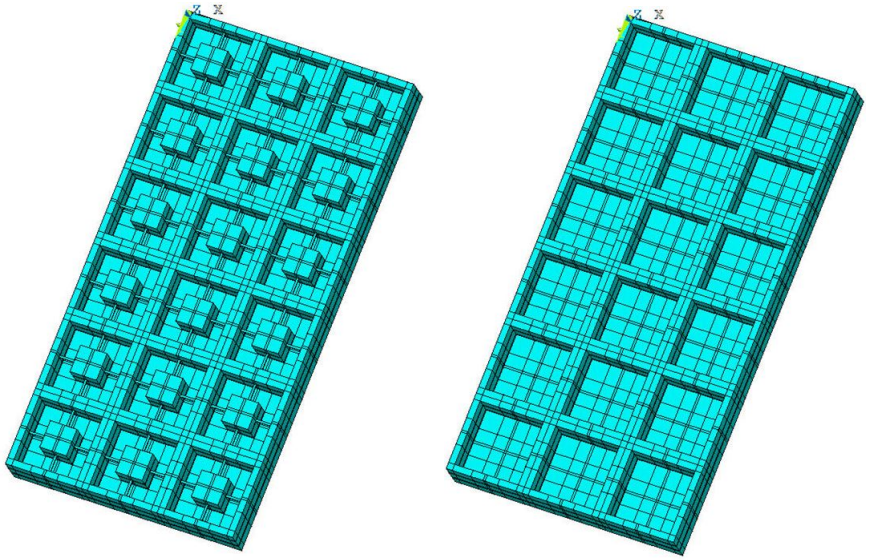

(a) (b)

Figure. 6.3: Plate with six slices with (a) and without (b) resonators.

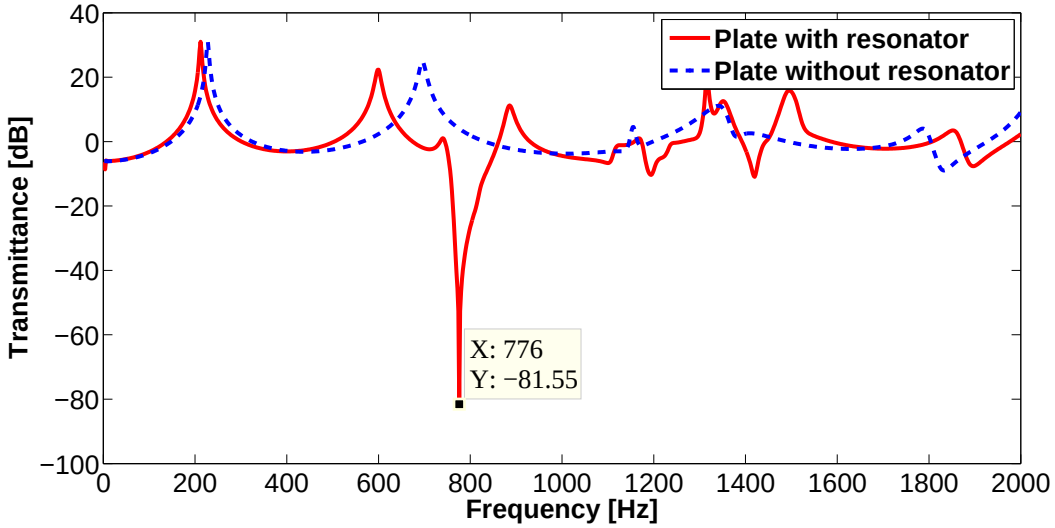

Figure. 6.4: Comparison of WFE for plates with resonators (blue sold line) and without (red dashed line) resonators.

6.3 Conclusion

Elastic metamaterial plates were investigated. A WFE method was proposed as engineering tool to calculate these elastic metamaterial plates with continuous local resonators. The vibration analysis was computed as well. Further, the results of proposed method (WFE) and FE (by ANSYS)

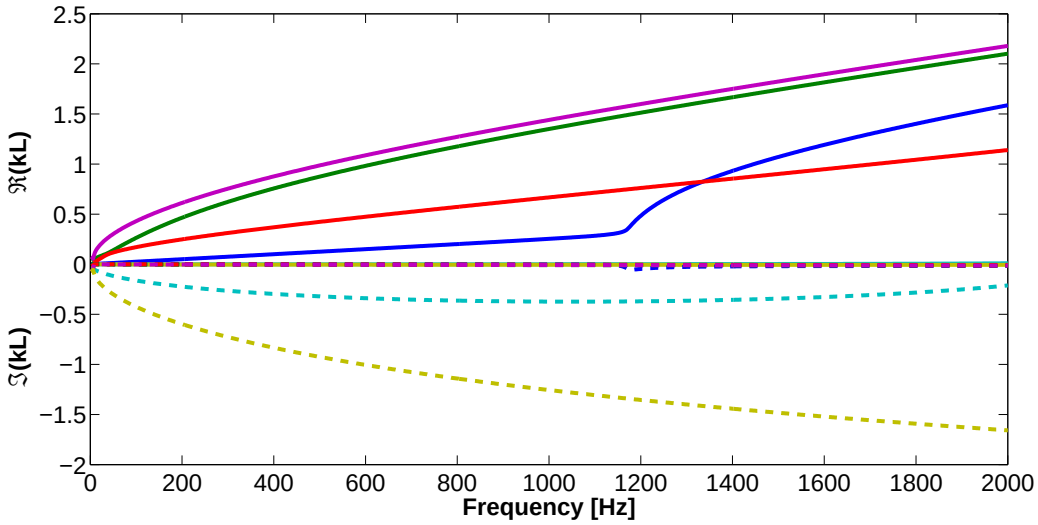

Figure. 6.5: Dispersion curves of the six first wave modes of slice: without resonators.

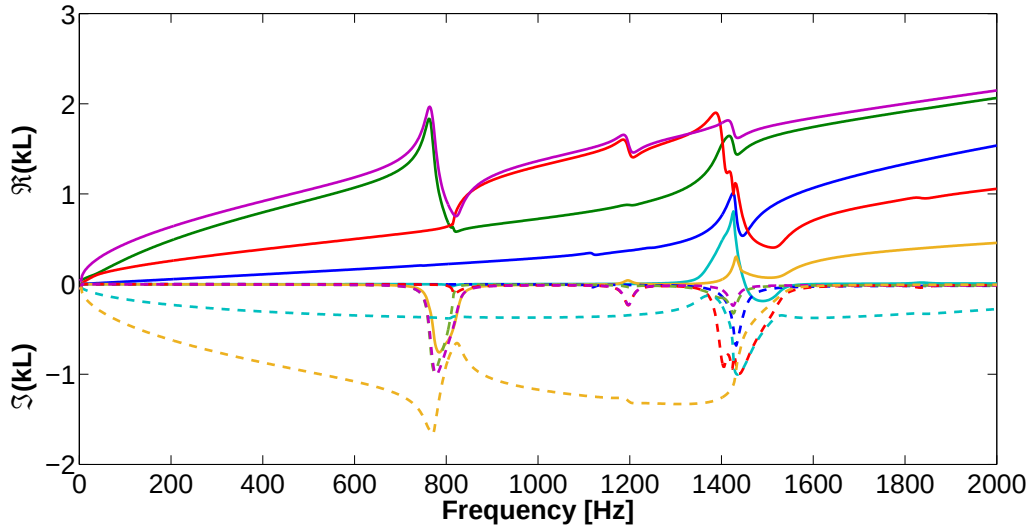

Figure. 6.6: Dispersion curves of the six first wave modes of slice: with resonators.

agree well. The comparison of plate with and without resonators shown that we can tune resonators to have band gaps in undesirable resonance frequencies. Furthermore, we shown that band gaps occur in the same frequency of the cell modes. Finally, the dispersion curves of a plate slice were shown and many modes had the similar frequency-band gap.

7 FLEXURAL WAVE BAND GAPS IN A ELASTIC METAMATERIAL PLATE WITH CONTINUOUS LOCAL RESONATOR

By using a real EM plate (Fig. 7.1) an experimental test is performed. An EM plate with square lattice is manufactured with a polymer (Vero White Plus) in a 3D printer with UV curing technology. Simulated results with finite element method (FEM), i.e. frequency response function (FRF), and with PWE method, i.e. band structure, are compared to the experimental data. Some different behaviors and mismatches between simulated and experimental results are found. These differences are reduced after a trial-and-error model updating by varying material property parameters (Young's modulus and mass density). The bandgap position and width can be localized from experimental, FE method and PWE formulations results, which are close each other. The details can be seen in Miranda *et al.* (2019). After this, new results was obtained, which include the WFE method with intention to compare FRF results and obtain the dispersion diagram. Furthermore, new results of numerical and experimental data were presented in this section using another excitation point.

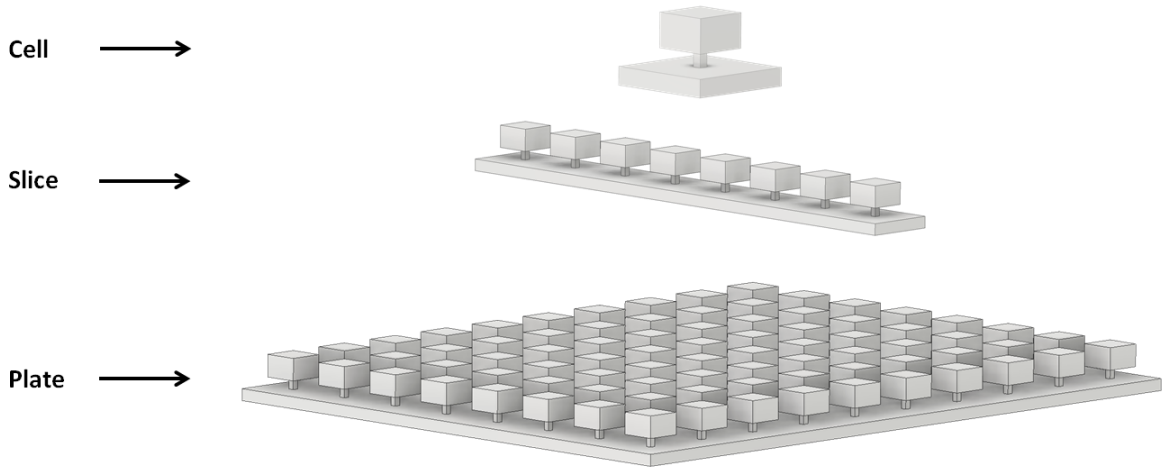

Figure. 7.1: EM plate model.

7.1 Modal analysis of EM plate

This analysis consists in a plate composed by 80 identical and symmetric unit-cells arranged as an array of 8 x 10 cells (Fig. 7.1). Each unit-cell consists of a plate with attached Continuous Local Resonator (CLR). The CLR is a local resonator made with a solid cubical block (mass) con-

nected by small beam (like spring) to the stiffener-beam. The cell is modeled with the first natural frequency tuned at $915\ Hz$, in order to create a bandgap around of this frequency. A numerical modal analysis of the CLR is performed with commercial software ANSYS with 993 DOFs using free mesh with the SOLID187 element. All displacement are fixed in the node included in all edges.. The results shows that the three first natural frequencies in a frequency band DC up to 2000 Hz are $915\ Hz$, $917\ Hz$, $1075\ Hz$ with the corresponding mode shapes torsional-x, torsional-y, torsional-z (Fig. 7.2).

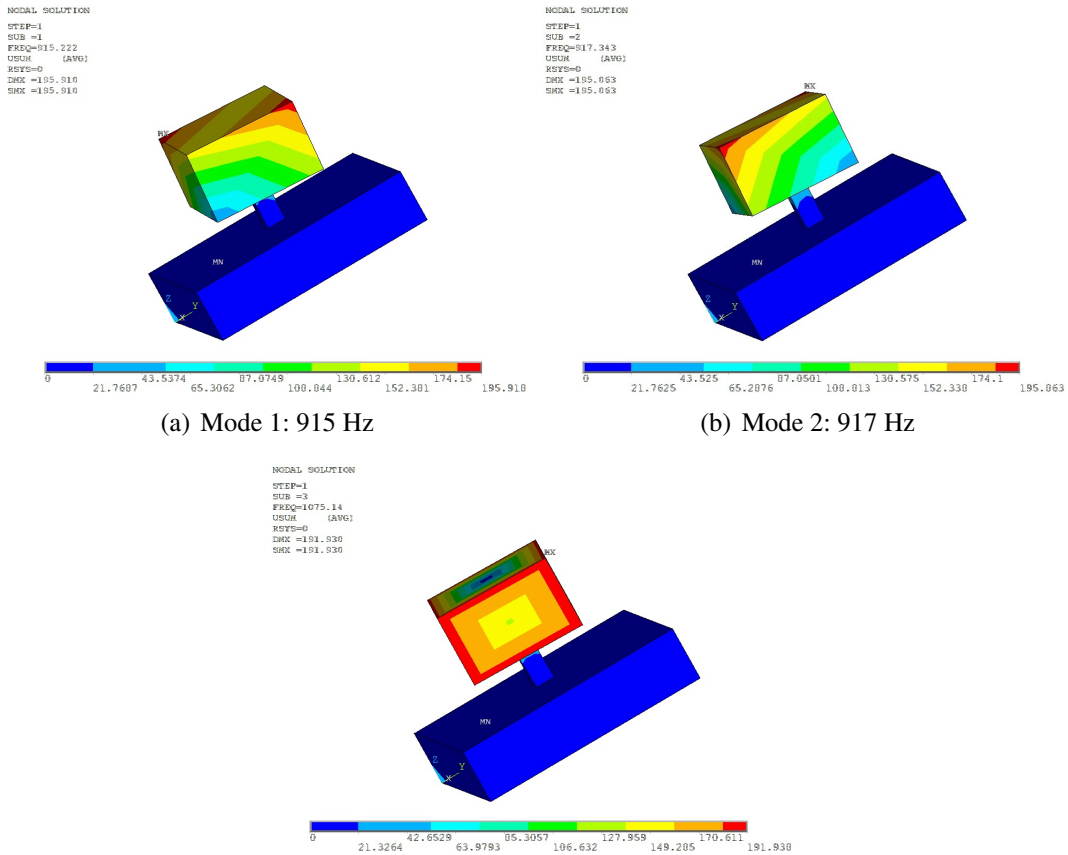

(a) Mode 1: 915 Hz

(b) Mode 2: 917 Hz

(c) Mode 3: 1075 Hz

Figure. 7.2: Modal analysis of EM plate cell with one attached local resonator.

In this second modal analysis, the EM plate (Fig. 7.1) is modeled free-free to obtain the vibration modes in order to see which band frequency the resonator have more influence on the plate behavior. As expected, it is possible to see in Fig. 7.3(a) that the plate is vibrating together with resonators, but the plate almost stop when it is vibe close to the resonants frequencies of cells (Fig. 7.3(b) and 7.3(c)) and start to vibe after these frequencies (Fig. 7.3(d)).

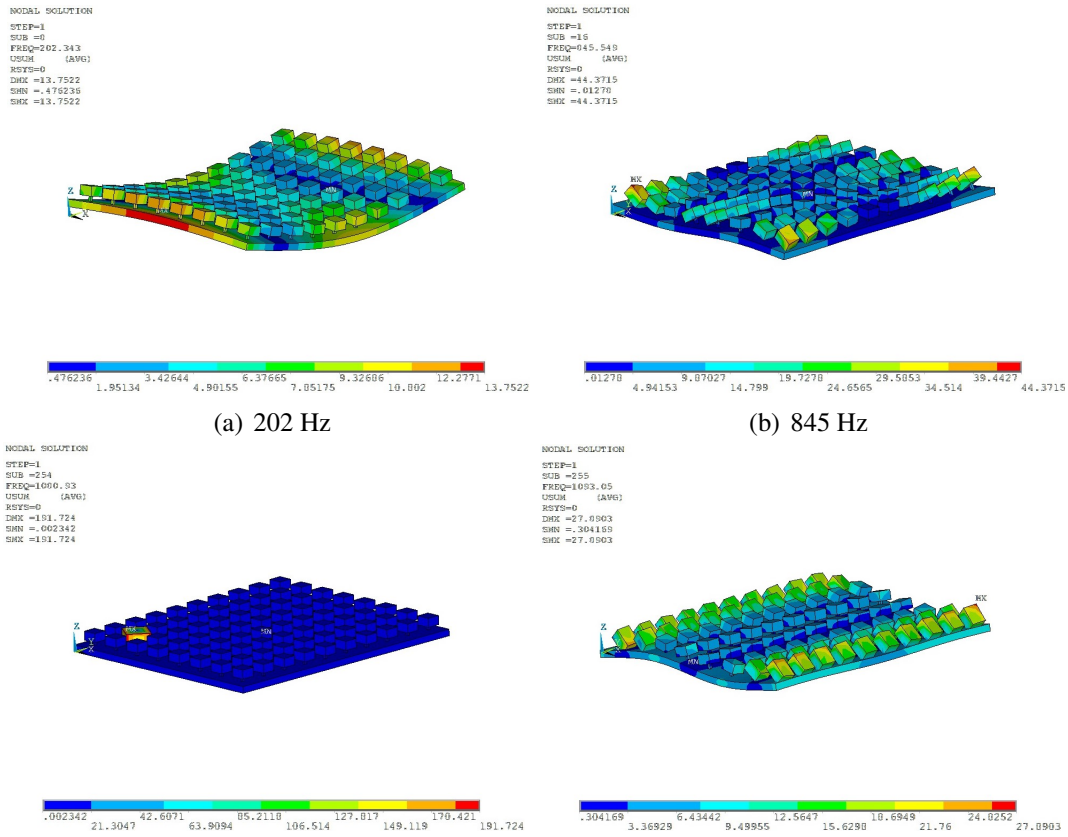

(a) 202 Hz (b) 845 Hz

(c) 1080 Hz (d) 1093 Hz

Figure. 7.3: Modal analysis of EM plate with 10 slices contain 8 cells with one attached local resonator each.

7.2 Harmonic analysis

In this section the force response by WFE method is verified by conventional FE method and dispersion curves of a metamaterial slice are calculated. The slice (Fig. 7.1) is modeled by commercial software ANSYS using 2479 nodes with solid element (SOLID187). Geometric parameters and material property are shown in Table 7.1. The plate was excited free-free in the direction z in the middle position $(48e^{-3}m, 0, 0)$ with a punctual load $F = 1\ N$. The material properties were obtain by means trial-and-error model updating.

The experiment results was obtain by means impact test as observed in the measurement setup in the figure 7.4(a). This also show a ordinary coherence function, which demonstrate that the results are consistent. The Table 7.2 contain the informations of the measurement instruments that were used in the experimental setup.

Table. 7.1: Geometric parameters and material properties of EM plate.

Geometry/Property	Value
Cell length[m]	$12x10^{-3}$
Plate thickness [m]	$2.8x10^{-3}$
Resonator beam cross section base [m]	$1x10^{-3}$
Resonator beam cross section height [m]	$1x10^{-3}$
Resonator beam length [m]	$2x10^{-3}$
Resonator mass side (cube) [m]	$3.8x10^{-3}$
Young's modulus (E) [Pa]	$0.86x10^{9}$
Mass density (ρ) [kg/m^3]	600
Structural damping (η)	0.02

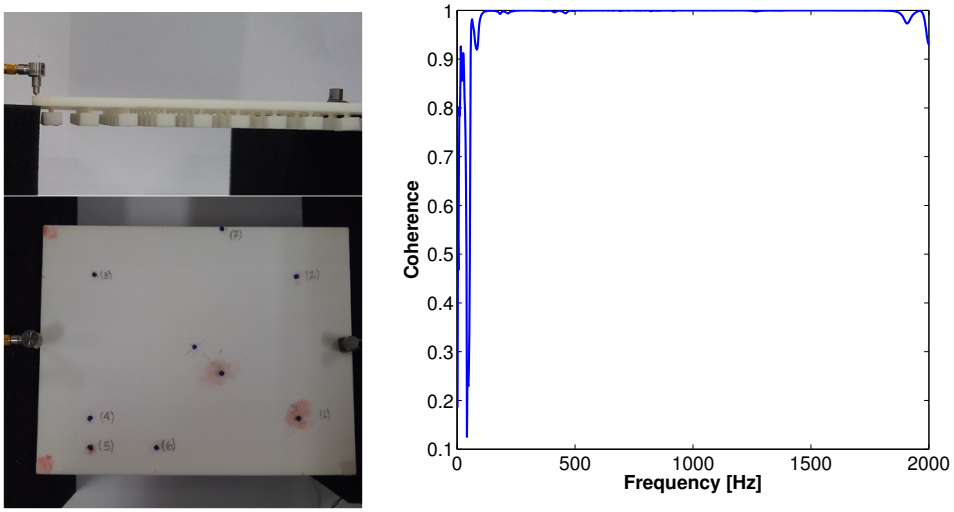

(a) (b)

Figure. 7.4: **a** - Experiment setup: EM plate exited with a Impact hammer in the middle of the left side and measured in the middle of the right side. **b** - Coherence of the experiment.

Table. 7.2: Measurement instruments.

Instrument	Manufacturer and model	Sensitivity	Measure range
Impact hammer	PCB 86E80	22.5 mV/N	222.0 N (peak)
Accelerometer	Kistler 8614A500M1	3.46 mV/g	0-25 kHz $\pm 5\%$
Data acquisition	LMS SCR05	-	-

The figure 7.5 shows FRF's comparisons between the results of WFE method with FEM and experimental testing. The WFE and FEM have a good agreement each other. It is possible see yet, that the experiment results shows a slight agreement with the modal analysis. In both numerical results, the width and position of the bandgap are coincident. The gap position is very close to the two first modes of the cell modal analysis. However, the same can not be said in relationship to

the experimental data. In this case, the result of the CLR do not create a gap, but the resonance frequencies around of local resonances (Fig. 7.2) are reduced. When it is made a comparison of this results with the modal analysis of the EM plate (Fig. 7.3), where in $845\ Hz$ and $1080\ Hz$ (Fig. 7.3(b) and 7.3(c)) the attached local resonators vibe almost alone. However, this study is not concluded doe to the bandgap appear clearly in the experiment. A comparison with a bare plate might need necessary to turn more clear the bandgap attenuation.

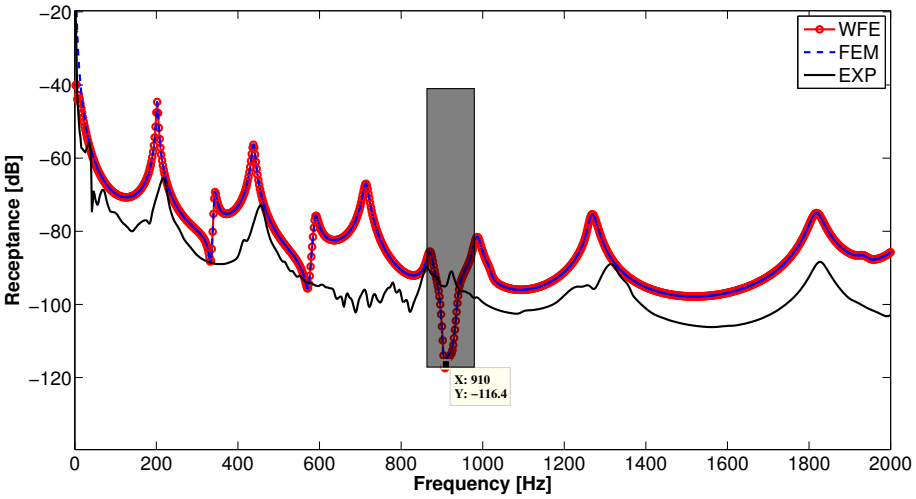

Figure. 7.5: FRFs Comparison of WFE, FE methods with experimental results. The bandgap is highlight.

The figure 7.6 shows a dispersion diagram with the seven first wave modes of a plate slice 7.1, where blue lines are real part of the wavenumber $k(\omega)L$ and red lines are the imaginary part ones. As highlighted in this figure, the bandgap appear in the same position as pointed in FRF of WFE and FEM. As commented in the last section (Chapter 6), the bandgap occur in all of the wave modes. This means that it is appear independent of the excitation type, which is different of local resonator with concentrated mass. Where Its bandgap depends of the DOFs attached local resonator.

7.3 Conclusion

A metamaterial plate was performed by Wave Finite Element method wherein the FRF and dispersion diagram were computed. As a objective to verifier the results, numerical and experimental tests were computed. In numerical comparison, modal analysis and displacement were obtained from of commercial FEM packets (ANSYS). The numerical results had a good agreement and the

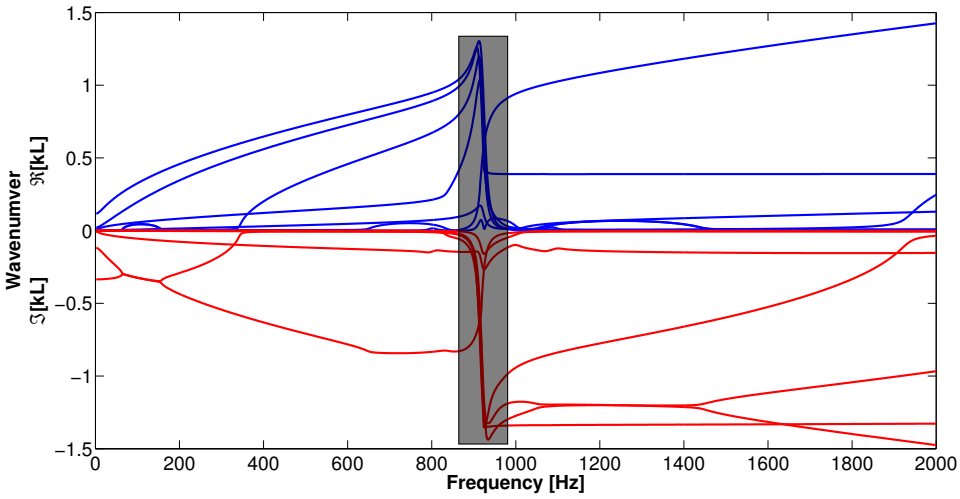

Figure. 7.6: Dispersion diagram the EM plate slice showing band gaps due to local resonance and coupling models.

band gap due to CLR appear clearly for both results. In experimental tests, it was obtained a displacement in FRF form. By comparing of the numerical and experimental tests, it was observed a slight agreement with the modal analysis and the numerical displacement. However, it was not possible to see the width and position of the band gap and more experiments with this metamaterial plate need to be made.

8 HIGHER ORDER ROD PHONONIC CRYSTAL

It is proposed formulations to calculate band gaps using Spectral Transfer Matrix (STM) and Wave Finite Element (WFE) methods from of Higher order Phononic Crystal (PC) with four cells as Fig. 8.1 . An usual transfer matrix is formulated from of a space-state vector that set the second-order ODE of a higher order rod in a first-order system analytically. Love (one wave mode), Mindlin-Herrmann (two wave modes) and Mindlin-McNiven (three wave modes) are high order rod theories presented in this work. Which besides of to use the WFE method, the Bloch-Floquet theorem to periodic rod structures is applied in the STM method to find dispersion diagrams and forced responses from Bragg wavenumbers and corresponding wave modes. The WFE method results are compared with STM method one and their numerical examples are validated with experimental data.

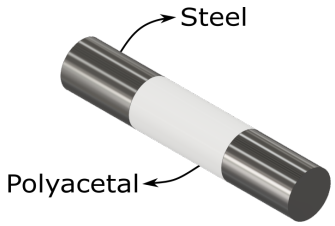

Figure. 8.1: Unit-cell PC rod scheme (steel-polyacetal-steel).

8.1 High Order Rod Models

High order rod models are mathematical formulations developed with greater complexity than the elementary rod model. The reason to use these models is due to the simplifications assumed when calculating the kinematics of deformation in the elementary rod model, where the Poisson effect associated with transverse deformations is neglected. At medium and high frequency bands, such simplifications are harmful and may lead to imprecise results. This section presents three high-order rod models formulated using energy equations, in order to obtain the transfer matrices required by WFE and STM to solve periodic structures and phononic crystal rods. For comparative purposes, it will also briefly present the formulation for the elementary rod model.

8.1.1 Elementary rod

The elementary rod model considers constant axial deformation along the cross section while disregard the transversal deformation due to Poisson's effect. Figure 8.2 shows a scheme of a two node 1D rod element with a constant cross-sectional area A, a length $L = 2a$ and a reference system positioned in the middle of the element. By using a non-dimensional coordinate $\xi = x/a$ in

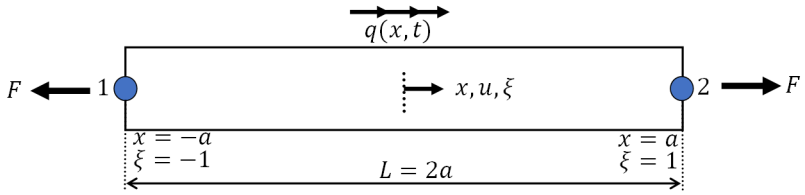

Figure. 8.2: 1D rod element and loads.

Fig. 8.2, the axial displacement can be written in matrix form as:

$$u = [N_1(\xi) \quad N_2(\xi)] \left\{ \begin{array}{c} u_1 \\ u_2 \end{array} \right\} = \mathbf{N}(\xi)\mathbf{u}, \tag{8.1}$$

where $N_j(\xi) = \frac{1}{2}(1+\xi_j\xi)$ and ξ_j are the coordinates of nodes j. The u_j is the axial displacement at node j. From of the strain and kinetic energies, (PETYT, 2010) it is obtained the mass and stiffness matrices of the elementary rod for a single element (Fig. 8.2), witch are given as:

$$\begin{aligned} \mathbf{K}_E^{(e)} &= \frac{EA}{2a} \begin{bmatrix} 1 & -1 \\ -1 & 1 \end{bmatrix} \\ \mathbf{M}_E^{(e)} &= \frac{\rho A a}{3} \begin{bmatrix} 2 & 1 \\ 1 & 2 \end{bmatrix} \end{aligned} \tag{8.2}$$

where E is the Young's modulus, ρ is mass density and A is the cross section area.

8.2 Love's rod

Like the elementary rod model, the Love's rod model has only one wave mode. However, it includes the transversal strain (contraction) due to the Poisson effect, caused by longitudinal strain of the structure (LOVE, 1927). This effect is included in the formulation as a transverse velocity of

strain in the kinetic energy calculation.

Consider the same two-node rod finite element scheme shown in Fig. 8.2, but now with a circular cross section of radius r. Its transverse strain is related to the axial strain by $\varepsilon_t = -\nu\varepsilon$, so the transverse velocity can be written as (LOVE, 1927),

$$\dot{u}_t = r\dot{\varepsilon}_t = -\nu r\dot{\varepsilon} = -\nu r\frac{\partial \dot{u}}{\partial x}, \tag{8.3}$$

where $\dot{u}$ e $\dot{u}_t$ are the longitudinal and transversal velocities, respectively, and ν is Poisson's rate. By using the kinetic energy of Love's rod, the mass matrix stay:

$$\mathbf{M}_L^{(e)} = \frac{\rho A a}{3}\begin{bmatrix} 2 & 1 \\ 1 & 2 \end{bmatrix} + \frac{\rho\nu^2 J}{2a}\begin{bmatrix} 1 & -1 \\ -1 & 1 \end{bmatrix}, \tag{8.4}$$

where J is the polar moment of inertia. The stiffness FE rod element matrix is the same as the one obtained with the rod elementary theory, i.e., $\mathbf{K}_L^{(e)} = \mathbf{K}_E^{(e)}$.

8.3 Mindlin-Herrmann's rod

The Mindlin-Herrmann rod theory, or the two wave modes approach, consists of adding the shear strain due to transversal displacement into Love's model. For the WFE approach, consider the two-node 2D rod element scheme shown in Fig. 8.3 with a circular cross section and reference system (x,y) positioned in the middle of the element.

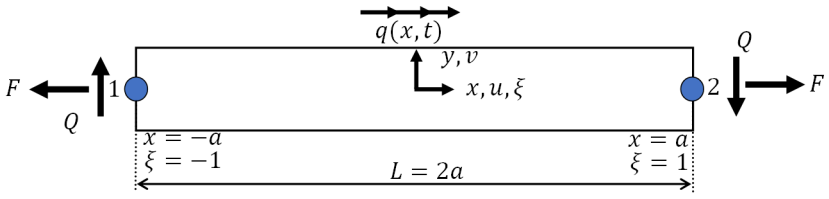

Figure. 8.3: 2D rod finite element model.

A simple strain field conformable with the axial motion is given by (MINDLIN AND HERRMANN, 1950):

$$\bar{u}(x,y) \approx u(x), \qquad \bar{v}(x,y) \approx \psi(x)y, \tag{8.5}$$

where these displacement equations consider lateral displacements, but ignore the distribution of axial displacement in the cross section. Taking Eq. (8.5) to obtain the stresses and strains, and then substituting it into the strain energy, it is possible to find the stiffness FE rod element matrix for Mindlin-Herrmann's rod theory:

$$\mathbf{K}_{MH}^{(e)} = \begin{bmatrix} \mathbf{K_u} & \frac{1}{2}\mathbf{K_a} \\ \frac{1}{2}\mathbf{K_a}^T & \mathbf{K}_\psi \end{bmatrix}, \tag{8.6}$$

where these stiffness sub-matrices are given as:

$$\begin{aligned} \mathbf{K_u} &= (2\mu+\lambda)\frac{A}{2a}\begin{bmatrix} 1 & -1 \\ -1 & 1 \end{bmatrix} \quad \mathbf{K_a} = \lambda A \begin{bmatrix} -1 & -1 \\ 1 & 1 \end{bmatrix}, \\ \mathbf{K}_\psi &= (2\mu+\lambda)\frac{Aa}{3}\begin{bmatrix} 2 & 1 \\ 1 & 2 \end{bmatrix} + \frac{\mu I}{2a}\begin{bmatrix} 1 & -1 \\ -1 & 1 \end{bmatrix} \end{aligned} \tag{8.7}$$

where $\lambda = \nu E/(1+\nu)(1-2\nu)$ and $\mu = E/2(1+\nu)$ are Lamé's parameters.

Similarly, from of the kinetic energy, the mass FE rod element matrix for Mindlin-Herrmann's rod theory is obtained as:

$$\mathbf{M}_{MH}^{(e)} = \begin{bmatrix} \mathbf{M_u} & \mathbf{0} \\ \mathbf{0} & \mathbf{M}_\psi \end{bmatrix}, \tag{8.8}$$

where the mass sub-matrices are given as:

$$\mathbf{M_u} = \frac{\rho A a}{3}\begin{bmatrix} 2 & 1 \\ 1 & 2 \end{bmatrix}, \quad \mathbf{M}_\psi = \frac{C_2 \rho I a}{3}\begin{bmatrix} 2 & 1 \\ 1 & 2 \end{bmatrix}. \tag{8.9}$$

8.4 Mindlin-McNiven's rod

This approach modifies Mindlin-Herrmann's rod theory, by adding a parabolic term that varies along the rod cross section into the longitudinal displacement.

Figure 8.3 shows a two nodes rod element scheme, where the deformations are expanded

in a Taylor series and an additional term is maintained at each expansion to obtain approximate displacements (DOYLE, 1997),

$$\bar{u}(x,y) \approx u(x) + \phi(x)h(1 - 12y^2/h^2), \quad \bar{v}(x,y) \approx \psi(x)y, \tag{8.10}$$

Using Eq. (8.10) to obtain the stresses and strains, and then substituting into the strain energy, the stiffness FE rod element matrix for Mindlin-McNiven's rod theory is obtained as:

$$\mathbf{K}_{MN}^{(e)} = \begin{bmatrix} \mathbf{K_u} & \frac{1}{2}\mathbf{K_a} & \mathbf{0} \\ \frac{1}{2}\mathbf{K_a}^T & \mathbf{K}_\psi & \frac{1}{2}\mathbf{K_b} \\ \mathbf{0} & \frac{1}{2}\mathbf{K_b}^T & \mathbf{K}_\phi \end{bmatrix}. \tag{8.11}$$

Similarly, the mass element matrix can be obtained as,

$$\mathbf{M}_{MN}^{(e)} = \begin{bmatrix} \mathbf{M_u} & \mathbf{0} & \mathbf{0} \\ \mathbf{0} & \mathbf{M}_\psi & \mathbf{0} \\ \mathbf{0} & \mathbf{0} & \mathbf{M}_\phi \end{bmatrix}. \tag{8.12}$$

The $\mathbf{K}_\phi$, $\mathbf{K}_b$ and $\mathbf{M}_\phi$ of Eqs. 8.11 and 8.12 are given as:

$$\begin{aligned} \mathbf{K}_\phi &= \frac{(2\mu+\lambda)A}{2a}\frac{4h^2}{5}\begin{bmatrix} 1 & -1 \\ -1 & 1 \end{bmatrix} + \frac{24^2\mu I a}{3h^2}\begin{bmatrix} 2 & 1 \\ 1 & 2 \end{bmatrix} \\ \mathbf{K}_b &= \frac{-48\mu I}{2h}\begin{bmatrix} -1 & -1 \\ 1 & 1 \end{bmatrix} \\ \mathbf{M}_\phi &= \frac{4\rho A h^2 a}{15}\begin{bmatrix} 2 & 1 \\ 1 & 2 \end{bmatrix}. \end{aligned} \tag{8.13}$$

8.5 Numerical and Experimental Results

To verify the performance and efficiency of the three high order rod models (Love, Mindlin-Herrmann, Mindlin-McNiven) using the WFE and STM to calculate band gaps and forced responses in periodic structures and phononic crystal rods, numerical simulations and an experimen-

tal test were executed.

Figure 8.4 shows a picture of the unit-cell PC rod arrangement made with steel and polyacetal. The PC rod sample (Fig. 8.4) was originally developed in the Vibroacoustic Laboratory (LVA)

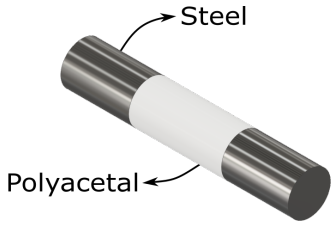

Figure. 8.4: Unit-cell PC rod scheme (steel-polyacetal-steel).

at UNICAMP to analyze and verify a PC rod model based on the elementary rod theory (SILVA *et al.*; GOLDSTEIN *et al.*, 2011b; 2011) and another PC beam model based on the Euler-Bernoulli theory (MIRANDA JR. AND SANTOS, 2017). The original design was focused manly on verifying the capacity of these theories to predict band gaps. The PC rod unit-cell material properties and geometry used in the numerical predictions are presented in Tables 8.1 and 8.2, respectively. The material properties of steel and polyacetal (Tab. 8.1) are nominal values extracted from engineering books and manufacturer catalogues (ASHBY; MAT, 2011; 2019). For the simulated numerical models the material properties of steel and polyacetal are updated (by try-and-error) in order to improve the adjustment between numerical and experimental curves. The dimensions in Tab. 8.2 were obtained by measurements of the PC rod parts (steel and polyacetal) using a digital caliper.

Table. 8.1: PC rod unit-cell nominal material property.

Property	Steel	Polyacetal
Elastic Modulus [GPa]	207	2.81
Density[kg/m^3]	7850	1580
Poisson's ratio	0.30	0.43
Loss factor	0.01	0.02

Table. 8.2: PC rod unit-cell geometry.

Phononic crystal	Cylindrical Rod	
Parameter	Steel	Polyacetal
Diameter [mm]	18.75	18.75
Length [mm]	29.40	40.90

The PC rod is built with cylindrical rods of steel and polyacetal made in a machine shop,

and then the parts are bonded with cyanoacrylate glue. The arrangement of unit-cell PC rod is Steel-Polyacetal-Steel and the whole structure is made with $N = 4$ unit-cells.

A free-free boundary condition was used for the experimental measurement of forced responses. Figure 8.5 shows the measurement setup (top) and the dimensions of the experimental PC rod (bottom). Figure 8.5 (top) shows the PC rod structure supported by foam, excited on the left end by an impulsive force hammer and the acceleration response measurement is obtained on the right end. For each hammer impact the inertance FRF and the ordinary coherence between output signal (acceleration) and input signal (force) are obtained in the Data Acquisition system at the frequency band of DC-20 kHz with 25 Hz frequency discretization (sample rate = 20480 Hz). Then Data Acquisition software makes the average with the next signal acquisition and the process is repeated until 15 averages are reached. Measurement instruments used in the experimental setup are listed in Table 8.3.

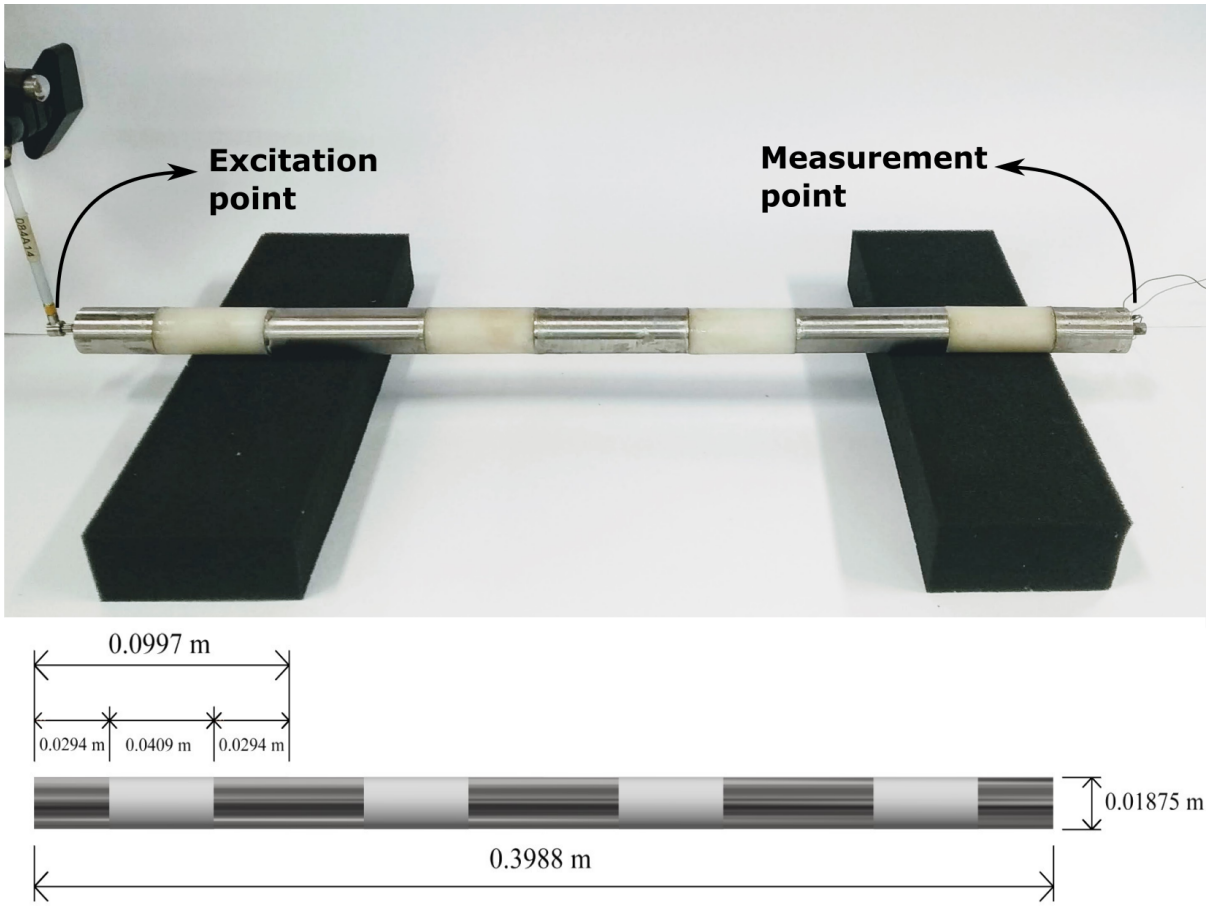

Figure. 8.5: Measurement setup (*top*) and PC rod dimensions (*bottom*).

Table. 8.3: Measurement instruments.

Instrument	Manufacturer and model	Sensitivity	Measure range
Impact hammer	PCB 86E80	22.5 mV/N	222.0 N (peak)
Accelerometer	Kistler 8614A500M1	3.46 mV/g	0-25 kHz $\pm 5\%$
Data acquisition	LMS SCR05	-	-

8.5.1 Numerical verification

Verification of WFE and STM methods was done with a numerical homogeneous periodic rod structure (PS-NH) made of polyacetal, with $N = 5$ cylindrical unit-cells of 25 mm diameter by 30 mm length. The PS-NH is evaluated using the elementary (EL), One mode or Love (LO), Two modes or Mindlin-Herrmann (M-H) and Three modes or Mindlin-McNiven (M-N) rod theories implemented in the WFE and STM methods. The PS-NH rod unit-cell is modeled using 03 STM rod elements of two nodes, while by WFE it is modeled using 75 two node FE rod elements. Dispersion diagrams and the inertance frequency response functions (FRF), with force excitation at one end and acceleration response at the opposite end, are calculated for the frequency band $f_b = [1.0Hz - 100.0kHz]$ with $25.0Hz$ frequency discretization as shown in Fig. 8.6.

Figure 8.6(a) shows the dispersion diagram and inertance FRF for the PS-NH calculated with the Elementary model (one mode) using WFE and STM. The results calculated by WFE are in good agreement with that of STM. The dispersion diagram presents a typical rod periodic structure result. The real part of dimensionless Bloch wavenumber ($\Re\{kL_c\} = 0 \sim \pi$) is a "zig-zag" of straight lines between zero and the Bragg limit (π), while the imaginary part is zero ($\Im\{kL_c\} = 0$). These results characterize a purely propagating wave mode. Also, the inertance FRF presents an expected result, with 16 peaks at the natural frequencies of the rod and a small attenuation along the analyzed frequency band due to material internal damping, which is included in the models as a complex loss factor. Similar results are observed for the one mode or Love's model (Fig. 8.6(b)). Although results calculated by both methods (WFE and STM) are in good agreement, some small changes where observed when compared to EL model. The dispersion diagram reveals an increase in the number of "zig-zags" of $\Re\{kL_c\}$ at the same frequency band used by the EL model. Likewise, there are twice the number of natural frequency peaks (32 peaks) in the Inertance FRF. These changes seem to be due to the inclusion of lateral strain in Love's model, which allows for it to take into account the displacement of an indirect transversal DOF related to lateral strain. Figure 8.6(c) shows the dispersion diagram and inertance FRF results for the two-mode or Mindlin-Herrmann's model. Results calculated by WFE and STM are in agreement. As expected, two wave modes appear in the dispersion diagram, where mode 1 (blue line) has similar behavior to EL and

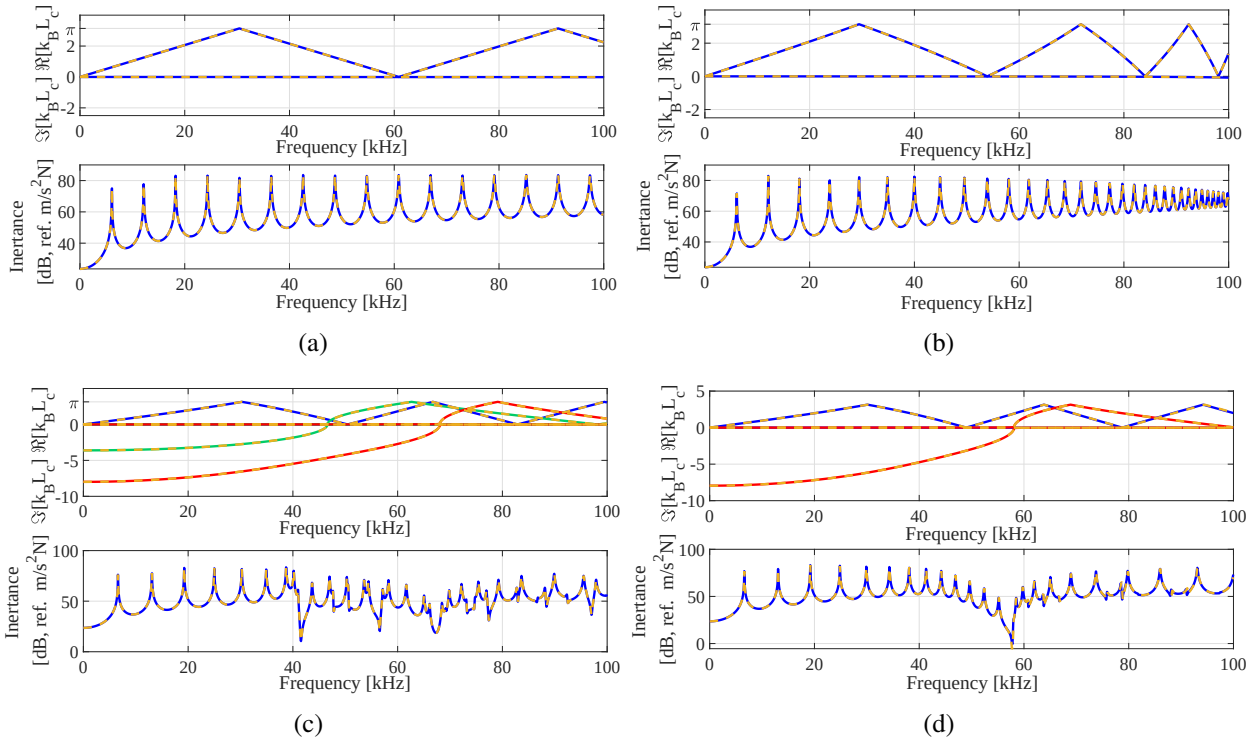

Figure. 8.6: Dispersion diagrams and Inertance FRFs for PS-NH obtained by STM (solid line) and WFE (dotted line) for rod models: a) Elementary (E); b) Love (L); c) Mindlin-Herrmann (M-H); d) Mindlin-McNiven (M-N); and corresponding Bloch wave modes: Mode 1 (−); Mode 2 (−); and Mode 3 (−).

LO models, in which only $\Re\{kL_c\} \neq 0$, while mode 2 (red line) is quite different. At $kL_c = 0$ mode 2 presents a *cut-off* frequency ($\omega_c = \sqrt{(2\mu + \lambda)A\rho IC_2}$) (DOYLE, 1997), below which mode 2 is purely evanescent ($\Re\{kL_c\} = 0$ and $\Im\{kL_c\} \neq 0$), and above which it is purely propagating ($\Re\{kL_c\} \neq 0$ and $\Im\{kL_c\} = 0$). Since ω_c is inversely proportional to the rod cross-section height or radius, slender rods present a high cut-off frequency. For the M-H model of PS-NH the cut-off frequency $\omega_c = 58.11$ kHz. The cut-off frequency also modifies the inertance FRF by increasing the mode 2 attenuation in a frequency band just before ω_c. Figure 8.6(d) shows the dispersion diagram and inertance FRF for the three modes or Mindlin-McNiven model. Results are similar to the M-H model with the inclusion of mode 3. Results for mode 3 are very close to that of mode 2, and there are two cut-off frequencies, given by $\omega_{c_1} = \sqrt{5\mu A/\rho I}$ and $\omega_{c_2} = \sqrt{(2\mu + \lambda)A/\rho IC}$ (DOYLE, 1997). In this case $\omega_{c_1} = 46.5$ kHz and $\omega_{c_2} = 68$ kHz. The attenuation effect due to the cut-off frequencies also appears in the M-N model inertance FRF.

8.5.2 Experimental validation

To validate high-order rod models using the WFE method, experimental tests have been carried out and the results are compared. The figure 8.7 shows the experimental FRF (top) and the corresponding ordinary coherence (bottom) measured on the PC rod shown in the figure 8.5. The FRF of experimental inertance of the PC rod exhibits a broadband attenuation (4.5-18 kHz), which corresponds to the Bragg numeric band interval. Within the bandgap region there are noise effects and a peak in the 8 to 10 kHz range. As expected, the corresponding coherence curve falls, indicating a loss of linearity in the bandgap region. The noise comes from the limit of the dynamic range of the accelerometer. The peak appears to be related to the beam mode generated in the excitation of the PC rod, due to errors of conformity and concentricity of the glue between the cylindrical parts of the PC rod due to the assembly process.

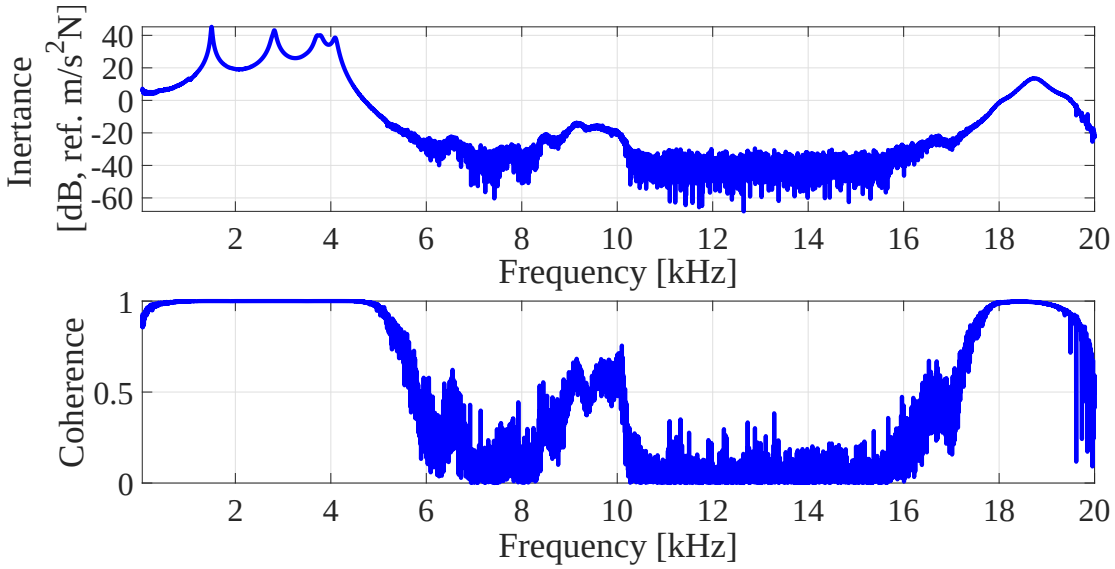

Figure. 8.7: Experimental data of the PC rod: inertance FRFs (*top*) and its coherence (*bottom*)

Numerical inertance FRFs are computed with the nominal material properties (MP) (Tab. 8.1) using WFE rod models (EL, LO, MH, MN) and its results were compared with the experimental FRF inertance (Fig. 8.8).

The numerical inertance FRFs calculated with the EL and LO models by the WFE combine between DC and 14.0 kHz. However, as the frequency increases, a shift between the curves appears, which was expected based on the differences in the formulations of the models. Numerical FRFs (EL and LO) are shifted to lower frequencies compared to the experimental one (Exp). The figure 8.8 shows that the numerical FRFs of the M-H and M-N models combine in the DC-14.0 kHz

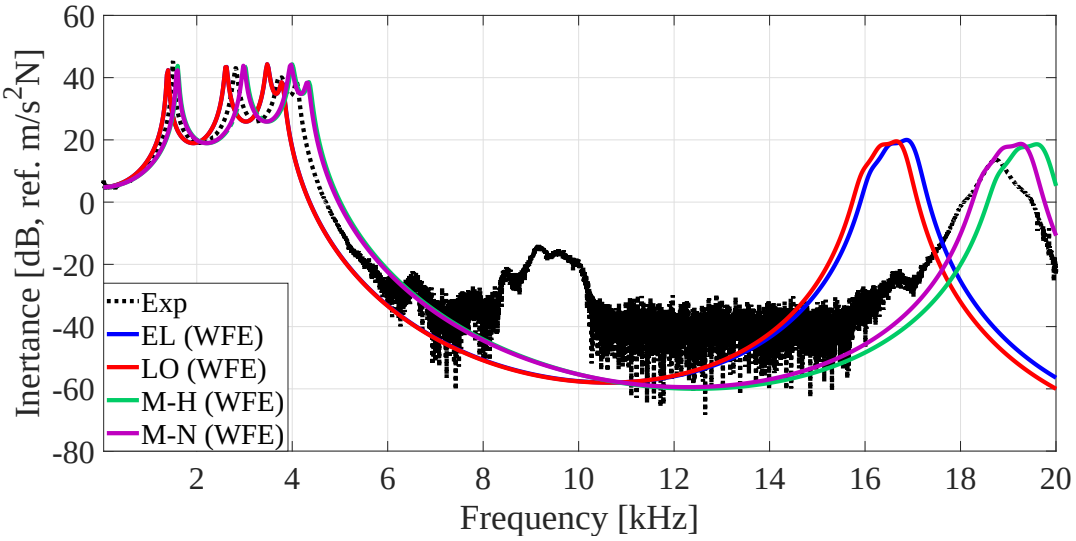

Figure. 8.8: PC rod Inertance FRFs experimental and numerical calculated with nominal material properties by WFE with EL, LO, M-H and M-N models.

frequency range, but disagree as the frequency increases. Comparing numerical (M-H and M-N) and experimental (Exp) FRFs, M-H and M-N are shifted to higher frequencies, as related to Exp. Based on these results (Fig. 8.8), it can note that all numerical curves are relatively close to the experimental data. Therefore, it is possible to infer that, using a simple model update procedure (trial and error), it is possible to obtain a good fit between the numerical and experimental curves. Considering that the material properties are important sources of uncertainties in the numerical/-analytical models, a try-and-error model update process was applied, where the model parameters (E, ρ and ν) are varied, one at a time, to obtain a FRF inertance curve that best fits the experimental one. The process is repeated until a reasonable fit between the curves is achieved and the updated material properties are recorded.

For the first update model, the Elementary and Love's models calculated by WFE were used and the best fit between the FRFs of experimental and numerical inertance was found using the material property values shown in Table 8.4.

Table. 8.4: First Updating - MP of PC rod unit-cell.

Property	Steel	Polyacetal
Elastic Modulus [GPa]	190	3.3
Density[kg/m^3]	7800	1410
Poisson's ratio	0.30	0.43

In the figure 8.9 the results obtained through WFE for the EL, LO, M-H and M-N models are compared with the experimental data (Exp). The EL and LO models converge in the DC-14 kHz

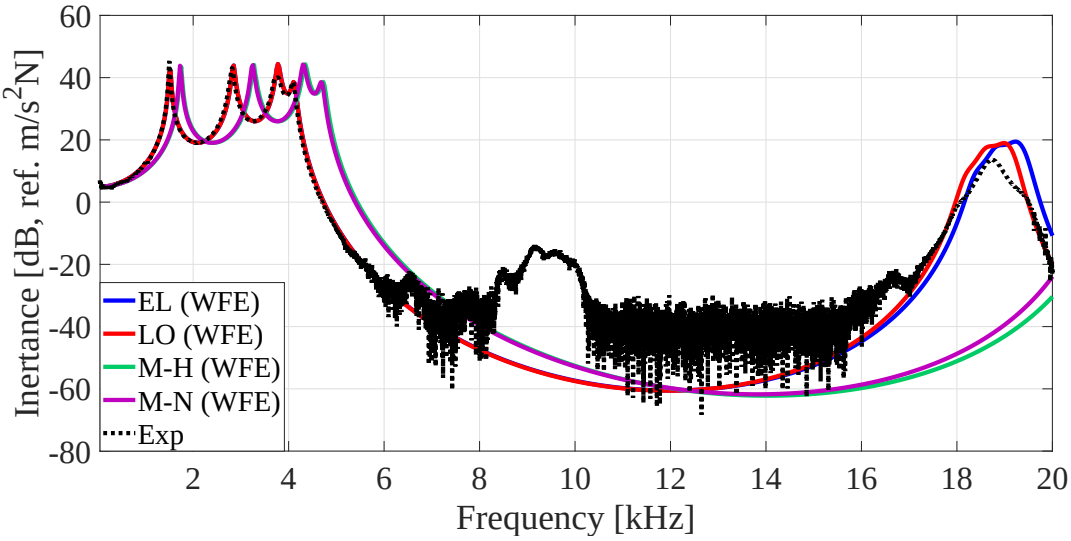

Figure. 8.9: PC rod Inertance FRFs experimental and numerical with 1st material properties updating by WFE with EL, LO, M-H, M-N models.

frequency range, whereas as the frequency increases these results start to diverge. When comparing these results with the experimental data, a better approximation for the LO model is observed. The same behavior is noticed when comparing the M-H and N-M models, where there is a good agreement between these models in the DC-14kHz frequency band, but soon after that band, the results start to diverge. It can be seen that the numerical results calculated by M-H and M-N are shifted to higher frequencies compared to the numerical results, in such a way that the last peak of the numerical result cannot be observed in the analyzed frequency band. Accordingly, a good approximation of the numerical curves (models M-H and M-N) with the experimental ones cannot be observed. Therefore, for this configuration of properties (Tab. 8.4) the low order models (EL and LO) present a good approximation for thin rod PC. This statement was also observed in Love's rod theory (DOYLE, 1997).

A new update of models properties was carried out in order to approximate models results of two and three modes (M-H and M-N) to the experimental results. In this analysis, it was possible to obtain better numerical results maintaining almost all the values in the table 8.4 except for the elasticity module, in which a reduction of 25.75 % was made from the current value, leaving $E_{poly} =$ 2.45 GPa.

The numerical results for this second parametric update are shown in the figure ref fig: high-FRF, where it is possible to observe an inverse behavior of the previous one. That is, the higher-order PC rod models (M-H and M-N) are closer to that of the experiment than the lower-order models (EL and LO).

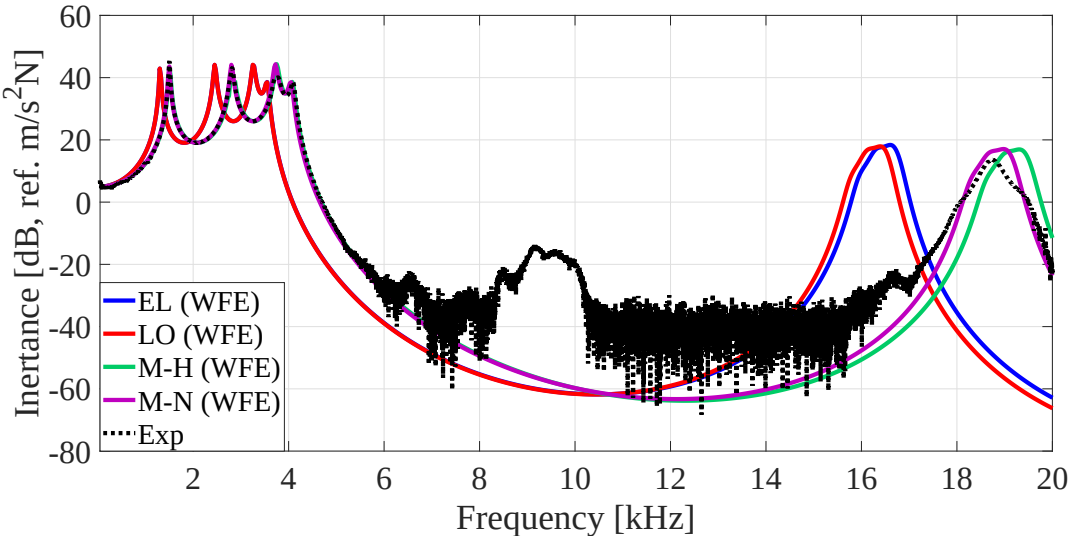

Figure. 8.10: PC rod Inertance FRFs experimental and numerical calculated with 2nd updating material properties by WFE with EL, LO, M-H, M-N models.

Observing the results of the 1st and 2nd update of the parameters, it is possible to see that, for both models, it was possible to obtain a good agreement by varying only the elasticity module: E = 3.3 GPa for the EL and LO models; and E = 2.45 GPa for models M-H and M-N). This was due to the differences in mathematical approximations of the models, where for the EL and LO models the PC rod becomes more rigid (models with only one degree of freedom). Whereas the highest order models (M-H and M-N) have two degrees of freedom, and therefore are more accurate at higher frequencies ref doyle1995.

In the observation of the numerical results of the dispersion diagram and the FRF of experimental inertance, it is possible to clearly see the predominant region of the band gap in relation to the two updates of the material properties (Fig. 8.11). In the figure 8.11(a) the first update is shown, in which the best approximation is for the EL and LO models. While the 8.11(b) figure shows the second update, where the best result compared to the experimental one occurs for the M-H and M-N models. In this case, the width of the band gap is observed in the dispersion diagram when the wave propagation mode becomes completely evanescent (highlighted area). This observation is confirmed by the attenuation that this behavior causes in the FRF of experimental inertance.

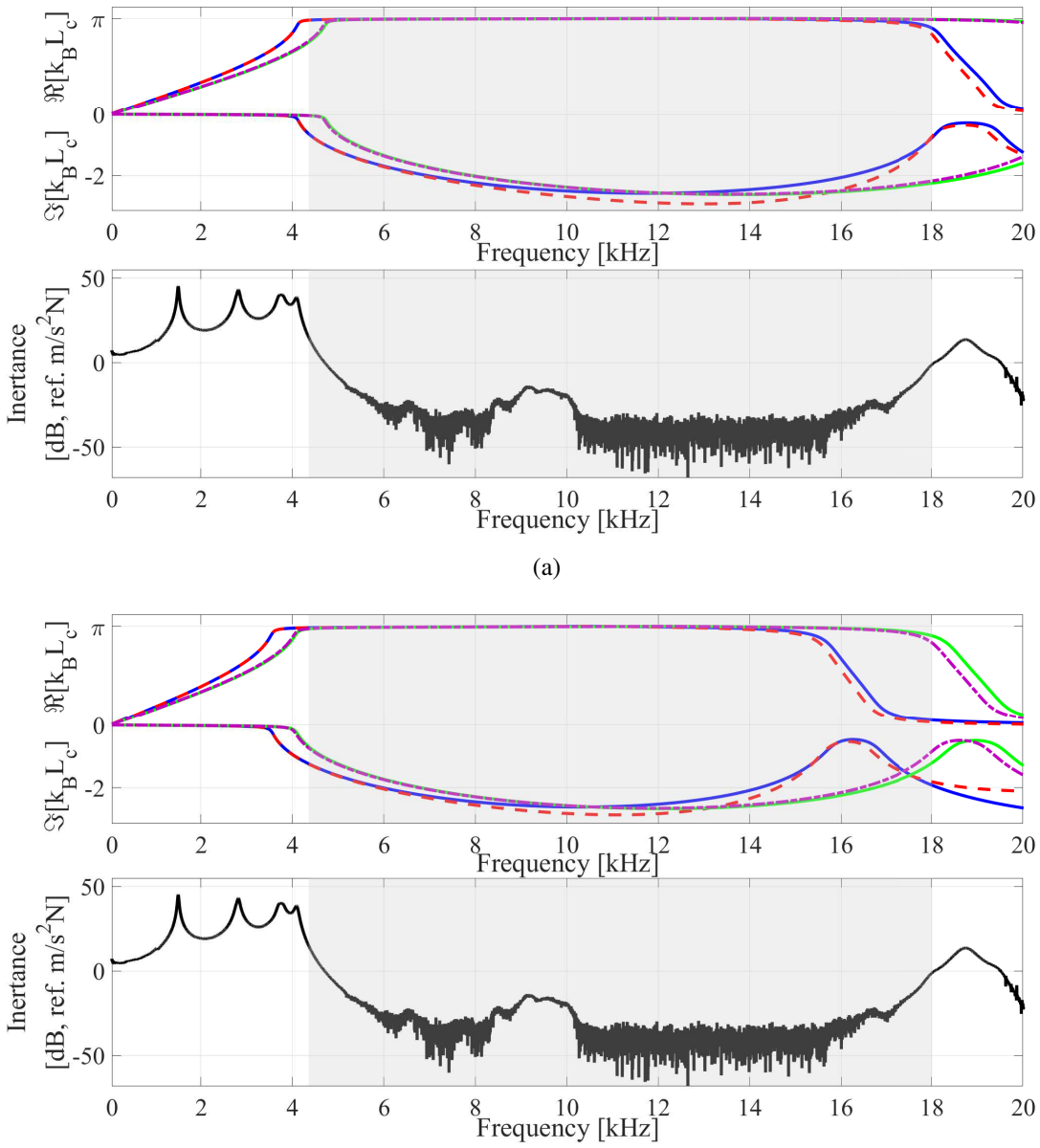

Figure. 8.11: PC rod experimental inertance FRF (bottom) and numerical dispersion diagram (*top*) calculated with EL (—); LO (— —); M-H (—); M-N (—.—) models by WFE using: (a) 1st and (b) 2nd model updating material properties.

8.6 Conclusion

Phononic Crystals were formulated using high order rod models (Love, Mindlin-Herrmann and Mindlin-McNiven) from of Wave Finite Element method. This formulations were numerically verified with the Spectral Transfer Matrix (STM) method wherein its dispersion diagrams and

forced responses of a homogeneous high order rod were compared. All numerical results has a good agreement in this comparison. In order to obtain the validation of PC rod results, a real structure was built, in which experimental tests were performed. In the comparison of experimental data to numerical results, it was observed that the nominal parameters of the real PC rod used to compute numerical result do not agree well. However, some updating parameters were performer with aim to approximate the experimental data with numerical tests. The challenge was choose a correct value parameter that agree for both high order models, because the lower-order models (Elementar and Love) do not agree with the higher-order (Mindlin-Herrmann and Mindlin-McNiven). Than, two model updating were made: a updating directed to lower-order models, in which the experimental data present a good agreement with numerical tests; and a updating in which the experimental data and numerical results agree well for higher-order models. As expected, for both updating, the comparisons has a good agreement. The dispersion diagrams result computed for both updating had the same behavior. In relationship to the Phononic Crystal analysis, It was possible to the band gap region with great clarity and it was possible to see such effect both in the inertance FRF and in the dispersion diagram. With this presented results, a great potential for higher-order rod models by WFE method was shown, in which the calculation of wave propagation and vibration problems of PC rod structures allowing an efficient and precise analysis.

9 CONCLUSION

A numerical method called Finite Wave Element (WFE), which makes a combination of the FEM and Floquet-Bloch theorem, has been proposed as an engineering tool to calculate elastic metamaterials and Phononic Crystals. This can create band gaps due to local resonance and Bragg scattering.

Elastic structures of metamaterial rods with periodic spatial distribution and local M-DOF resonators were presented with the aim of creating band gaps. This type of structure was modeled using the WFE method and its verification was made using the Spectral Elements Method (WSEM). Its efficiency in terms of precision in modeling EM rods has been demonstrated. The EM rods with attached S-DOF and 2-DOF resonators were evaluated using the WFE method. A good approximate solution for EM rod systems was obtained from a comparison of the WFE method with the WSEM. An important feature of the WFE method used was the commercial FEM (software ANSYS), which allows modeling complex geometry or non-uniform structures. Experimental results were performed with the objective of obtaining a real validation of the modeling of EM rods using the WFE method. In the comparison between the results, the methods presented (WSEM) and applied (WFE and WFE with ANSYS) were able to obtain a good agreement with the experimental results and also find the position and width of the band gap.

The WFE method was considered and implemented to calculate the wave modes in homogeneous and PC frames. The convergence of the WFE and FE methods was observed. The coupling of the wave modes was shown in straight line frames, as well as in the periodic change of the wave propagation direction. It was demonstrated that the topology of the patterns in the wave propagation properties positively influences the formation of the band gap. The increase in the number of band gap is one of them. After that, the structures of the PC plates arranged along a triangular pattern are modeled using the WFE method. Two types of periodicity were analyzed, the first due to the change in the material and the other due to the variation in the angle between the waveguides. The numerical results are compared with the classic FE method and its efficiency was analyzed in terms of accuracy and computational time. To make these comparisons, the frequency responses of the PC plate structures are computed. These periodicities create effects of band gaps that can be seen in the transmittance vibration. However, even for small angles of triangular shape, the band's attenuation effect is more efficient than alternating the material with similar properties, such as steel and aluminum.

The WFE method was proposed to calculate EM reinforced plates with CLR structures, where the vibration analysis was investigated from the modal transmittance analysis. The results were validated with the commercial method of FE (ANSYS). The effect of band gaps was used at undesirable resonance frequencies by means of tuned resonators, as demonstrated in the comparison of plates with and without a resonator. In a modal analysis of a cell it was possible to obtain its corresponding vibration modes and it was shown that the modes appear at the same frequency as the band gap. In addition, the plate dispersion diagram cuts the gap effect in all observed wave modes.

An experimental analysis was performed with a real thin EM plate with resonators in a square network. The modal analysis and the forced response were calculated using the FE method. It was demonstrated that the WFE and FE methods had a good agreement with each other. The experimental results show a good agreement regarding the band width attenuated in comparison with the numerical results.

Wave propagation and dynamic behavior of periodic structures and phononic crystals with high-order rod models (Elementary, Love, Mindlin-Herrmann and Mindlin-McNiven) are formulated by the Wave Finite Element (WFE) method and compared with the spectral transfer matrix (STM). The results for all models calculated by WFE and STM are in agreement. Experimental tests were performed to validate the numerical model of high-order PC rod by WFE. The band gap region in the dispersion diagrams, calculated with the WFE PC rod model, is compared to the attenuation region in the FRF experimental inertance and the results indicate the same region. The formulations, analyzes and results presented show the potential of high-order rod models by the WFE method to calculate wave propagation and vibration problems, allowing an efficient and accurate analysis of periodic structures and Phononic Crystals.

Future works

In the following, new studies are being developed about phononic materials and their influence on the wave propagation properties in elastic structures. Two of this topics appear as future prospects for continuation of the research developed in this thesis are listed.

- **Scattering Matrix Coupling**: In this study, a transfer matrix is formulated by the scattering matrix with objective of to obtain a relation of the left and right wave amplitudes between

a considerable number of coupling structures. Consequently, we will may extract the forced response more fast than the others method and the wave properties.

- **Two Dimensional Wave Finite Element applied to metamaterials and Phononic Crystals**. In this proposal, will be studied the WFE method for two dimension in elastic structures. For this, will be used the Floquet-Bloch's theorem in two periodic directions to condense the periodic structure for a cell. The challenge will to find the appropriated method to solve the eigenvalue problem.

List of publications

Articles in indexed journals:

- NOBREGA, E.D.; GAUTIER, F.; PELAT, A.; DOS SANTOS J.M.C. Vibration band gaps for elastic metamaterial rods using wave finite element method. **Mechanical Systems and Signal Processing**, v. 79, 192-202, 2016.
- MIRANDA Jr., E.J.P.; NOBREGA, E.D.; FERREIRA, A.H.R.; DOS SANTOS, J.M.C. Flexural wave band gaps in a multi-resonator elastic metamaterial plate using KirchhoffLove theory. **Mechanical Systems and Signal Processing**, v. 116, 480-504, 2019.
- GOTO, A. M.; NOBREGA, E.D.; PEREIRA, F.N.; DOS SANTOS, J.M.C. Numerical and experimental investigation of higher order phononic crystal waveguides by STM and WFE. **International Journal of Mechanical Sciences** (accepted to review), 2020.
- MIRANDA Jr., E.J.P.; NOBREGA, E.D.; RODRIGUES, S.F.; ARANAS Jr., C.; DOS SANTOS, J.M.C. Wave attenuation in elastic metamaterial thick plates: Numerical and experimental investigations. **International Journal of Solids and Structures** (under review), 2020.

Full Papers and Abstracts in Conference Proceedings:

- NOBREGA, E. D.; and DOS SANTOS, J. M. C. Vibration bandgaps for elastic metamaterial rods using wave finite element method, In Proceedings of the **International Conference on Structural Engineering Dynamic (ICEDyn)**, Lagos, Algarve, Belgium, june 22-24 2015.

- MACHADO, M. R.; NOBREGA, E.D.; DOS SANTOS, J.M.C. Wave propagation in a beam-like structure with random, In Proceedings of the **International Conference Noise and Vibration Engineering (ISMA)**, Leuven, Belgium, 22-24 June, 4141-4152, 2016.

- NOBREGA, E. D.; and DOS SANTOS, J. M. C. Bandas proibidas em vigas de metamaterial elástico modeladas por elementos finitos de propagação de ondas, In Proceedings of the **IX Congresso Nacional de Engenharia Mecânica (CONEM)**, Fortaleza, Ceará, Brasil, 21-25 August, 2016

- NOBREGA, E. D.; GOBERT, M.-L.; DOS SANTOS, J.M.C.; MENCIK, J.-M. Investigating simple designs of phononic crystal plates and their influence on the wave propagation properties, In Proceedings of the **International Conference Noise and Vibration Engineering (ISMA)**, Leuven, Belgium, 17-19 September, 2483-2496, 2018.

- NOBREGA, E. D.; DOS SANTOS, J.M.C. Metamaterial Plate Vibration with WFE Method using Continuous Local Resonator, In Proceedings of the **XVIII International Symposium on Dynamic Problems of Mechanics Modeling (DINAME)**, Buzios, Rio de Janeiro, Brazil, 10-15 March, 2019.

- GOTO, A. M.; NOBREGA, E. D.; PEREIRA, V.S.; COSTA, D.I.G.; DOS SANTOS, J.M.C. One-dimensional phononic crystal dynamic analysis by spectral transfer matrix method, In Proceedings of the **XVIII International Symposium on Dynamic Problems of Mechanics Modeling (DINAME)**, Buzios, Rio de Janeiro, Brazil, 10-15 March, 2019.

- FERREIRA, A.; NOBREGA, E. D.; MIRANDA, E.J.P., Jr.; DOS SANTOS, J.M.C. Flexural wave band gaps in locally resonant elastic metamaterial plate using Reissner-Mindlin theory, In Proceedings of the **XVIII International Symposium on Dynamic Problems of Mechanics Modeling (DINAME)**, Buzios, Rio de Janeiro, Brazil, 10-15 March, 2019.

- GOTO, A. M.; NOBREGA, E. D.; DOS SANTOS, J.M.C. Dynamic analysis of phononic crystal curved beam using the spectral transfer matrix method, In Proceedings of the **International congress and exhibition on noise control engineering (INTER-NOISE)**, Madri, Spain, 16–19 June, 2019.

- GOTO, A. M.; NOBREGA, E. D.; PEREIRA, F.N.; DOS SANTOS, J.M.C. Spectral transfer matrix method for higher order phononic crystal waveguides, In Proceedings of the **International Conference on Structural Engineering Dynamics (ICEDyn)**, Viana do Castelo, Portugal, 24-26 June, 2019.

- MACEDO, P.; NOBREGA, E. D.; DOS SANTOS, J.M.C. Wave propagation in a tunable metamaterial beam with periodic piezoelectric shunts, In Proceedings of the **International Conference on Structural Engineering Dynamics (ICEDyn)**, Viana do Castelo, Portugal, 24-26 June, 2019.

- NOBREGA, E. D.; PEREIRA, V.S.; COSTA, D.I.G.; DOS SANTOS, J.M.C. Energy flow analysis applied to dynamic behavior of metamaterials, In Proceedings of the **XL Ibero-Latin-American Congress on Computational Methods in Engineering (CILAMCE)**, Natal, Rio Grande do Norte, Brazil, 11-14 November, 2019

- FERNANDES, Y.M.S.; MACHADO, M. R.; NOBREGA, E. D.; Vibrational analysis of power transmission tower by spectral element method: a numerical validation, In Proceedings of the **25th ABCM International Congress of Mechanical Engineering (COBEM)**, Uberlândia, MG, Brazil, 20-25 October, 2019.

REFERENCES

Matweb - material property data. 2019.
URL: *http://www.matweb.com/index.aspx*

ALLEMANG, A.J. The modal assurance criterion (mac): Twenty years of use and abuse. **Sound Vib**, pp. 14–21, 2003.

ASHBY, M.F. **Material Selection in Mechanical Design**. Elsevier, 4 ed., 2011.

ASSOUAR, M.B. and OUDICH, M. Enlargement of a locally resonant sonic band gap by using double-sides stubbed phononic plates. **Applied Physics Letters**, v. 100, n. 12, 123506, mar 2012.

ASSOUAR, M.B.; SUN, J.H.; LIN, F.S. and HSU, J.C. Hybrid phononic crystal plates for lowering and widening acoustic band gaps. **Ultrasonics**, v. 54, n. 8, 2159–2164, dec 2014.

BELI, D.; FABRO, A.T.; RUZZENE, M. and ARRUDA, J.R.F. Wave attenuation and trapping in 3d printed cantilever-in-mass metamaterials with spatially correlated variability. **Scientific Reports**, v. 9, n. 1, apr 2019.

BELI, D.; MENCIK, J.M.; SILVA, P.B. and ARRUDA, J.R.F. A projection-based model reduction strategy for the wave and vibration analysis of rotating periodic structures. **Computational Mechanics**, v. 62, n. 6, 1511–1528, may 2018.

BEN SOUF, M.A.; BAREILLE, O.; ICHCHOU, M.N.; BOUCHOUCHA, F. and HADDAR, M. Waves and energy in random elastic guided media through the stochastic wave finite element method. **Physics Letters A**, v. 377, 2255–2264, 2013a.

BEN SOUF, M.A.; BAREILLE, O.; ICHCHOU, M.N.; TROCLET, B. and HADDAR, M. Variability of coupling loss factors through a wave finite element technique. **Journal of Sound and Vibration**, v. 332, 2179–2190, 2013b.

BHUDDI, A.; GOBERT, M.L. and MENCIK, J.M. On the acoustic radiation of axisymmetric fluid-filled pipes using the wave finite element (WFE) method. **Journal of Computational Acoustics**, v. 23, n. 03, 1550011, jun 2015.

BLOCH, F. Über die quantenmechanik der elektronen in kristallgittern. **Zeitschrift für Physik**, v. 52, n. 7-8, 555–600, jul 1928.

BOUCHOUCHA, F.; ICHCHOU, M.N. and HADDAR, M. Stochastic wave finite element method in uncertain elastic media through the second order perturbation. **Journal of Applied Mechanics and Technical Physics**, v. 58, n. 2, 362–370, mar 2017.

BRILLOUIN, L. **"Wave Propagation in Periodic Structures: Electric Filters and Crystal Lattices**. Dover Publications, New York, 1946.

CASADEI, F. and BERTOLDI, K. Wave propagation in beams with periodic arrays of airfoil-shaped resonating units. **Journal of Sound and Vibration**, v. 333, n. 24, 6532–6547, dec 2014.

CHEN, Y.; HUANG, G.; ZHOU, X.; HU, G. and SUN, C.T. Analytical coupled vibroacoustic modeling of membrane-type acoustic metamaterials: Membrane model. **The Journal of the Acoustical Society of America**, v. 136, n. 3, 969–979, sep 2014.

COLOMBI, A.; ROUX, P. and RUPIN, M. Sub-wavelength energy trapping of elastic waves in a metamaterial. **The Journal of the Acoustical Society of America**, v. 136, n. 2, EL192–EL198, aug 2014.

CROËNNE, C.; PONGE, M.F.; DUBUS, B.; GRANGER, C.; HAUMESSER, L.; LEVASSORT, F.; VASSEUR, J.O.; LORDEREAU, A.; THI, M.P. and HLADKY-HENNION, A.C. Tunable phononic crystals based on piezoelectric composites with 1-3 connectivity. **The Journal of the Acoustical Society of America**, v. 139, n. 6, 3296–3302, jun 2016.

DOYLE, J.F. **Wave propagation in structure: spectral analysis using fast discrete Fourier transforms**. Springer Verlag, 1997.

DUHAMEL, D.; MACE, B.R. and BRENNAN, M.J. Finite element analysis of the vibrations of waveguides and periodic structures. **Journal of Sound and Vibration**, v. 294, n. 1-2, 205–220, jun 2006.

DURANTEAU, M.; VALIER-BRASIER, T.; CONOIR, J.M. and WUNENBURGER, R. Random acoustic metamaterial with a subwavelength dipolar resonance. **The Journal of the Acoustical Society of America**, v. 139, n. 6, 3341–3352, jun 2016.

FAROOQUI, M.; ELNADY, T. and AKL, W. Sound attenuation in ducts using locally resonant periodic aluminum patches. **The Journal of the Acoustical Society of America**, v. 139, n. 6, 3277–3287, jun 2016a.

FAROOQUI, M.; ELNADY, T. and AKL, W. Validation of low frequency noise attenuation using locally resonant patches. **The Journal of the Acoustical Society of America**, v. 139, n. 6, 3267–3276, jun 2016b.

FLOQUET, G. Sur les équations différentielles linéaires à coefficients périodiques. **Annales scientifiques de l'É.N.S. 2e série**, v. 12, 47–88, 1883.

GOLDSTEIN, A.L.; SILVA, P.B. and ARRUDA, J.R.F. The wave spectral finite element method applied to the design of periodic waveguides. In **International Congress on Sound and Vibration**. 2011.

GUO, Y.; DEKORSY, T. and HETTICH, M. Topological guiding of elastic waves in phononic metamaterials based on 2d pentamode structures. **Scientific Reports**, v. 7, n. 1, dec 2017.

HUSSEIN, M.I.; LEAMY, N.J. and RUZZENE, M. Dynamics of phononic materials and structures: Historical origins, recent progress, and future outlook. **Applied Mechanics Reviews**, v. 66, n. 4, 38pp, may 2014.

HVATOV, A. and SOROKIN, S. Free vibrations of finite periodic structures in pass- and stop-bands of the counterpart infinite waveguides. **Journal of Sound and Vibration**, v. 347, 200–217, jul 2015.

ICHCHOU, M.; BOUCHOUCHA, F.; BEN SOUF, M.; DESSOMBZ, O. and HADDAR, M. Stochastic wave finite element for random periodic media through first-order perturbation. **Computer Methods in Applied Mechanics and Engineering**, v. 200, n. 41-44, 2805–2813, oct 2011.

ICHCHOU, M.N.; MENCIK, J.M. and ZHOU, W. Wave finite elements for low and mid-frequency description of coupled structures with damage. **Computer Methods in Applied Mechanics and Engineering**, v. 198, 1311–1326, 2009.

KHAJEHTOURIAN, R. and HUSSEIN, M.I. Dispersion characteristics of a nonlinear elastic metamaterial. **AIP Advances**, v. 4, n. 12, 124308, dec 2014.

LEE, M.K. and KIM, Y.Y. Add-on unidirectional elastic metamaterial plate cloak. **Scientific Reports**, v. 6, n. 1, feb 2016.

LEE, U. **Spectral element method in structural dynamics**. John Wiley and Sons (Asia), 2009.

LI, Y. and BRIK, P.Y. **Design, Implementation and Vibration Test of a Meta-Beam**. ENSIM-LAUM-Université du Maine, Research Report, (in French), 2014.

LIU, Z.; RUMPLER, R. and FENG, L. Broadband locally resonant metamaterial sandwich plate for improved noise insulation in the coincidence region. **Composite Structures**, v. 200, 165–172, sep 2018.

LIU, Z.Y.; ZHANG, X.X.; MAO, Y.W.; ZHU, Y.Y.; YANG, Z.Y.; CHAN, C.T. and SHENG, P. Locally resonant sonic materials. **Science**, v. 289, 1734–1736, 2000.

LOVE, A.E. **A treatise on the mathematical theory of elasticity**. Dover Publications, 1927.

LUCKLUM, R.; KE, M. and ZUBTSOV, M. Two-dimensional phononic crystal sensor based on a cavity mode. **Sensors and Actuators B: Chemical**, v. 171-172, 271–277, aug 2012.

MACE, B. and MACONI, E. Modelling wave propagation in two-dimensional structures using finite element analysis. **Journal of Sound and Vibration**, v. 318, 884–902, 2008.

MACE, B.R.; DUHAMEL, D.; BRENNAN, M.J. and HINKE, L. Finite element prediction of wave motion in structural waveguides. **The Journal of the Acoustical Society of America**, v. 117, n. 5, 2835–2843, may 2005.

MACHADO, M.R.; NOBREGA, E.D. and DOS SANTOS, J.M.C. Wave propagation in a beam-like structure with random parameter using wave finite element method. In **PROCEEDINGS OF ISMA2016 INCLUDING USD2016**. 2016.

MEAD, D.J. Free wave propagation in periodically supported, infinte beams. **Journal of Sound and Vibration**, v. 11(2), 181–197, 1970.

MEAD, D.J. A general theory of harmonic wave propagation in linear periodic systems with multiple coupling. **Journal of Sound and Vibration**, v. 27(2), 235–260, 1973.

MEAD, D.J. Wave propagation and natural modes in periodic systems: I. mono-coupled systems. **Journal of Sound and Vibration**, v. 40(1), 1–18, 1974.

MEAD, D.J. Wave propagation and natural modes in periodic systems: Ii. multi-coupled systems, with and without damping. **Journal of Sound and Vibration**, v. 40(1), 19–39, 1975.

MENCIK, J.M. **Approche numerique pour la propagation multi-modale guidee**. Universite Francois Rabelais de Tours, 2008.

MENCIK, J.M. On the low- and mid-frequency forced response of elastic structures using wave finite elements with one-dimensional propagation. **Computers and Structures**, v. 88, 674–689, 2010.

MENCIK, J.M. Model reduction and perturbation analysis of wave finite element formulations for computing the forced response of coupled elastic systems involving junctions with uncertain eigenfrequencies. **Computer Methods in Applied Mechanics and Engineering**, v. 200, n. 45-46, 3051–3065, oct 2011.

MENCIK, J.M. A model reduction strategy for computing the forced response of elastic waveg-

uides using the wave finite element method. **Computer Methods in Applied Mechanics and Engineering**, v. 229-232, 68–86, jul 2012.

MENCIK, J.M. A wave finite element-based formulation for computing the forced response of structures involving rectangular flat shells. **International Journal for Numerical Methods in Engineering**, v. 95, n. 2, 91–120, may 2013.

MENCIK, J.M. New advances in the forced response computation of periodic structures using the wave finite element (WFE) method. **Computational Mechanics**, v. 54, n. 3, 789–801, apr 2014.

MENCIK, J.M. A wave finite element strategy to compute the dynamic flexibility modes of structures with cyclic symmetry and its application to domain decomposition. In **Proceedings of the 6th International Conference on Computational Methods in Structural Dynamics and Earthquake Engineering (COMPDYN 2015)**. Institute of Structural Analysis and Antiseismic Research School of Civil Engineering National Technical University of Athens (NTUA) Greece, 2017.

MENCIK, J.M. and DUHAMEL, D. A wave-based model reduction technique for the description of the dynamic behavior of periodic structures involving arbitrary-shaped substructures and large-sized finite element models. **Finite Elements in Analysis and Design**, v. 101, 1–14, 2015.

MENCIK, J.M. and DUHAMEL, D. A wave finite element-based approach for the modeling of periodic structures with local perturbations. **Finite Elements in Analysis and Design**, v. 121, 40–51, nov 2016.

MENCIK, J.M. and ICHCHOU, M. Wave finite elements in guided elastodynamics with internal fluid. **International Journal of Solids and Structures**, v. 44, n. 7-8, 2148–2167, apr 2006.

MENCIK, J.M. and ICHCHOU, M.N. Multi-mode propagation and diffusion in structures through finite elements. **European Journal of Mechanics A/Solids**, v. 24, n. 5, 877–898, sep 2005.

MINDLIN, R.D. and HERRMANN, G. A one-dimensional theory of compressional wave in an elastic rod. In **Proceedings of First U.S National Congress of Applied Mechanics**, pp. 187–191. 1950.

MIRANDA, E.J.P.; NOBREGA, E.D.; FERREIRA, A.H.R. and DOS SANTOS, J.M.C. Flexural wave band gaps in a multi-resonator elastic metamaterial plate using kirchhoff-love theory. **Mechanical Systems and Signal Processing**, v. 116, 480–504, feb 2019.

MIRANDA JR., E.J.P. and SANTOS, J.M.C.D. Flexural wave band gaps in phononic crystal euler-bernoulli beams using wave finite element and plane wave expansion methods. **Materials Research**, v. 20, 2017.

MITCHELL, S.J.; PANDOLFI, A. and ORTIZ, M. Metaconcrete: designed aggregates to enhance dynamic performance. **Journal of the Mechanics and Physics of Solids**, v. 65, 69–81, apr 2014.

MITROU, G.; FERGUSON, N. and RENNO, J. Wave transmission through two-dimensional structures by the hybrid FE/WFE approach. **Journal of Sound and Vibration**, v. 389, 484–501, feb 2017.

MOHAMMADI, S.; EFTEKHAR, A.A.; KHELIF, A.; HUNT, W.D. and ADIBI, A. Evidence of large high frequency complete phononic band gaps in silicon phononic crystal plates. **Applied Physics Letters**, v. 92, n. 22, 221905, jun 2008.

NASCIMENTO, R. F. **Propagação de ondas usando modelos de elementos finitos de fatias de guias de ondas estruturais**. 2009. PhD Thesis. Universidade Estadual de Campinas.

NEWTON, I. **"Principia" Book II**. 1687.

NOBREGA, E. D. **Análise de Modelos de Barra de Alta Ordem Usando Métodos das Fatias de Guia de Ondas**. 2015. University of Campinas.

NOBREGA, E.D. and DOS SANTOS, J.M.C. Vibration bandgaps for elastic metamaterial rods using wave finite element method. In **International Conference on Structural Engineering Dynamic - ICEDyn**, v. 1, pp. 22–24. 2015.

NOBREGA, E.D. and DOS SANTOS, J.M.C., editores. **Metamaterial Plate Vibration with WFE Method using Continuous Local Resonator**. XVIII International Symposium on Dynamic Prob-

lems of Mechanics Modeling - DINAME, 2019.

NÓBREGA, E.D. and DOS SANTOS, J.M.C. Metamaterial plate vibration with WFE method using continuous local resonator modeling. In **DINAME2019**. ABCM, 2019.

NOBREGA, E.D.; GAUTIER, F.; PELAT, A. and DOS SANTOS, J. Vibration band gaps for elastic metamaterial rods using wave finite element method. **Mechanical Systems and Signal Processing**, v. 79, 192–202, 2016.

NOBREGA, E.D.; GOBERT, M.L.; DOS SANTOS, J. and MENCIK, J.M. Investigating simple designs of phononic crystal plates and their influence on the wave propagation properties. In **International Conference Noise and Vibration Engineering - ISMA**, v. 1, pp. 2483–2496. 2018.

PATEL, R. On computing the eigenvalues of a symplectic pencil. **Linear Algebra and its Applications**, v. 188-189, 591–611, jul 1993.

PENG, H.; PAI, P.F. and DENG, H. Acoustic multi-stopband metamaterial plates design for broadband elastic wave absorption and vibration suppression. **International Journal of Mechanical Sciences**, v. 103, 104–114, nov 2015.

PETYT, M. **Introduction to finite element vibration analysis**. Cambridge University Press, New York, USA, 2010.

POGGETTO, V.F.D.; SERPA, A.L. and DE FRANÇA ARRUDA, J.R. Optimization of local resonators for the reduction of lateral vibrations of a skyscraper. **Journal of Sound and Vibration**, v. 446, 57–72, apr 2019.

PONGE, M.F.; CROËNNE, C.; VASSEUR, J.O.; MATAR, O.B.; HLADKY-HENNION, A.C. and DUBUS, B. Control of elastic wave propagation in one-dimensional piezomagnetic phononic crystals. **The Journal of the Acoustical Society of America**, v. 139, n. 6, 3288–3295, jun 2016.

QI, S.; OUDICH, M.; LI, Y. and ASSOUAR, B. Acoustic energy harvesting based on a planar acoustic metamaterial. **Applied Physics Letters**, v. 108, n. 26, 263501, jun 2016.

RENNO, J.M. and MACE, B.R. On the forced response of waveguides using the wave and finite element method. **Journal of Sound and Vibration**, v. 329, n. 26, 5474–5488, dec 2010.

RENNO, J.M. and MACE, B.R. Calculating the forced response of two-dimensional homogeneous media using the wave and finite element method. **Journal of Sound and Vibration**, v. 330, n. 24, 5913–5927, nov 2011.

RENNO, J.M. and MACE, B.R. Calculation of reflection and transmission coefficients of joints using a hybrid finite element/wave and finite element approach. **Journal of Sound and Vibration**, v. 332, n. 9, 2149–2164, apr 2013.

RENNO, J.M. and MACE, B.R. Vibration modelling of structural networks using a hybrid finite element/wave and finite element approach. **Wave Motion**, v. 51, n. 4, 566–580, jun 2014.

SHU, F.; LIU, Y.; WU, J. and WU, Y. Band gap in tubular pillar phononic crystal plate. **Ultrasonics**, v. 71, 172–176, sep 2016.

SILVA, P. B. **Dynamic analysis of periodic structures via wave-based numerical approaches and substructuring techniques**. 2015. PhD Thesis. University of Campinas, Brazil.

SILVA, P.B.; ARRUDA, J.R.F. and GOLDSTEIN, A.L., editores. **Study of elastic band-gaps in finite periodic structure using finite element models**. XIV International Symposium on Dynamic Problems of Mechanics - DINAME, 2011a.

SILVA, P.B.; ARRUDA, J.R.F. and GOLDSTEIN, A.L. Study of elastic band-gaps in finite periodic structure using finite element models. In **Proceedings of the XIV International Symposium on Dynamic Problems of Mechanics**. 2011b.

SILVA, P.B.; GOLDSTEIN, A.L. and ARRUDA, J.R.F. Building spectral element dynamic matrices using finite element models of waveguide slices and elastodynamic equations. **Shock and Vibration**, v. 20, n. 3, 439–458, 2013.

SILVA, P.B.; MENCIK, J.M. and ARRUDA, J.R.F. On the forced harmonic response of coupled

systems via a wfe-based super-element approach. In **Proceedings of ISMA**, v. 1, pp. 1–13. 2014.

SILVA, P.B.; MENCIK, J.M. and ARRUDA, J.R.F. On the use of the wave finite element method for passive vibration control of periodic structures. **Advances in Aircraft and Spacecraft Science**, v. 3, n. 3, 299–315, 2016.

SILVA, P.B.; MENCIK, J.M. and DE FRANCA ARRUDA, J.R. Wave finite element-based superelements for forced response analysis of coupled systems via dynamic substructuring. **International Journal for Numerical Methods in Engineering**, v. 107, n. 6, 453–476, dec 2015.

SINGH, R.; DROZ, C.; ICHCHOU, M.; FRANCO, F.; BAREILLE, O. and ROSA, S.D. Stochastic wave finite element quadratic formulation for periodic media: 1d and 2d. **Mechanical Systems and Signal Processing**, v. 136, 106431, feb 2020.

SUN, J.H. and WU, T.T. Propagation of acoustic waves in phononic-crystal plates and waveguides using a finite-difference time-domain method. **Physical Review B**, v. 76, n. 10, sep 2007.

TITOVICH, A.S.; NORRIS, A.N. and HABERMAN, M.R. A high transmission broadband gradient index lens using elastic shell acoustic metamaterial elements. **The Journal of the Acoustical Society of America**, v. 139, n. 6, 3357–3364, jun 2016.

TORRENT, D.; PENNEC, Y. and DJAFARI-ROUHANI, B. Effective medium theory for elastic metamaterials in thin elastic plates. **Physical Review B**, v. 90, n. 10, sep 2014.

WAKI, Y. **On the application of finite element analysis to wave motion in one-dimensional waveguides**. 2007. PhD Thesis. University of Southampton, United Kingdom.

WAKI, Y.; MACE, B. and BRENNAN, M. Free and forced vibrations of a tyre using a wave/finite element approach. **Journal of Sound and Vibration**, v. 323, n. 3-5, 737–756, jun 2009a.

WAKI, Y.; MACE, B.R. and BRENNAN, M.J. Numerical issues concerning the wave and finite element method for free and forced vibrations of waveguides. **Journal of Sound and Vibration**, v. 327, n. 1-2, 92–108, oct 2009b.

WANG, G.; WEN, X.; WEN, J. and LIU, Y. Quasi-one-dimensional periodic structure with locally resonant band gap. **Journal of Applied Mechanics**, v. 73, 167–170, 2006.

WANG, T.; SHENG, M.P.; GUO, Z.W. and QIN, Q.H. Flexural wave suppression by an acoustic metamaterial plate. **Applied Acoustics**, v. 114, 118–124, dec 2016a.

WANG, X.P.; JIANG, P.; CHEN, T.N. and ZHU, J. Tuning characteristic of band gap and waveguide in a multi-stub locally resonant phononic crystal plate. **AIP Advances**, v. 5, n. 10, 107141, oct 2015.

WANG, Y.F.; WANG, Y.S. and ZHANG, C. Two-dimensional locally resonant elastic metamaterials with chiral comb-like interlayers: Bandgap and simultaneously double negative properties. **The Journal of the Acoustical Society of America**, v. 139, n. 6, 3311–3319, jun 2016b.

WANG, Y.F.; WANG, Y.Z.; WU, B.; CHEN, W. and WANG, Y.S. Tunable and active phononic crystals and metamaterials. **Applied Mechanics Reviews**, v. 72, n. 4, feb 2020.

XIANG, H.J. and SHI, Z.F. Analysis of flexural vibration band gaps in periodic beams using differential quadrature method. **Computers and Structures**, v. 87, 1559–1566, 2009.

XIANG, H.J.; SHI, Z.F.; WANG, S.J. and MO, Y.L. Periodic materials-based vibration attenuation in layered foundations: experimental validation. **Smart Materials and Structures**, v. 21, n. 11, 112003, sep 2012.

XIAO, Y.; MACE, B.R.; WEN, J. and WEN, X. Formation and coupling of band gaps in a locally resonant elastic system comprising a string with attached resonators. **Physics Letters A**, v. 375, n. 12, 1485–1491, mar 2011.

XIAO, Y.; WEN, J. and WEN, X. Broadband locally resonant beams containing multiple periodic arrays of attached resonators. **Physics Letters A**, v. 376, n. 16, 1384–1390, mar 2012a.

XIAO, Y.; WEN, J. and WEN, X. Longitudinal wave band gaps in metamaterial-based elastic rods containing multi-degree-of-freedom resonators. **New Journal of Physics**, v. 14, n. 3, 033042,

2012b.

XIAO, Y.; WEN, J.; YU, D. and WEN, X. Flexural wave propagation in beams with periodically attached vibration absorbers: Band-gap behavior and band formation mechanisms. **Journal of Sound and Vibration**, v. 332, n. 4, 867–893, feb 2013.

YANG, Y.; MACE, B.R. and KINGAN, M.J. Prediction of sound transmission through, and radiation from, panels using a wave and finite element method. **The Journal of the Acoustical Society of America**, v. 141, n. 4, 2452–2460, apr 2017.

ZHANG, Y.; HE, J. and JIANG, L.H. Flexural vibration band gaps characteristics in phononic crystal euler beams on two-parameter foundation. **Advances in Mechanical Engineering**, v. 5, 935258, jan 2013.

ZHONG, W. and WILLIAMS, F. On the direct solution of wave propagation for repetitive structures. **Journal of Sound and Vibration**, v. 181, n. 3, 485–501, mar 1995.